Evaluating the Combined Use of Three-Dimensional Hydrodynamic Modeling and Polyethylene Passive Sampling in the Lower Duwamish Waterway

by

Catherine Elizabeth Sobchuk

B.S. Civil Engineering
Syracuse University, 2014

SUBMITTED TO THE DEPARTMENT OF CIVIL AND ENVIRONMENTAL ENGINEERING IN PARTIAL FULFILLMENT OF THE REQUIREMENTS FOR THE DEGREE OF

MASTER OF ENGINEERING IN CIVIL AND ENVIRONMENTAL ENGINEERING
AT THE
MASSACHUSETTS INSTITUTE OF TECHNOLOGY

JUNE 2018

Signature redacted

Signature of Author: _____
Department of Civil and Environmental Engineering
May 11, 2018

Signature redacted

Certified by: _____
E. Eric Adams
Senior Lecturer, Senior Research Engineer
Thesis Supervisor

Signature redacted

Accepted by: _____
Jesse Kroll
Professor of Civil and Environmental Engineering
Chair, Graduate Program Committee

Evaluating the Combined Use of Three-Dimensional Hydrodynamic Modeling and Polyethylene Passive Sampling in the Lower Duwamish Waterway

by

Catherine Elizabeth Sobchuk

Submitted to the department of Civil and Environmental Engineering
on May 11, 2018 in partial fulfillment of the
Requirements for the Degree of Master of Engineering in
Civil and Environmental Engineering

ABSTRACT

Polyethylene (PE) passive samplers are capable of measuring in-situ, freely dissolved, time-averaged concentration distributions of contaminants in air, surface water, and sediment bed porewater. This sampling technique can be coupled with a three dimensional (3D) hydrodynamic model of a given surface water body to identify where sources contributing to the measured concentration distribution are most likely located and what mass flux is required to produce the measured concentrations. This evaluation was completed for the Lower Duwamish Waterway (LDW), a salt wedge estuary located in Seattle, Washington. The LDW was selected for its idealized conditions (straight channel with relatively uniform cross-section), established 3D hydrodynamic model (Environmental Fluid Dynamics Code [EFDC]), and availability of measured data.

Density-driven circulation in the LDW drives saltwater upstream and freshwater downstream, influencing residence times, mixing times, and the resulting concentration distributions of potential sources. The dependence of simulated, unit strength concentration distributions on source location was evaluated by spatially comparing EFDC-simulated sources introduced at various points in the LDW. This determined how far apart potential sources need to be, referred to as a distinguishable distance, to be "resolved" by measured or modeled concentrations at the LDW centerline. East and west bank sources were generally distinguishable within 0.8 miles of introduction; water surface and sediment bed sources were generally distinguishable throughout the LDW; longitudinally distributed sources were distinguishable for 0.4 to 1.1 miles from the source location. PE passive samplers placed at the centerline of the LDW with spacing at or near the distinguishable distance will likely be able to differentiate between various source locations.

Inverse model techniques were applied to measured concentration distributions in the water column using numerous cases of potential source locations with distinguishable, unit strength concentration distributions. The resulting mass fluxes ranged from 0.034 mg/s to 0.072 mg/s (average 0.043 mg/s), an order of magnitude higher than known source fluxes (i.e., sediment diffusive flux and air-water exchange flux). Therefore, one or more "missing sources" were determined to exist; based on this evaluation, it is possible the sources originate from the midstream sediment bed, upstream sediment bed, and upstream water surface.

Thesis Supervisor: E. Eric Adams
Title: Senior Lecturer, Senior Research Engineer

Acknowledgements

I would like to thank my advisor Dr. Eric Adams for his guidance during the year. I would also like to thank Dan Prendergast for his EFDC training, technical support, and contributions. Lastly, I would like to thank Dr. Phil Gschwend, Dr. Peter Israelsson, and Dr. Aaron Chow for their contributions.

Contents

List of Tables

List of Figures

1.0 Introduction

Surface water contamination is a risk to human health, the environment, and surrounding wildlife until it has been appropriately remediated. Remediation consists of source identification, evaluation of clean-up options, execution of the chosen strategy, and long-term monitoring to confirm recontamination will not occur. The critical step in the remediation process is source identification; if sources have not been properly identified and controlled, the chosen remedial strategy will be ineffective.

Polyethylene (PE) passive samplers have been established as a method to measure *in-situ*, freely dissolved, time-averaged concentration distributions of contaminants in air, surface water, and sediment bed porewater (Apell & Gschwend, 2016). This sampling technique can be coupled with a three dimensional (3D) hydrodynamic model of the surface water body to identify where the sources contributing to the measured concentration distribution are most likely located. In this process, measured concentration distributions are compared to concentration distributions that originate from potential source locations, of unit strength, as simulated in the 3D hydrodynamic model. The relationship between the measured concentration distribution and the simulated unit concentration distribution is assumed to be linear. As such, the potential source locations are assigned a weight based on the linear least square fit of the data. Source location weights can guide surface water remediation, leading to a more efficient and effective remediation procedure.

The combined use of 3D hydrodynamic modeling and PE passive sampling was evaluated for the Lower Duwamish Waterway (LDW), an estuary located in Seattle, Washington. The LDW is a 5-mile segment between the freshwater Green/Duwamish River and the saltwater Elliott Bay that historically supported numerous industrial and manufacturing facilities. These processes used polychlorinated biphenyls (PCBs), polycyclic aromatic hydrocarbons (PAHs), and many other chemicals, which impacted the environment in and surrounding the LDW. While remediation efforts are ongoing, as described in Section 2.0, the LDW water column continues to be impacted by contamination.

Ultimately, this method could be modified and applied to any contaminated site. The LDW was selected for this evaluation for three reasons:

1. Idealized conditions. As described in Section 2.0, the LDW was dredged to become a navigation channel in the early 1900s (US EPA, 2014). This process created a straighter channel with a relatively uniform cross-section. These conditions are assumed in many

theoretical equations, such as longitudinal dispersion and transverse mixing time, and they can be applied accurately within the LDW.

2. Previously developed 3D hydrodynamic model. The LDW Environmental Fluid Dynamics Code (EFDC) model was first developed by Virginia Institute of Marine Sciences and is described further in Section 3.0 (Dynamic Solutions International, LLC, EFDC Explorer, 2016). This model was calibrated and validated prior to this assessment and could immediately be used for simulation of unit concentration sources in the LDW.
3. Availability of measured data. Massachusetts Institute of Technology (MIT) collected water column, sediment bed porewater, and air samples throughout the LDW in 2012, 2014, 2015, and 2016 (Apell & Gschwend, 2016) (Prendergast et al., 2018) (Apell & Gschwend, 2017). The PE passive sampling process is described further in Section 4.0. Measured concentration distributions are essential to assign weights to simulated unit concentration distributions and to identify where potential sources are located. In addition to data collection and analysis, a linear least square fit of measured water column concentrations to potential sediment bed source locations was conducted as described in Section 4.4.

As described in Section 5.0, the study begins by evaluating characteristics of the LDW with the LDW EFDC model, such as its salinity distribution, estuary classification, flow patterns, and typical residence and mixing times. Next, the dependence of simulated unit source concentration distribution on source location was evaluated by spatially comparing LDW EFDC-simulated sources introduced at various locations, as described in Section 6.0. A linear least square fit, referred to as Inverse Modeling, of simulated unit source concentration distributions to measured concentration distributions was conducted for potential sediment bed sources and potential water surface sources. Section 7.0 describes the result and analysis of LDW characteristics, LDW EFDC unit source concentration distributions, and Inverse Modeling. Finally, a comparison of modeled and measured fluxes to known source information was completed in Section 8.0 to evaluate if modeled potential source contributions align with measured concentration distributions in the LDW.

2.0 Lower Duwamish Waterway Background

2.1 Physical Characteristics

Historically, the LDW was a naturally meandering estuary that flowed between the Green/Duwamish River in Tukwila, Washington and Elliott Bay in Seattle, Washington. The engineered navigation channel as it exists today was dredged in the early 1900s for commercial use. Waterway construction and subsequent industrial development between river mile (RM) 0, at Elliott Bay, and RM 5, the most upstream point of the LDW, resulted in the elimination of natural wetlands and mudflats in the immediate vicinity of the estuary (US EPA, 2014).

The navigation channel is maintained between 20 and 30 feet below mean lower low water (MLLW) by dredging every one to three years. For comparison, the waterway mouth at Elliott Bay can be as deep as 47 feet below MLLW, while the banks of the channel are much shallower and consist of sloped embankments, subtidal areas, or intertidal areas (US EPA, 2014). The LDW and Early Action Areas (EAAs, discussed in Section 2.3.2), are shown in Figure 1.

Average flow through the LDW is approximately 1,340 cubic feet per second (cfs), much less than historical flow rates. Rivers that historically discharged to the Green/Duwamish River were diverted around the same time as the navigation channel was dredged, decreasing the volume of water flowing through the LDW. Water volume was further decreased in 1961 when the Howard Hanson Dam began operation. A smaller volume of water combined with a larger cross-sectional area resulted in lower water velocities through the LDW. The reduced flow and lower velocities caused less erosion along the banks and more sediment deposition on the bed (US EPA, 2014).

As previously mentioned, the LDW is an estuary between the freshwater Green/Duwamish River and the saltwater Elliott Bay. Density differences between the freshwater and saltwater creates a two-layer effect in the LDW; less-dense freshwater flows at the water surface while more-dense saltwater flows at the waterway bottom. The interface of freshwater and saltwater is referred to as a "salt wedge," and it can move upstream and downstream as influenced by the tides and river flow. The wedge is always present between RM 0 and 2.2, sometimes present between RM 2.2 and 4, and has extended between RM 4 and 5 during extreme circumstances. During high river flow, the wedge forces freshwater to flow above saltwater, reducing sediment erosion and resuspension (US EPA, 2014).

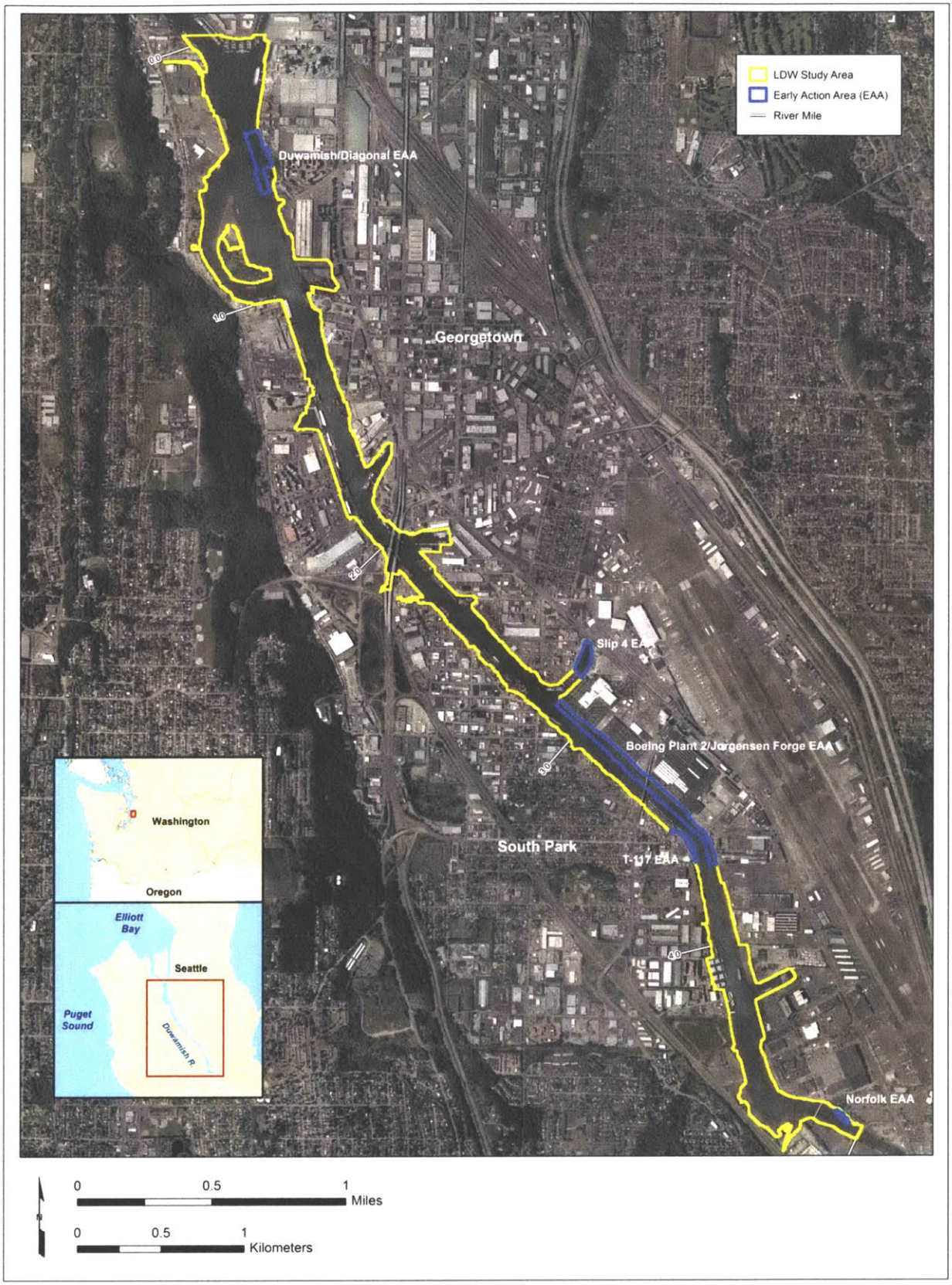

Figure 1: LDW Study Area and EAAs (US EPA, 2014)

2.2 Nature and Extent of Contamination

Supported by the construction of the waterway, the LDW and surrounding area transitioned from agricultural uses to a variety of industrial uses. Early industrialization included lumber, brick, and steel operations, in addition to marine-related construction. These industries grew and expanded to meet the growing demands of World War II (US EPA, 2014). A treatment facility opened in 1938 on Diagonal Way to manage the new sources of sanitary sewerage. Its outfall discharged into the LDW (Washington State Department of Ecology, 2004). Other solid and liquid waste disposal practices included landfills, soil infiltration, and direct disposal into the waterway itself (US EPA, 2014).

By 1955, the LDW transitioned again from industrial uses to manufacturing and storage operations, including cargo storage, metal manufacturing, petroleum storage, and various shipyard operations. A larger sanitary sewer system capable of serving boring sides of the LDW was constructed in the 1970s (US EPA, 2014). As a result, the Diagonal Way Treatment Plant ceased operations (Washington State Department of Ecology, 2004).

The history of industrial, manufacturing, and storage operations adjacent to the LDW led to the waterway impacts observed today. Heavy metals, polychlorinated biphenyls (PCBs), polycyclic aromatic hydrocarbons (PAHs), and other chemicals were used in daily industrial and manufacturing operations that have since been phased out. Inappropriate waste management practices (such as spills, leaks, and dumping), pipe discharges, overland flow, groundwater, and soil erosion carried these chemicals to the LDW, causing its contamination (US EPA, 2014). Sediment contamination remained in the LDW due to high sediment deposition and low resuspension, compounding the problem. In addition to historical management methods, combined sewer overflows (CSOs), industrial wastewater, waterway operations, in-waterway spills, atmospheric deposition, and the transport of contaminated sediments continue to contribute to contamination by causing new sources, creating new pathways, or by carrying historical contamination to the LDW (US EPA, 2014).

The Remedial Investigation and Feasibility (RI/FS) reports completed by Lower Duwamish Waterway Group (LDWG) reviewed data collected between 1990 and 2010 to evaluate the nature and extent of impacts in and around the LDW. Analyzed samples included surface and subsurface sediment samples, fish and shellfish tissue samples, surface water samples, seep samples, porewater samples, and toxicity tests where required by contamination levels. Concentrations of PCBs were detected throughout the surface and subsurface sediment. PCBs, in addition to arsenic,

PAHs, dioxins, and furans, were detected at greater than background concentrations in fish, shellfish, and benthic invertebrate tissue. High concentrations of PCBs, arsenic, and PAHs were also detected in surface water samples (US EPA, 2014).

To better understand how sediment, both contaminated and non-contaminated, travels through the LDW, the LDWG developed a sediment transport model (STM). The STM estimated more than 200,000 metric tons of sediment enters the LDW each year; 99% of this sediment is from upstream, non-impacted sources, while 1% is from potentially impacted storm drains, CSOs, and small streams. The flow through the LDW carries approximately 50% of the sediment to Elliott Bay, and 50% of the deposited sediment is dredged for navigation channel maintenance purposes. Therefore, 25% of the sediment that enters the LDW settles to its bed (US EPA, 2014). Approximately 1% of the deposited sediment originates from point sources and can have a much higher contaminant concentration than upstream, non-impacted sediment (US EPA, 2014). This can cause "hotspots" of concentrations near discharge locations. Further studies by Ecology have identified direct discharges and stormwater pathways as the highest remedial priorities, which are the focus of many of the Early Action Areas (EAA) described below (US EPA, 2014).

2.3 Remediation Efforts and Progress

2.3.1 Regulatory Agencies and Contributing Parties

The United States Environmental Protection Agency (EPA) and the Washington State Department of Ecology (Ecology) declared the LDW to be a high-priority study area in 1981 due to growing concerns about water quality and sediment contamination. Numerous studies were conducted on the LDW contamination, sources, and cleanup options in the 1980s. To reduce sewerage and stormwater inputs to the LDW, three sewer separation projects were constructed in the late 1980s and early 1990s. The Elliott Bay/Duwamish Restoration Program (EBDRP) was created in 1991 and required the City of Seattle (City) and King County to conduct restoration, remediation, and source control projects. Four restoration programs were completed by the EBDRP along the LDW in the early 2000s. Additional restoration projects were completed by the Port of Seattle (Port) in the late 1990s, which included removal of abandoned ships, excavation of fill soil, and reintroducing native marsh and vegetation (Lower Duwamish Waterway Group, n.d.).

In 2000, the Port, the City, King County, and the Boeing Company (Boeing) volunteered to investigate the contamination of LDW sediments and formed the Lower Duwamish Waterway Group (LDWG). Shortly after, the LDW was placed on the EPA's National Priority List and on Ecology's Hazardous Sites List. In 2003, the LDWG proposed seven EAAs to focus early remediation

efforts on (Lower Duwamish Waterway Group, n.d.). EPA and Ecology selected five of the proposed EAAs; Once all EAAs have been remediated, the PCB weighted average concentration in surface sediment will be reduced by about 50% (US EPA, 2014).

The LDWG investigation culminated in a RI submitted to the EPA in 2010 and a FS submitted to the EPA in 2012. Together, the RI/FS documents describe what is known about the LDW and evaluate remedial alternatives. This includes its history, sediment transport processes, contamination nature and extent, potential historical and ongoing sources, source control identification and strategy, and human and environment risk assessments (Windward Environmental, LLC, 2010) (AECOM, 2012). With this information, the EPA issued a proposed cleanup plan in 2013 identifying its preferred remedial alternative. After public comment and Ecology agreement, EPA issued its Record of Decision (ROD) in 2014 (AECOM, 2012). The ROD outlines the strategy for in-waterway remediation, including specific Remedial Action Objections, sediment cleanup objectives (SCOs), and cleanup screening levels (CSLs) (US EPA, 2014). In-waterway remediation will address the levels of contamination detected in sediment, surface water, and in-water organisms and will commence after the completion of EAA remediation and source control, described in the following sections.

2.3.2 Early Action Areas

2.3.2.1 Norfolk CSO/SD

A 1991 Consent Decree between the City of Seattle (the City) and King County with the National Oceanic and Atmospheric Association spurred the remediation of the Norfolk CSO/storm drain (SD) EAA, located at the south end of the LDW. The Norfolk CSO is part of the King County wastewater system, and sediments near its outfall contained mercury, bis(2-ethylehexyl)phthalate (BEHP), and PCBs at high concentrations. Between February 1999 and March 1999, approximately 5,190 cubic yards (CY) of sediment was dredged to an average depth of two to three feet (King County, 2016). This area was then backfilled, capped, and monitored for 5 years following remediation to ensure recontamination by phthalates would not occur (King County Department of Natural Resources, 2005). Remediation efforts were shared between EPA, Ecology, King County, and the City.

Following dredging in 1999, evidence of recontamination on the sediment cap was observed. Higher than expected concentrations of PCBs were measured near the Boeing SD outfall in 2000. A sediment characterization in June 2002 verified these results and identified the Boeing SD outfall to be the most likely source of recontamination. Though PCB concentrations in the area decreased during the 2002 and 2003 monitoring events, Boeing subsequently extracted 60 CY of impacted

sediments from the area of the SD outfall in September 2003. An increase in PCB concentrations in two sampling stations was measured post-remediation; however, the detections appeared to be residual concentrations and were not a result of recontamination due to the Norfolk CSO (King County Department of Natural Resources, 2005). The project is considered complete and the EPA will review the EAA as part of the ROD conditions to ensure the work completed meets current remediation goals (US EPA, 2014) .

2.3.2.2 Duwamish/Diagonal CSO/SD

As part of the same Consent Decree, four outfalls between Harbor Island and Kellogg Island were identified by the City, King County, and NOAA for a separate remediation effort conducted by EPA, Ecology, King County, and the City. The Diagonal Way SD, the Duwamish CSO, the Diagonal Avenue South SD, and the former Diagonal Way Treatment Plant outfall impacted an area of seven acres within the northern portion of the LDW (US EPA, 2014). Between November 2003 and January 2004, approximately 68,000 CY of sediment was dredged to a maximum depth of five feet. A cap consisting of 75,000 CY of material was constructed between January and March 2004 to isolate the remaining sediment and encourage salmon foraging (EcoChem, Inc., Anchor Environmental, LLC, 2005).

During large dredging projects, some residual sediment is expected to migrate outside of the remediation area. However, during post-construction sampling, an area of approximately 4 acres to the southeast of the remediation boundary contained higher concentrations of residual PCBs than the areas to the northeast. Poor management practices during the initial phases of dredging released enough sediment to cause concentration buildup outside of the remediation boundary. King County placed an average of 9 inches of clean sand over this area in February 2005 as a method of Enhanced Natural Recovery (ENR) (Anchor Environmental, LLC, 2007).

The final post-construction monitoring events occurred in 2011 and 2012, over 5 years after the ENR remediation. While some chemicals still exceeded sediment quality standards (SQS) and/or CSLs, such as PCBs, BEHP, and PAHs, many exceedances were determined to likely be transient due to changes in sediment chemistry and discharge influences from nearby outfalls (King County Water and Land Resources Division, 2016). Along with the Norfolk County CSO/SD project, the Duwamish/Diagonal CSO/SD remediation is complete and will be reviewed by the EPA as part of the ROD conditions (US EPA, 2014).

2.3.2.3 Slip 4

The City and King County entered an Administrative Settlement Agreement and Order on Consent with the EPA to enable the remediation of sediments within Slip 4, located at the approximate middle of the LDW on the east bank. Six active outfalls discharge to Slip 4: the I-5 SD, the Georgetown SD, the King Country International Airport SD No. 3 and PS44 emergency overflow, and two private outfalls (Windward Environmental, LLC, 2017).

Prior to in-slip remediation, source control actions at the Georgetown Steam Plant (GTSP) and North Boeing Field (NBF) were required. GTSP was originally constructed next to the Duwamish River in 1906 to provide power during periods of high electricity use. It was most recently operated by the City between 1951 and 1973 and is now a National Historic Landmark. An open-air flume was constructed in 1913, when the straightened navigation channel was constructed, to carry cooling water to Slip 4. In 2009, this flume was cleaned, disposed, and replaced with a closed pipe to reduce potential contamination entering Slip 4. In addition, two soil removal events were conducted in 1985 and 2006 by the City. Accessible PCB impacted soil was excavated from low-elevation areas where runoff and sediment historically pooled near the GTSP (Washington State Department of Ecology, n.d.).

NBF is owned by King County and has been operated by Boeing since the 1940s for aircraft and aerospace manufacturing, maintenance, and research. In 2011, additional accessible PCB and petroleum impacted soil between NB and GTSP was excavated from low-elevation areas or capped to prevent off-property migration to Slip 4. To further reduce the volume of sediments leaving the site and entering Slip 4, Boeing installed a stormwater treatment system in 2011 and cleaned, repaired, and/or replaced many storm drains located on the north end of the property. Boeing is continuing to remove PCB impacted building materials and surface debris in compliance with TSCA regulations (Washington State Department of Ecology, n.d.).

In 2011 and 2012, 3.4 acres of Slip 4 were dredged or excavated, resulting in the disposal of 10,250 CY of sediment and bank soil with associated impacted debris, timber, piles, and concrete pier structures. Engineered soil caps and an expanded natural habitat were constructed in its place using 53,000 tons of material (Windward Environmental, LLC, 2017). During post-construction monitoring in 2012, elevated concentrations of PCBs were detected in the surface sediment outside the delineated EAA, but within the Slip 4 monitoring area. EPA approved the placement of a 9-inch cap as a method of isolating the impacted sediment, which was installed in 2012 (Integral Consulting, Inc., 2015).

The most recent post-construction sampling event conducted in 2015 indicated concentrations at five sampling stations exceeded one or more SQS or CSL, typically for PCBS, BEHP, and/or benzyl alcohol. Identified potential sources included vessel propwash-induced resuspension from active piers, tidal fluctuations, additional dredging, and storm drain outflows. As source control efforts are ongoing in Slip 4 and in the LDW, impacted sediment will continue to deposit and will be measured in long-term monitoring (Integral Consulting, Inc., 2015).

While outside of the Slip 4 EAA, Boeing dredged and backfilled the southern area of Slip 4 under a RCRA Administrative Order on Consent. Construction was completed in 2015, and post-construction sampling events in 2015 and 2016 indicated PCB concentrations were below SCO (Windward Environmental, LLC, 2017).

2.3.2.4 Terminal 117

Terminal 117 (T-117) was historically an asphalt production plant, primarily for roofing shingles, on the west bank of the LDW near RM 3.5. Prior to the non-time critical removal action (NTCRA) associated with the EAA, two time-critical removal actions (TCRA) and two independent cleanups. The first TCRA was conducted by the Port in 1999. Per an EPA Consent Order, approximately 2,100 tons of accessible PCB impacted soil was removed while inaccessible soil was capped. Some impacted soil was left *in-situ* as required for building stability. This soil became accessible in 2006 and approximately 3,100 tons of PCB impacted soil removed in a second TCRA. The area was subsequently backfilled and capped with asphalt. Two independent cleanups were conducted between 2004 and 2005 which involved the removal of petroleum-impacted soil from a below-grade utility corridor, a boat storage yard, a roadway, and residential yards (US EPA, 2010).

The T-117 EAA was divided into three areas to facilitate remediation: Sediment/Upland area, Residential Yards area, and Streets/Stormwater area. The Residential Yards area was completed in March 2013 and consisted of removing impacted sod and vegetation, excavating and disposing impacted soil and debris, placing clean backfill and topsoil, and restoring landscaping. This work resulted in approximately 2,300 tons of soil excavated from 8 residential properties, nearby planting strips, and an alleyway (Integral Consulting, LLC, 2013).

Following the completion of the Residential Yards area, construction of the Sediment/Upland began. Between March 2013 and January 2015, approximately 76,000 tons of soil and debris and 22,000 tons of sediment and in-water debris were removed. Excavated areas were backfilled and restored pre-construction grade (in-waterway) or below pre-construction grade (upland). During

construction, five underground storage tanks (USTs) were removed and approximately 4.8 million gallons of project-related water was treated in an on-site water treatment facility (AECOM, 2016).

The Street/Stormwater area began construction in July 2015 and involved the installation of new stormwater structures within the T-117 streets/neighborhood. Installation required the demolition and removal of pavement, removal and disposal of 28,300 tons of soil, backfilling excavations with clean materials, and restoring and improving paving and landscaping. A temporary water storage facility was used to collect, treat, and store water generated during construction. Construction finished in the Street/Stormwater area in August 2016, completing the T-117 remediation (Integral Consulting, LLC, 2017).

2.3.2.5 Boeing Plant 2/Jorgenson Forge

Although treated as one EAA, Boeing Plant 2 and Jorgenson Forge are treated as two cleanup actions. A 1994 RCRA Consent Order is controlling remediation at Boeing Plant 2. Sediment remediation at Jorgenson Forge is controlled by the EPA (under a 2012 CERCLA Removal Consent Order) while Ecology (most recently a 2017 Agreed Order) controls on-land remediation efforts (US EPA, 2014). The EAA is located to the south of Slip 4 on the east bank of the LDW.

Boeing Plant 2 historically operated as a major aircraft manufacturing facility and is now classified as a RCRA hazardous waste facility. Under the RCRA Consent Order, Boeing removed contaminated joint caulk, cleaned impacted storm drains, removed or treated contaminated soil and groundwater, and ultimately demolishing the Plant 2 building between 2010 and 2012 (US EPA, 2018) (Boeing, n.d.). Between 2013 and 2015, Boeing dredged and removed approximately 265,000 CY of contaminated sediments and bank soil along the waterfront (Boeing, n.d.). This was followed by a mile-long habitat restoration project to reintroduce native wetland plants to the waterfront and provide a habitat for in-waterway fish and land species (Boeing, n.d.). In addition to monitoring the in-waterway work for recontamination, Boeing is continually completing upland remediation, such as the installation of stormwater treatment systems or soil/groundwater treatment, to control ongoing sources of contamination to the LDW (US EPA, 2018).

Jorgenson Forge borders the Boeing Plant 2 site and has housed heavy industrial uses since the 1940s, including fabrication of structural steel, tractors and road equipment, manufacturing of large-scale aircraft and marine parts, and processing of nickel, titanium, and specialized alloys (Washington State Department of Ecology, n.d.). Remediation has been required by both the EPA and Ecology, but sediment remediation has only been completed to some extent under the 2012 CERCLA Consent Order. The EPA required the previous land owner, Earle M Jorgenson (EMJ), to

remove impacted sediments and bank material in 2014. The excavated area was replaced with clean backfill; however, post-construction sampling indicated the impacted sediment left in place exceeded the appropriate cleanup levels. EMJ conducted additional sampling between 2015 and 2016 with the same results. The EPA is requiring EMJ to prepare an Engineering Evaluation/Cost Analysis to address the remaining PCB contamination (US EPA, 2017).

On-land remediation was initialized in 2007 under an Agreed Order between the most recent land owner, Jorgenson Forge Corporation (JFC), and Ecology. The Order was amended in 2013 and required JFC to investigate sources migrating from the property to the LDW sediments and waterway and conduct an interim cleanup action. After the requirements were met in 2014, Ecology issued an Enforcement Order to JFC to further investigate and develop and cleanup action plan for the property. JFC subsequently filed bankruptcy in 2016. A new Agreed Order between former land owner EMJ and Ecology was agreed upon in 2017 and will result in a RI/FS with a draft cleanup plan to initiate remedial efforts (Washington State Department of Ecology, n.d.).

2.3.3 Source Control

Concurrently with EAA remediation, Ecology identified 24 non-waterway source areas that contributed to surface water and sediment contamination in the LDW. Contamination from source areas must be controlled (i.e., removed or reduced to the extent possible) prior to in-waterway remediation to minimize the risk of recontamination during and post-waterway remediation. Source control will be prioritized in upriver locations, followed by mid-reach locations and downriver locations. This reduces the risk of recontamination of remediated downstream areas by un-remediated upstream areas (Washington State Department of Ecology, n.d.).

Of the 20,400 acres that ultimately discharge to the LDM, approximately half of this area is considered a source area. Contamination from these areas follow specific pathways to the LDW, such as through CSOs, surface runoff, and groundwater discharges, shown in Figure 2. Source control can be completed by either removing the pathway between the source and the LDW or by removing the source altogether. Removing one of these aspects will prevent continued contamination to the LDW and will allow in-waterway cleanup to begin (Washington State Department of Ecology and Leidos, 2016).

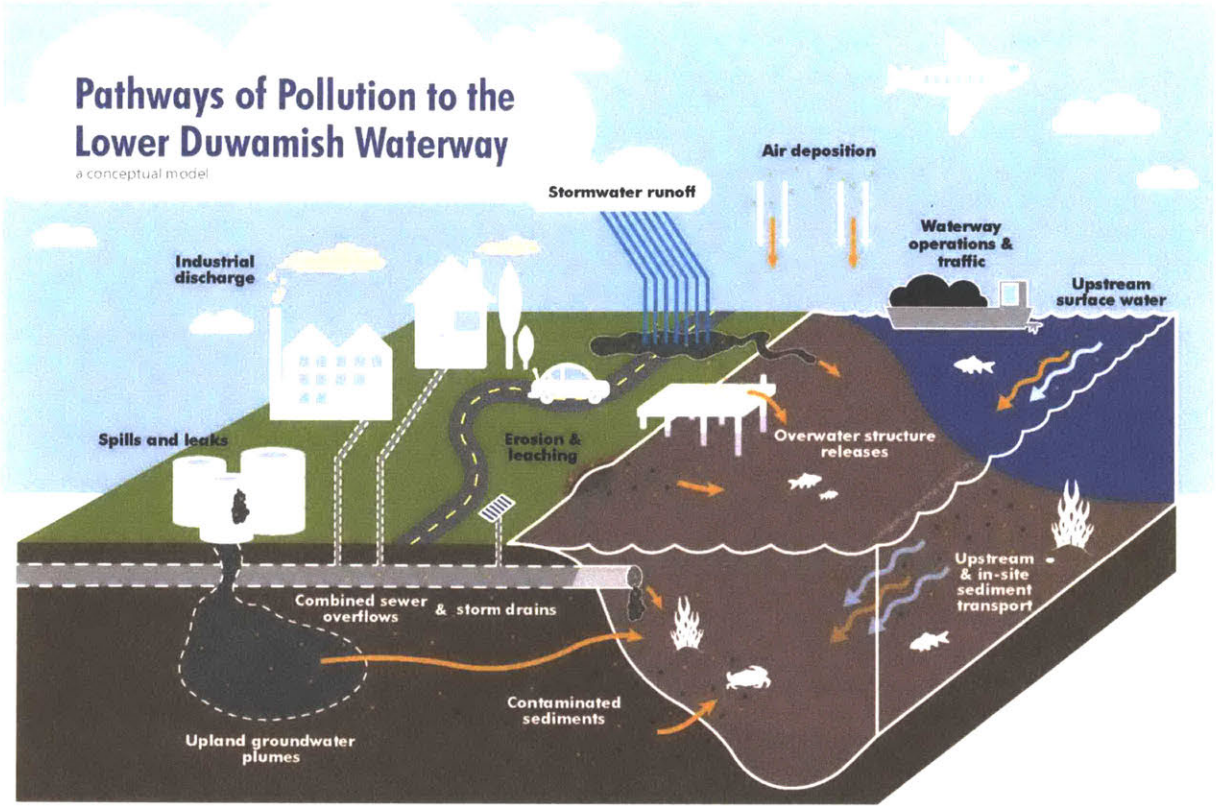

Figure 2: Pathways of Pollution to the LDW (Washington State Department of Ecology and Leidos, 2016)

Ecology is working with the City, King County, and EPA to create and enforce Source Control Action Plans (for each source area) and Source Control Implementation Plans (for each regulatory agency). Ecology is the lead agency for direct discharge properties and upland contaminated properties; the City is the lead agency for their storm drain system; King County is the lead for wastewater or CSO systems; and EPA provides technical assistance and coordination with their on-going sediment investigations and cleanups (Washington State Department of Ecology, n.d.). In addition to these agencies, local agencies and associated regulations will manage and enable remediation within the source control areas. At the completion of source control area remediation, Ecology will evaluate the work done and determine if chemical concentrations were reduced enough to facilitate in-waterway sediment remediation in the LDW. If the work is deemed sufficient, a monitoring and sampling program will be enforced to evaluate the effectiveness of the source area remediation and reduce the risk of recontamination (Washington State Department of Ecology and Leidos, 2016).

2.3.4 In-Waterway Remediation

The Final ROD, issued by EPA in 2014, outlined the in-waterway remediation strategy for the LDW. Approximately 177 acres will undergo active cleanup and remediation using one of the following methods:

1. Dredge (or partially dredge) and engineered sediment cap (105 acres): These areas contain highly contaminated sediments that have the potential for erosion, that must maintain a specific water depth, that must be compatible with current or anticipated human use, and/or must maintain its fish and wildlife habitat. EAAs will address an additional 29 acres for a total of 134 acres dredged and capped.
2. Engineered sediment caps (24 acres): These areas contain highly contaminated sediments and sufficient water depth to engineer a 3 to 4 feet sediment cap without disrupting human use.
3. Enhanced natural recovery (48 acres): These areas are less contaminated than those listed above, but still require 6-9 inches of clean material to provide a new surface of clean sediments. The clean sediment mixes with underlying contaminated sediment and reduces contaminant concentrations faster than natural processes. These areas may include *in-situ* treatment with activated carbon to further enhance the natural degradation of contaminants.

Location-specific plans will be developed to address areas with structural or access restrictions, such as piers, bulkheads, and engineered shorelines. In addition to active cleanup, approximately 235 acres will undergo Monitored Natural Recovery (MNR). These areas are less contaminated than those undergoing active cleanup and are located such that deposition of cleaner, upstream sediments will reduce surface sediment concentrations and bury contaminated sediment. MNR areas are divided into two subsets based on its initial chemical concentrations: areas that exceed the SCO are categorized MNR to benthic SCO, while areas that are below the SCO but above sediment cleanup levels for human health are categorized as MNR below benthic SCO. Long-term monitoring of the top 10 cm of surface sediments will be conducted to confirm concentrations are decreasing over time and re-evaluate the remediation if necessary (US EPA, 2014).

Additional sampling and monitoring will be conducted throughout the LDW as part of baseline, construction, post-construction, and long-term evaluations. As in-waterway remediation is completed, institutional controls will be introduced to reduce human exposure to remaining contaminants and to ensure the remedy is in-tact and effective. These controls can include land use

restrictions, seafood consumption advisories, and in-waterway cap protections. Community outreach about the current waterway condition, conducted remediation, and post-remediation conditions will educate the surrounding community and reduce the reliance on institutional controls (US EPA, 2014).

3.0 Environmental Fluid Dynamics Code

3.1 Background

The Environmental Fluid Dynamics Code (EFDC) is a public domain software which models flow, transport, and biogeochemical processes in 3D surface water systems. The model was originally developed by the Virginia Institute of Marine Sciences and has since been supported by the EPA for use by university, government, and consulting organizations. EFDC numerically solves the equations of motion and coupled transport equations for a variable-density fluid over a horizontal and vertical coordinate system. The model supports Cartesian horizontal coordinates, curvilinear-orthogonal horizontal coordinates, stretched vertical coordinates, and sigma vertical coordinates; users creating the model select which coordinate system aligns with their goals and the physical characteristics of the surface water body. This enables EFDC to simulate sediment transport, dilution fields from multiple source, fate and transport of dissolved or sorbed contaminants, and a variety of nutrient processes through complicated surface water systems (Dynamic Solutions International, LLC, EFDC Explorer, 2016).

Sediment fate and transport can be incorporated into the model, including cohesive, non-cohesive, and variable size sediments. Users can define multiple size classes and specify options for settling velocities. A separate flocculation model can be activated to appropriately model cohesive sediment. EFDC can also enable a multiple-bed layer option to reflect how the bed elevation changes as sediments settles (Dynamic Solutions International, LLC, EFDC Explorer, 2016).

Two internal sub-models simulate toxic contaminant fate and transport. The first sub-model resolves dissolved and sorbed sediment transport and computes mass per unit area in the sediment bed of a single contaminant. This factors in contaminant-specific equilibrium partitioning and first-order reactions. The second sub-model can simulate multiple dissolved or sorbed contaminants with a numerical-transport model that has improved accuracy over other models. The second sub-model improves on the first sub-model by modeling sorption between dissolved and sorbed phases as either equilibrium or nonlinear processes. In addition, contaminants in the second sub-model can re-enter the water column via sediment resuspension, porewater diffusion, and porewater expulsion, altering the contaminant distribution in the water column (Dynamic Solutions International, LLC, EFDC Explorer, 2016).

Within EFDC, an integrated hydrodynamic eutrophication model spatially and temporarily resolves water quality parameters and various nutrient cycles, such as dissolved oxygen, algae, and fecal

coliform bacteria. The eutrophication model was developed by coupling a water quality model consisting of 21 state variables with a sediment model consisting of 27 state variables to predict long-term water quality parameters and their response to varied nutrient loadings (Dynamic Solutions International, LLC, EFDC Explorer, 2016).

In tidally-influenced estuaries, areas exist that may flood or drain as the tide changes, such as discharge control structures or naturally shallow areas. If wetting and drying cycles area not accommodated within the model, negative concentrations of dissolved and sorbed materials may arise in these areas. EFDC couples the mass transport equations with a wetting/drying scheme to allow for proper submerging and emerging within tidally influenced estuaries, such as the LDW (Dynamic Solutions International, LLC, EFDC Explorer, 2016).

An EFDC model was developed for the LDW, referred to as the LDW EFDC model, and is described in Section 3.2. This work assumes PCBs are conservative in the LDW and does not use the full capabilities of EFDC described above. Instead, the model provided the hydrodynamics of the LDW and simulated the movement of a conservative tracer.

3.2 LDW EFDC Model

The LDW EFDC model was initially developed by King County in 1999 to use as a mass balance and to evaluate CSO chemical loadings. The mass balance allowed King County to estimate the amount of unattributed chemical contributions to the LDW given known CSO, ambient, and boundary contributions. Further, King County simulated concentration distributions if CSOs were removed as a source and determined how removing CSOs would impact risks to human health, wildlife, and aquatic life (King County, 1999). The LDW EFDC model was updated by King County in 2006 for use in the RI/FS phase of superfund remediation (Prendergast et al., 2018).

Elliott Bay, the LDW, and a 7-mile upriver section are represented in the LDW EFDC model with a curvilinear-orthogonal horizontal grid with stretched-sigma vertical layers. The LDW portion of the model, as shown in Figure 3, was built with 115 cells, consisting of 35 longitudinal cells, at least three lateral cells. Within each cell, 20 evenly spaced vertical layers are placed between the water surface and sediment bed (Prendergast et al., 2018). The average cell area in this section is 240 meters long by 60 meters wide, while cell thickness varies with total water depth due to the evenly spaced vertical layers. A maximum time step of 2 seconds is incorporated into the model to prevent negative cell depths and concentrations (Prendergast et al., 2018).

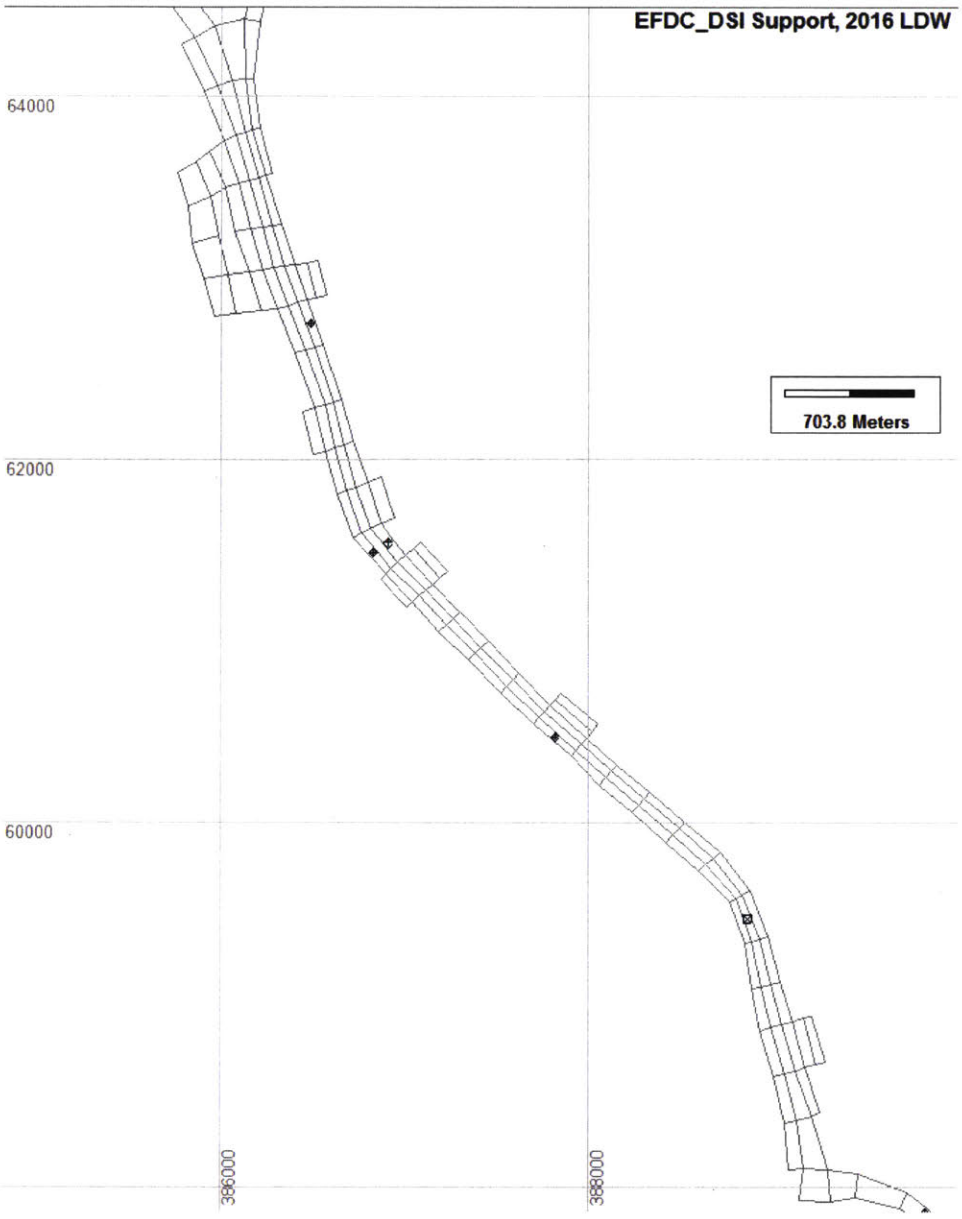

Figure 3: Two-Dimensional Map of the LDW Generated in EFDC

Boundary conditions were updated by Massachusetts Institute of Technology (MIT) for the summer of 2014 and again for the summer of 2016. This included updating the tidal forcing at the west end of Elliott Bay, updating Green River discharge rates from upriver locations, matching LDW bathymetry from surveys conducted in 2003, and calculating stormwater outfall flow with a runoff model and rainfall data (Prendergast et al., 2018).

3.2.1 Calibration and Validation

LDW EFDC model calibration and validation was completed as part of a separate modeling exercise in 2016 (Prendergast et al., 2018); the following is a summary of that process. Calibration was

completed by adjusting model water levels to match gauged water levels near the Seattle Pier, located approximately 1 mile north of Harbor Island. Validation was completed by comparing various measured water quality and physical parameters to the model results. Acoustic doppler current profiler (ADCP) profiles were collected to evaluate velocities in the water column, which were supplemented by conductivity, temperature, and depth measurements. Modeled depths were accurate within 0.5 m of measured depths; modeled velocities were accurate within 0.4 m/s of measured velocities; and modeled salinity was within 0.3 practical salinity units (PSU) of measured salinity for most areas (Prendergast et al., 2018).

However, it was noted that the model tends to soften the vertical salinity gradient when compared to the measured salinity gradient. This was attributed to insufficient resolution of the vertical grid, which resulted in somewhat higher vertical diffusion in the model than in the estuary (Prendergast et al., 2018). The sigma coordinate is not exactly horizontal due to the bathymetry of the LDW, and the overmixing is an artifact of the numerical coordinate system.

4.0 Massachusetts Institute of Technology's Role

Since MIT became involved with research efforts, it has particularly focused on *in-situ* passive sampling and source identification. The LDW is a suitable candidate for research because it is somewhat idealized (it is a mostly straight channel with a relatively uniform cross-section) and has been well-characterized. Observations in the field can be compared with theoretical equations for evaluate if what is observed aligns with what is expected.

Sampling efforts were conducted by MIT in the LDW in 2012, 2014, and 2016, followed by data analysis, EFDC model calibration, and various evaluations. Ultimately, the projects study where the LDW is contaminated, evaluate potential source fluxes, and attempt to identify source locations. Selected projects are summarized in the following sections.

4.1 *In-situ* Polyethylene Passive Sampling

At many sites impacted by halogenated organic compounds (HOCs), the transport of HOCs from contaminated sediment to the impacted water body is modeled using porewater concentrations. Traditionally, porewater concentrations are estimated by measuring sediment concentrations and applying an estimated sorption coefficient derived from the equilibrium partitioning theory. However, polyethylene (PE) samplers placed in the sediment can directly measure the porewater concentration without specific knowledge of sorption properties. This theory was tested in 2012 to measure PCB porewater concentrations within the LDW (Apell & Gschwend, 2016).

Prior to *in-situ* deployment, PE strips were cleaned and loaded with performance reference compounds (PRCs). The PRCs were selected and loaded to a concentration that would match the retardation factors of the PCBs, such that the PCBs would diffuse onto the PE sampler at the same rate as the PRCs would diffuse out of the PE sampler. If the concentration of PCBs on the PE samplers did not reach equilibrium at the end of sampling time, the measured loss of PRCs from the PE strip could then be used to adjust measured PCB concentrations (Apell & Gschwend, 2014). After the PE strips were loaded with PRCs, they were mounted to aluminum frames and deployed into the sediments of the LDW by MIT. After several weeks of *in-situ* equilibration, the PE samplers were removed and taken to a laboratory for processing before transport back to MIT (Apell & Gschwend, 2016)

At the time of PE sampler deployment, sediment cores were collected near deployment locations and were homogenized in glass jars. The core samples would undergo an *ex-situ* sampling process to evaluate the effectiveness of *in-situ* PE sampling. The same PE strips were placed in the sediment

jars and the jars were tumbled for the duration of *in-situ* sampling. When sampling was completed, the *ex-situ* PE strips were extracted and processed in the same manner as *in-situ* PE strips to ensure a fair comparison (Apell & Gschwend, 2016).

In-situ passive PE samples and *ex-situ* active PE samples generally agreed within a factor of two, with *in-situ* concentrations generally lower that *ex-situ* concentrations. While *ex-situ* porewater concentration may be preferred as a conservative estimate of contamination levels, it may not accurately represent the freely-dissolved concentrations, leading to overestimation of bed fluxes and bioaccumulation in benthic species. *In-situ* passive samplers detected individual HOCs over a range of properties at picogram per liter (pg/L) concentrations, providing information about the fate and transport of HOCs that may not have been detected before (Apell & Gschwend, 2016).

4.2 Diffusive Sediment-Water Flux

In-situ PE samplers were deployed again in 2014 to evaluate if the molecular diffusive flux from the sediment bed is the primary source of PCB contamination in the water column. PE samplers were prepared in the same method described in Section 4.1 and were deployed *in-situ* (to target freely dissolved concentrations) or buoyed 1m above the sediment bed (to target water column concentrations) by MIT in 2014. Samplers were deployed between July 21-23, 2014 and recovered between October 6-8, 2014 (Prendergast et al., 2018).

During deployment, ADCP measurements were taken to characterize the diffusive boundary layer along the LDW bed. The measured boundary layer thickness and fitted shear velocities were used to calibrate a mass transfer coefficient and congener-specific PCB fluxes between the bed and water column. Significant spatial heterogeneity of PCB fluxes was revealed, as were three hotspots. Outside these hotspots, the net PCB flux was generally into the water column in the downstream half of the LDW, while the net PCB flux was generally into the sediment bed in the upstream half of the LDW. Calculated upward flux was generally composed of lighter PCBs, while the heavier PCBs appeared to have reached near-equilibrium along the sediment bed. The area-weighted diffusive flux for the sum of 20 PCBs was approximately 130 ng/m^2/day (Prendergast et al., 2018).

Individually calculated fluxes were used as boundary conditions in the EFDC model to simulate water column concentrations due to diffusive mass input from the sediment bed. When compared to the water column concentrations, as measured by PE samplers buoyed above the sediment bed, the modeled water column concentrations were an order of magnitude lower. A full mass balance of individual congeners considering the diffusive flux, residence times, and water column

concentrations confirmed additional modeled sources were needed to match the measured water column concentrations. Suggested sources to investigate include bioirrigation, which could influence the release of light congeners, and resuspension of contaminated sediments, which could allow heavy congeners to desorb into the water column (Prendergast et al., 2018).

4.3 Air-Water Exchange

During the RI phase, concerns arose that continuous low-level sources of contamination could compromise the long-term remediation of the LDW. Air-water exchange was identified as a potential pathway for PCBs in the LDW, and King County later recognized it as a knowledge gap. To evaluate if air-water exchange was a significant source or sink of PCBs, MIT deployed PE samplers in the surface water and in the air approximately 1 m above high tide in 2015. The measured PCB concentrations in air and surface water facilitated calculations of the magnitude and direction of air-water exchange (Apell & Gschwend, 2017).

PE samplers were prepared as described in Section 4.1, with one exception: thicker PE was used in air samplers to allow for higher detection limits of lighter PCBs which may approach equilibrium during sampling time. Estimated transfer velocities of PCBs in air and water were applied to the measured concentrations of freely dissolved PCBs in air and surface water to estimate the flux magnitude and direction. Calculated fugacity ratios of surface water to air indicated the net transport of dissolved PCBs was from water to air, so that the atmosphere was a sink of PCBs in the LDW. The difference between the air water exchange flux (68 ng/m^2/day) and the reported wet and dry depositional flux (5.5 ng/m^2/day) resulted in an approximate net flux of 62.5 ng/m^2/day from the water to the air (Apell & Gschwend, 2017).

As the atmosphere was no longer considered a source to the LDW, the LDW had to be considered a source of contamination to the atmosphere. The contribution of the LDW to atmospheric PCB impacts was calculated using a conservative residence time of air above the LDW (1 day), the volume of the LDW, the calculated air-water exchange flux, and the measured surface water concentrations. The expected sum of PCB air concentrations from the LDW was calculated to be less than 12% of measured atmospheric PCBs. As such, other sources, such as consumer products, were determined to be contributing more to the PCB contamination in the atmosphere than the LDW (Apell & Gschwend, 2017).

4.4 Inverse Model Source Identification

One of MIT's main objectives is to trace the sources of contamination in the LDW by developing a method to fit possible source locations and strengths to the concentration distributions measured by the PE samplers. The first effort to do so was executed in 2017 (Prendergast, 2017); a second parallel effort is described as part of this thesis in Section 6.2. The LDW EFDC model was used to simulate the transport of PCBs by introducing a dissolved-phase, conservative tracer with a unit loading at specified locations in the LDW. The resulting unit concentration distributions were weighted to fit the observed concentration distributions by least-squares fitting, referred to as inverse modeling. The number of potential source locations and the number of observations used to fit the data was chosen by the modeler. A visualization of the inverse modeling algorithm is provided as Figure 4.

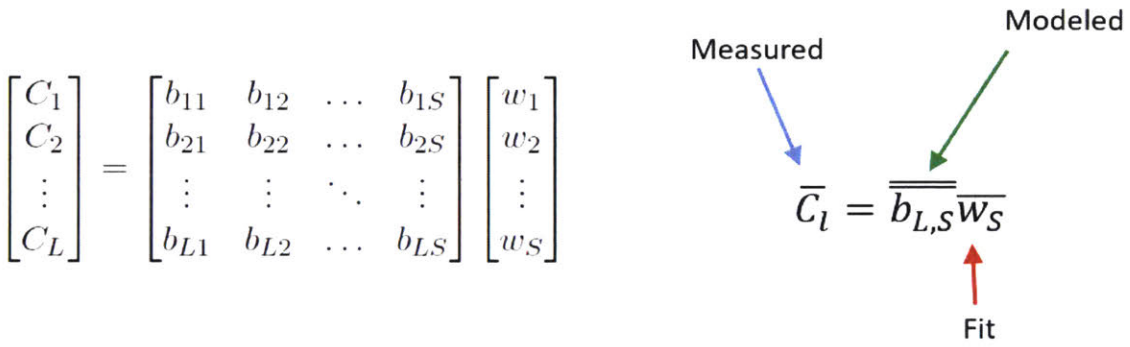

Figure 4: Inverse Modeling Schematic (Prendergast, 2017)

Following the completion of the 2014 *in-situ* bed and water column data analysis, it was determined more data would be required to adequately represent concentration distributions in the LDW. Specifically, only five water column samples were collected in the 2014 sampling efforts, which was determined to be an insufficient amount (Prendergast, 2017). Additional PE samplers were deployed by MIT in 2016 using the same method as described in Section 4.1, focusing particularly on water column samples. When analyzed, the 2016 data will be input to the inverse modeling technique; until then, the 2014 dataset, which measured freely dissolved bed concentrations at 19 locations and water column concentrations at five locations, was used to test the method.

The chosen number of potential source locations to model was 6, while the chosen number of measured concentrations was 5. This results in an underdetermined system with an infinite number of solutions because there are fewer known concentrations than unknown source strengths. The solution is determined by minimizing the weights (W) such that C=bW. Further

details of this process are provided in Section 6.24. Of the 19 locations measured in the 2014 dataset, every combination of 6 source locations was considered. The inverse modeling focused on sediment bed source locations and predicted the magnitude and direction of sediment bed fluxes. An example of the flux predicted by inverse modeling compared to the measured flux is shown in Figure 5.

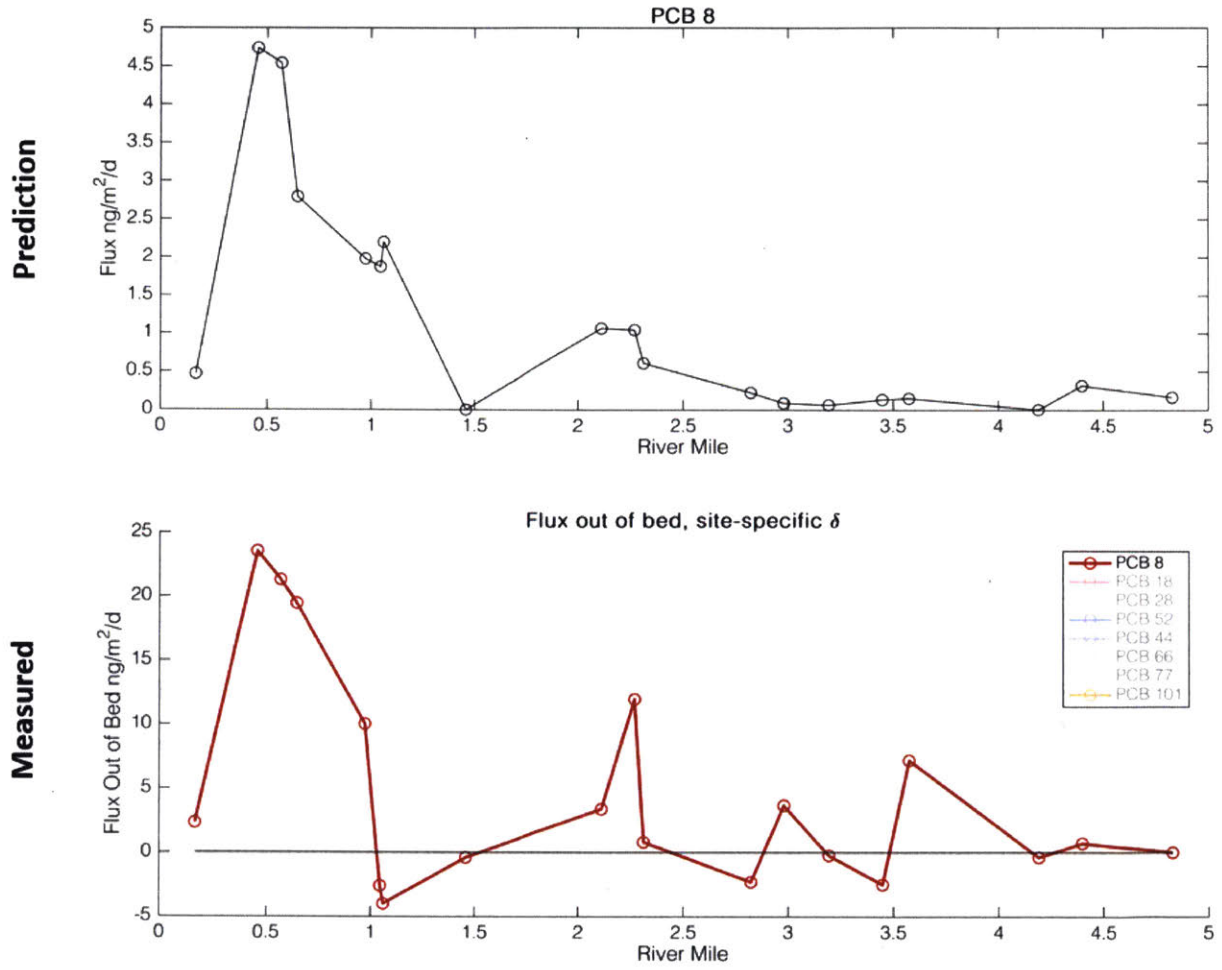

Figure 5: Predicted and Measured PCB-8 Flux Out of the Sediment Bed (Prendergast, 2017)

The inverse modeling technique generally predicted the direction and relative magnitudes of the flux at different source locations. However, the modeled flux magnitudes varied from the measured and calculated fluxes by a factor of 2 to 5. This further supported the conclusion that missing sources are contributing to concentration distributions within the LDW (Prendergast, 2017).

5.0 Focus of Present Thesis

PCB contamination in the LDW is widespread, as evidenced by historical investigations, on-going remediation, and MIT's research efforts. PE samplers have been proven to be an effective way to measure the freely dissolved PCB concentrations in the LDW porewater, sediment, and airspace. Potential sources of this contamination can be located in three dimensions within the LDW: laterally (left bank or right bank), vertically (water surface or river bed), and longitudinally (upstream or downstream). This work evaluates the combined use of modeling and passive sampling to understand contamination source locations to facilitate more economical remediation. The evaluation was completed in four stages:

1. Characterize the LDW using the LDW EFDC model. EFDC-simulated salinity gradients and conservative dye distributions were evaluated to determine estuary classification, salinity intrusion, flow patterns, and residence time.
2. Input conservative, continuous point sources at various locations in the LDW EFDC model. The resulting concentration distributions were evaluated and compared to each other to study how they could provide insight to the source location, and therefore, PE sampler location. One goal was to determine how far apart potential sources need to be in order to be "resolved" by measured concentrations or modeled concentrations.
3. Apply inverse modeling techniques to measured water column concentration measurements. Sources with distinguishable concentration signatures were included in the model to calculate the required fluxes to produce the measured concentration distribution.
4. Compare the modeled fluxes to previously studied fluxes (i.e., sediment diffusive flux) and known source information to evaluate if the modeled source contribution aligns with measured concentration distributions.

Related to Step 2 above, for this work, sources were considered distinguishable from each other if the resulting concentration distribution were significantly different. As measured concentrations will be collected *in-situ* with a PE passive sampler, significantly different was interpreted to be the measurement error for PE samplers, approximately 20% (Apell & Gschwend, 2016). Two source locations become indistinguishable at the location where the resulting concentration distributions fall within this range; therefore, a PE passive sampler placed in that area is unlikely to provide insight on the source origin. However, if a PE passive sampler is placed in an area with two distinguishable sources, the sampler may be able to provide insight on the source origin because the concentration distributions are distinguishable. Determining the distances at which PE passive

samplers are most effective will allow for more efficient sampling and a higher chance of source location identification.

As previously discussed, the LDW was selected for this study due to its idealized conditions and the availability of measured data. In a sense, the LDW is acting as a "laboratory" to study the effects of source location on concentration distribution and how it can guide source identification and remediation. This study approached the contamination in the LDW as if no prior knowledge of potential source locations exists. While measured data was available throughout the LDW, including sediment bed concentrations, only measured water column data and surface water data were considered to guide source identification. Ultimately, this method could be modified and applied to any contaminated site with an established hydrodynamic model and available measured data.

6.0 Method

The LDW EFDC model was the main computational tool used in this study. While the full capabilities described in Section 3.0 were not used, the model provided the hydrodynamics of the LDW and the concentration distribution of a conservation tracer. Following numerous simulations, Matlab was used to extract and process the data for further analysis. Matlab was selected for its ability to calculate time-average concentration distributions to compare to the time-average PE sampler concentrations. The method used for each computation tool is discussed further below.

6.1 LDW EFDC Method

The LDW EFDC model was calibrated and validated in 2016 for a previous modeling exercise, as described in Section 3.2. Within the model, the salinity and dye modules were activated for the current modeling exercises. The salinity module, in conjunction with the model's hydrodynamic capabilities, simulates the movement of saltwater and freshwater in the LDW. The model reflects a semi-diurnal tidal cycle of approximately 12.4 hours and a spring-neap cycle of approximately 14.7 days. After a simulating a period of one spring-neap cycle to "forget" initial conditions, the extent of salinity intrusion to the LDW was observed at typical high tide levels and typical low tide levels.

The dye module was activated to input a conservative, continuous, dissolved tracer at various locations in the LDW EFDC model. A unit loading of 1 mg/s, corresponding to a dye concentration of 0.1 mg/L and a flow rate of 0.01 m^3/s, was introduced at each chosen location in separate model simulations. The model hydrodynamics were not expected to be significantly altered by the low dye flow rate. Separate simulations of a unit loading were executed to facilitate direct comparisons of individual concentration distributions.

Simulated source locations were selected by RM to facilitate spatial comparison of time-averaged concentration distributions in one of the following categories. RM is measured upstream from the mouth of the LDW at Elliott Bay:

1. Comparison of east bank and west bank sources. A location always within the salt intrusion area (RM 0.5) and a location sometimes within the salt intrusion area (RM 3.7) were selected for this analysis. At each RM, sources were introduced at the bank surface or at the bank bed. A source introduced at the bank bed was generally introduced at a higher elevation than the bed of the LDW navigation channel; this is because the banks of the LDW are generally shallower than the navigation channel.

2. Comparison of surface and bed sources. A location always within the salt intrusion area (RM 1.0), a location mostly within the salt intrusion area (RM 2.3), and a location sometimes within the salt intrusion area (RM 4.1) were selected for this analysis. At each RM, sources were introduced at the centerline of the LDW, within the navigation channel.
3. Comparison of longitudinal source locations. The LDW was divided into 16 approximately equal segments. At the approximate center of each segment, dye was introduced at the bed or surface of the navigation channel.

A total of 44 EFDC model runs were completed, calculating elevation at each horizontal location and salinity and dye concentrations for each of the 115 grid cells in the LDW. The model simulated conditions between May 1, 2016 and July 1, 2016. Data simulated between May 1, 2016 at 00:00 and May 17, 2016 at 22:00 is considered the "warm-up" period to forget initial conditions, since this is considerably longer than the residence times of order 2 days. Output from this "warm-up" period was not considered. Model results were simulated between May 17, 2016 at 22:00 and July 1, 2016 at 00:00, representing approximately 3 spring-neap cycles. As discussed in Section 4.1, PE samplers measure average, freely-dissolved concentrations in the LDW over a period of several weeks (Apell & Gschwend, 2016). Therefore, the simulated data must also be collected over a modeled period of several weeks to enable averaging and comparison to the PE sampler measurements.

6.2 Matlab Method

Calculations to characterize the LDW, estimate residence time, visualize concentration distributions, and locate potential source locations were executed in Matlab (version 2017b). The LDW EFDC model results were extracted and time-averaged over the simulation period. Data analysis focused on the centerline of the LDW, in the shipping channel, and was visualized with a "heat" map or with a simple line plot. Unless otherwise noted, time-averaged data was used for all calculations and visualizations.

6.2.1 Estuary Classification

The LDW is classified as a salt wedge estuary (US EPA, 2014). The LDW EFDC model outputs were used to evaluate this classification by calculating the Estuary Richardson number (R) (Fischer et al., 1979):

Equation 1: Estuary Richardson Number (R)

$$R = \frac{\Delta\rho_0 g Q_f}{\rho W {u_t}^3}$$

A typical density difference between salt water and fresh water ($\Delta\rho_0/\rho$) of 0.025 was used in the above calculation. The freshwater flow rate (Q_f) was taken to be the average tide-filtered discharge rate measured at USGS station 12113390, located approximately 3 miles southeast of the LDW, during the simulation time (United States Geological Survey, 2018). The root mean squared (RMS) tidal velocity (u_t) is required for this calculation due to the changing direction of tidal flow between high and low tides. RMS tidal velocity was estimated as a fraction of the tidal amplitude ($u_t=0.71u_{max}$). The width of the estuary (W) was taken to be the average width of the LDW calculated from the width of individual grid cells.

The Estuary Richardson number is a ratio of the potential and kinetic energy rates of the estuary. It provides insight to the degree of mixing within the LDW, which helps to predict the subsequent transport and mixing of contaminated materials (Fischer et al., 1979). It is important to note that the amount of upstream salinity intrusion constantly changes the salinity profile and that the Estuary Richardson number provides a typical classification without considering transition periods between tides.

6.2.2 Residence Time

To understand the movement of the tracer within the LDW, the dye residence time was determined for each input location. The residence time (τ) is the amount of time dye typically spends within the LDW, and is calculated for a continuous dye source by integrating dye concentration (C) over the volume of the LDW (V) and dividing by the mass flux of dye ($\dot{m}_{dye}$) (Hilton et al., 1998):

Equation 2: Residence Time

$$\tau = \frac{\int_0^V C\, dV}{\dot{m}_{dye}}$$

The volume of each grid cell was calculated with the length, width, and average depth, and the concentration of each grid cell was calculated as a depth-averaged, time-averaged concentration. The volume of dye in each cell was calculated by multiplying the cell volume by its concentration. Finally, the total dye volume was divided by the mass flux of dye (1 mg/s) to calculate residence time. This process was repeated for each dye input location; resulting residence times were averaged to determine typical residence times.

6.2.3 Typical Mixing Time

Typical mixing times were calculated for the LDW to determine if simulated concentration distributions were reasonable given the dimensions, river flow rate, and tidal forcing. The

evaluation focused on lateral and longitudinal mixing as significant vertical mixing was not anticipated. Freshwater at the surface of the LDW flows from the Green/Duwamish River towards Elliott Bay, while saltwater at the bottom of the LDW flows upstream. The resulting density stratification inhibits vertical mixing between the surface and bottom of the LDW, preventing sources from mixing over the salt wedge.

Lateral (transverse) mixing was evaluated by comparing the calculated transverse mixing time to the residence time calculated in Section 6.2.2. First, the tidal excursion ($2\xi_0$) was estimated from its relationship with the tidal prism (P_u) based on the modified tidal prism method. This method assumes the net mass transport over one tidal cycle is the mass contained in the tidal prism, so that the high tide volume of an upstream channel segment is equal to the low tide volume of the downstream segment (Ketchum, 1951). The length of each segment is the same, which provides the relationship between the tidal excursion and the tidal prism shown in Equation 3. The average cross-sectional area (A, 1,830,000 m^2), the tidal range ($2a_0$, 3.6 m), the average depth of the river (h, 7.7 m), and the width (W, 260 m) and length (L, 8050 m) of the LDW are also used in the derivation.

Equation 3: Tidal Prism

$$P_u = V_{high\ tide} - V_{low\ tide} = (2a_0)WL$$

$$2\xi_0 A = P_u$$

Equation 4: Tidal Excursion

$$2\xi_0 = \frac{(2a_0)L}{h}$$

A maximum tidal velocity (u_{max}) was calculated from the tidal excursion and tidal period (T_t, 1 day). This was used to estimate the average tidal velocity (u_t) and ultimately calculate the transverse mixing coefficient (E_T).

Equation 5: Maximum Tidal Velocity

$$u_{max} = \frac{2\pi\xi_0}{T_t}$$

Equation 6: Average Tidal Velocity

$$u_t = 0.71u_{max}$$

Equation 7: Transverse Mixing Coefficient

$$E_T = 0.6u_* h = 0.6(0.1u_t)h$$

Dimensional analysis was used to determine a typical transverse mixing time (t_{TM}) from the transverse mixing coefficient and the average width of the LDW (W). Only half of the width is considered in the below equation because sources originating from the east bank or west bank will migrate to the middle of the channel and then mix together.

Equation 8: Transverse Mixing Time

$$t_{TM} = \frac{(W/2)^2}{2E_T}$$

A typical longitudinal mixing time was not directly calculated; the tidally-influenced nature of the LDW causes flow in both directions which makes it difficult to calculate one mixing time. Instead, the longitudinal dispersion coefficient (E_L) was calculated from simulated data. The LDW EFDC simulations provided concentration profiles for 16 longitudinally distributed sources. From these profiles, the distance from a given source to where that source was indistinguishable from an adjacent source was estimated. This distinguishable distance (L_D) was compared to the tidal excursion to evaluate the influence of the tidal excursion on the longitudinal dispersion coefficient. The distinguishable distance was used to calculate the longitudinal dispersion coefficient.

Equation 9: Distinguishable Distance

$$L_D{}^2 = 2E_L \frac{T_t}{2}$$

Equation 10: Longitudinal Dispersion Coefficient

$$E_L = \frac{L_D{}^2}{T_t}$$

Half of the tidal period (T_t) was used in Equation 9 to calculate the dispersion that occurs before the tide changes from high to low.

6.2.4 Inverse Modeling

An inverse modeling procedure using least-squares fitting was completed to weigh the contributions of selected source locations to collected data. The procedure is parallel to the method described in Section 4.4 and included the potential for both sediment bed sources and water surface sources. Seven cases of potential source locations were for this analysis; all potential source locations were chosen at the center of the LDW. As the 2016 data is not available at the time of this evaluation, the inverse modeling focused on measured concentrations from the 5 water column PE samplers deployed at RMs 0.1, 0.5, 2.2, 4.3, and 4.8 in 2014 (Apell & Prendergast, 2015).

In addition, measured concentrations from the 3 water surface PE samplers deployed at RMs 0.9, 2.0, and 4.7 in 2015 were included for the final case (Apell & Gschwend, 2017).

1. Case A: Three locations (upstream sediment bed source, downstream sediment bed source, and downstream water surface source) were selected as potential sources for the 5 water column PE samplers deployed in 2014.
2. Case B: Three locations (upstream water surface source, downstream sediment bed source, and downstream water surface source) were selected as potential sources for the 5 water column PE samplers deployed in 2014.
3. Case C: Three locations (upstream, middle, and downstream sediment bed sources) were selected as potential sources for the 5 water column PE samplers deployed in 2014.
4. Case D: Three locations (two middle sediment bed sources and one upstream sediment bed source) were selected as potential sources for the 5 water column PE samplers deployed in 2014.
5. Case E: Four locations (upstream sediment bed source, upstream water surface source, downstream sediment bed source, and upstream water surface source) were selected as potential sources for the 5 water column PE samplers deployed in 2014.
6. Case F: Four locations (upstream sediment bed source, upstream water surface source, downstream sediment bed source, and upstream water surface source) were selected as potential sources for 3 of the water column PE samplers deployed in 2014 and 2 of the water surface PE samplers deployed in 2015.
7. Case G: Four locations (upstream sediment bed source, upstream water surface source, downstream sediment bed source, and upstream water surface source) were selected as potential sources for the 5 water column PE samplers deployed in 2014 and the 3 water surface PE samplers deployed in 2015.

Numerous additional iterations of 3 to 4 source locations could be chosen for this analysis. Unlike Section 4.4, this system is an overdetermined system with no exact solution because there are more known concentrations than unknown source weights. The solution is determined by minimizing the difference between measured concentrations (5x1 matrix C) and the unit concentrations (5x3 matrix B) multiplied by the calculated weights (3x1 matrix w), also known as minimizing the sum of square error (E). The error is minimized by taking its derivative with respect to matrix w and setting it equal to zero (Polytechnic Institute of New York University, 2013).

Equation 11: Sum of Least Squares Error

$$E = \|C - Bw\|^2 = (C - Bw)^T(C - Bw) = C^TC - 2C^TBw + w^TB^TBw$$

Equation 12: Minimizing Sum of Least Squares Error

$$\frac{\partial E}{\partial w} = -2B^TC + 2B^TBw = 0$$

This results in the following least squares solution:

Equation 13: Sum of Least Squares Solution for Matrix w

$$w = (B^TB)^{-1}B^TC$$

The unit source concentrations (C) at each measurement location were extracted from the modeled unit concentration distributions. As the measured and modeled concentrations must both be nonnegative values, it was important that the calculated weights of the potential source locations are also nonnegative. The Matlab internal function lsqnonneg was used to solve for the least squares solution such that the weights of the potential sources were not less than zero.

It is important to note that the water column PE samplers were tethered approximately 1 m from the sediment bed. The LDW EFDC model vertically divides each cell into 20 even layers based on water depth, defining layer 1 as the closest to the sediment bed and layer 20 as the closest to the water surface. Therefore, 1 m from the sediment bed may fall in a different layer at each location. The appropriate layer (k) was determined with the average modeled water depth at each measurement location (h) and calculating which layer was approximately 1 m from the sediment bed.

Equation 14: EFDC grid cell location of PE passive sampler

$$k = \frac{1}{h}(20\ layers)$$

This calculation was not necessary for water surface PE samplers and the average depth of water surface PE passive samplers is listed as not applicable (N/A). Input information to the inverse model is provided in Tables 1 through 3. Samples designated "WS" are water surface samples; sampled designated "SB" are sediment bed samples.

Table 1: Inverse Model Input Information

RM	Average Depth, h (m)	PE Sampler Location in LDW EFDC Model		
		I (lateral)	J (longitudinal)	K (vertical)
0.1 SB	14.7	14	32	2
0.5 SB	5.2	15	30	4
0.9 WS	N/A	12	27	20
2.0 WS	N/A	14	21	20
2.2 SB	6.4	12	19	3
4.3 SB	4.1	12	5	5
4.7 WS	N/A	14	3	20
4.8 SB	4.0	15	3	5

Table 2: Inverse Model Measured Concentration Matrix C

RM	Measured Total PCB Concentration, C_m (pg/L)
0.1 SB	220
0.5 SB	470
0.9 WS	280
2.0 WS	280
2.2 SB	960
4.3 SB	870
4.7 WS	420
4.8 SB	480

Table 3: Example Inverse Model Simulated Concentration Matrix B

RM	RM 4.1 SB (pg/L)	RM 1.4 WS (pg/L)	RM 0.8 SB (pg/L)
0.1 SB	4,080	3,184	1,2526
0.5 SB	5,589	3,665	15,344
2.2 SB	13,513	5,686	22,756
4.3 SB	44,888	6,031	14,665
4.8 SB	34,599	4,381	9,937

The Inverse Model was evaluated by calculating the root-mean-squared error (RMSE) between the measured total PCB concentrations (C_m) and the calculated total PCB concentrations (C_c) for the number (n) of measured concentrations. A case with a relatively high RMSE compared to other cases indicates the Inverse Model does not fit the measured concentrations as well in that case.

Equation 15: Root mean squared error

$$RMSE = \sqrt{\frac{(C_{m1} - C_{s1})^2 + (C_{m2} - C_{s2})^2 + \ldots + (C_{mn} - C_{sn})^2}{n}}$$

7.0 Results and Analysis

7.1 LDW Characterization

7.1.1 Estuary Classification

LDW EFDC simulated salinity gradients conservative dye distributions were evaluated to determine the estuary classification, the extent of salinity intrusion, typical flow patterns, and typical residence time for the LDW. First, the tidal cycle was evaluated by simulating water depths at RM 0.1, located at the mouth of the LDW near Elliott Bay.

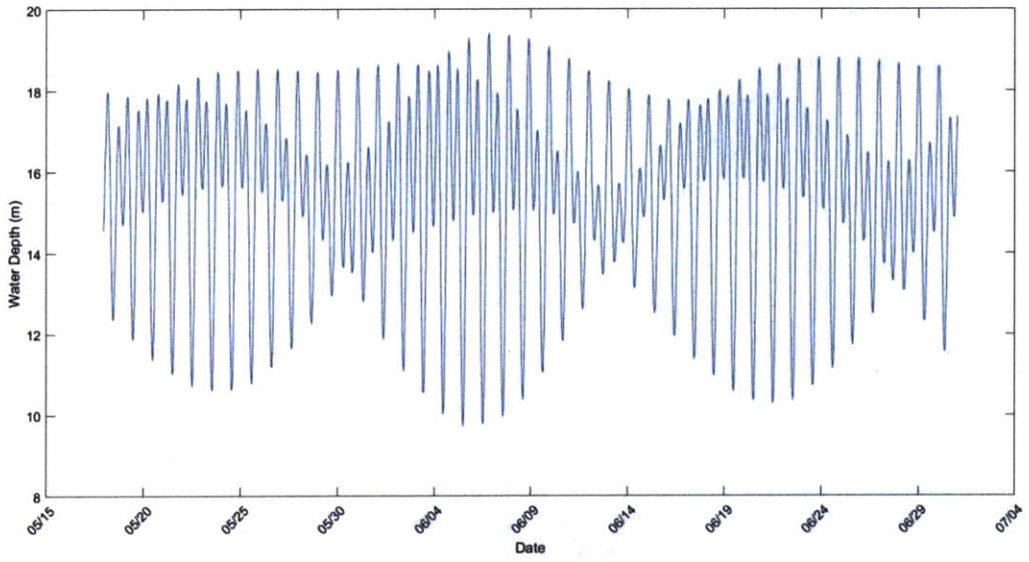

Figure 6: Simulated Water Depth Between 5/17/2016 and 7/1/2016

As observed in Figure 6, the LDW follows a semi-diurnal tidal cycle and experiences two high tides and two low tides each lunar day (24.8 hours). One tide is stronger than the other, such that two weak tides follow two strong tides. Spring tides (relatively stronger tides) and neap tides (relatively weaker) are also observed approximately every 14.7 days, which aligns with typical spring-neap tidal cycles. Longitudinal and cross-section "heat maps" of salinity were observed to evaluate the movement of saltwater in three dimensions for typical spring and neap tides (Figures 7-14).

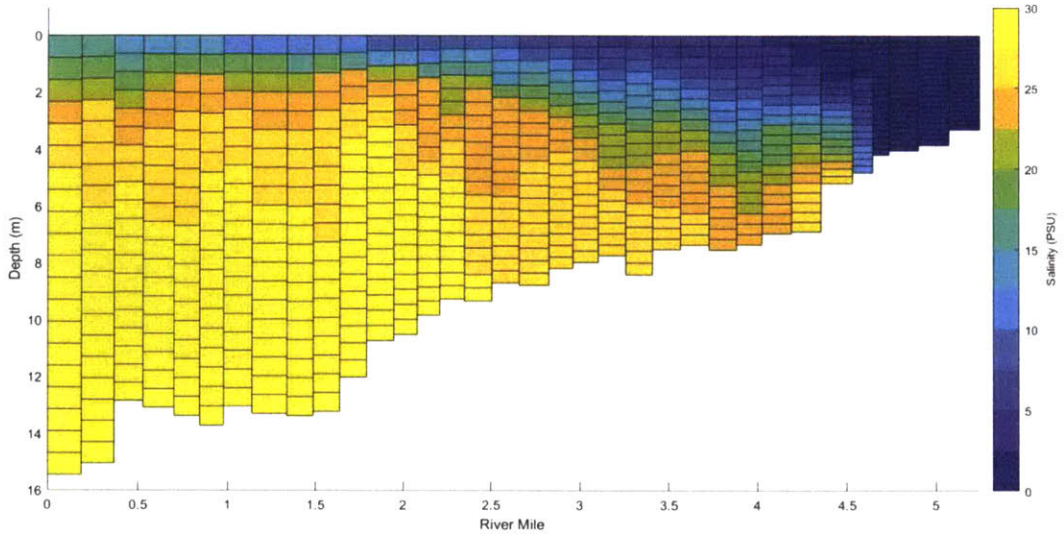

Figure 7: Longitudinal Salinity Distribution for a Typical Neap Low Tide

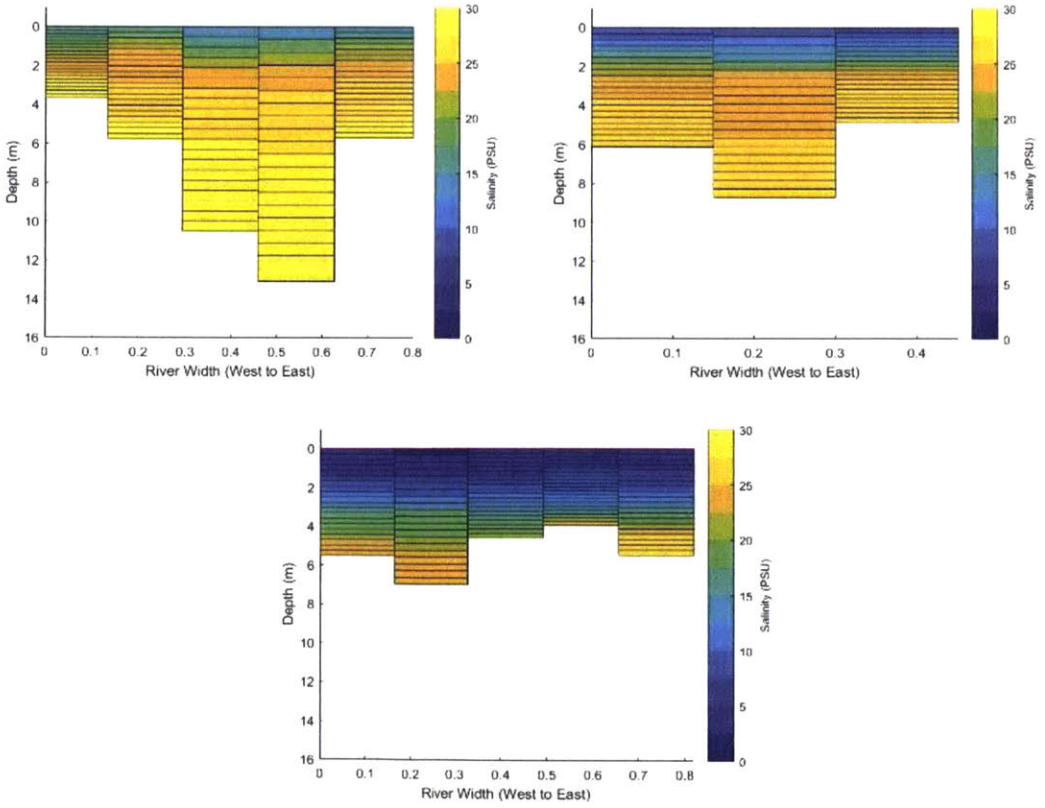

Figure 8: Selected Cross-Section Salinity Distributions of a Typical Neap Low Tide at RM 0.6 (top left), RM 2.3 (top right), and RM 4.1 (center bottom)

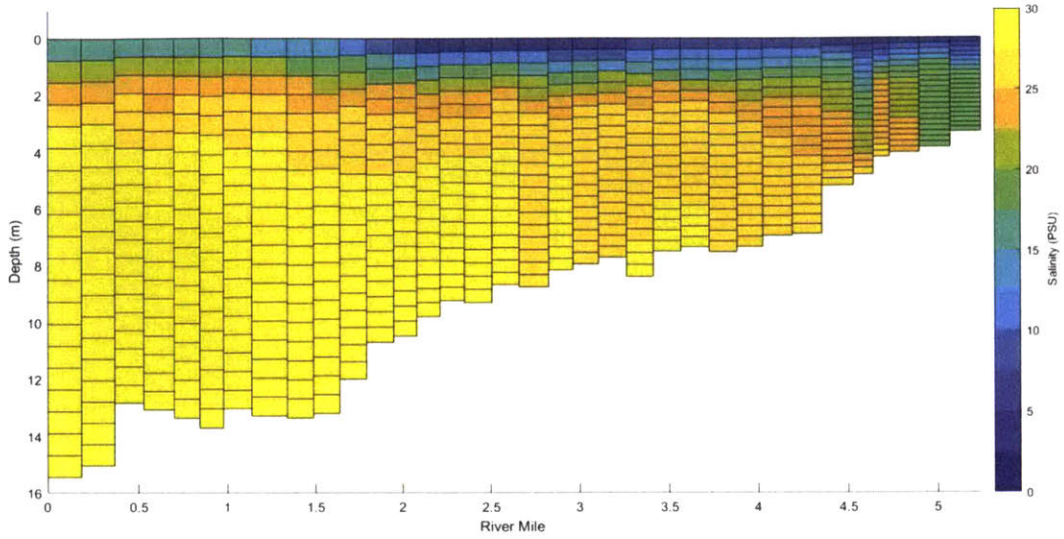

Figure 9: Longitudinal Salinity Distribution for a Typical Neap High Tide

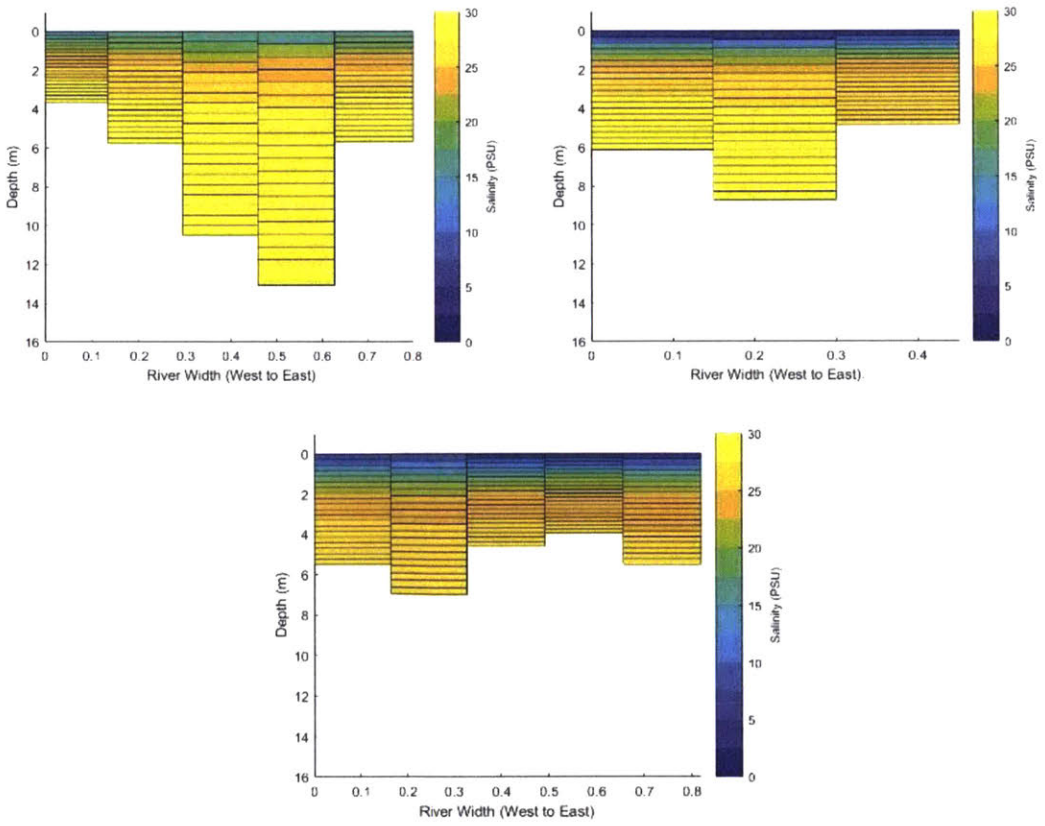

Figure 10: Selected Cross-Section Salinity Distributions of a Typical Neap High Tide at RM 0.6 (top left), RM 2.3 (top right), and RM 4.1 (bottom center)

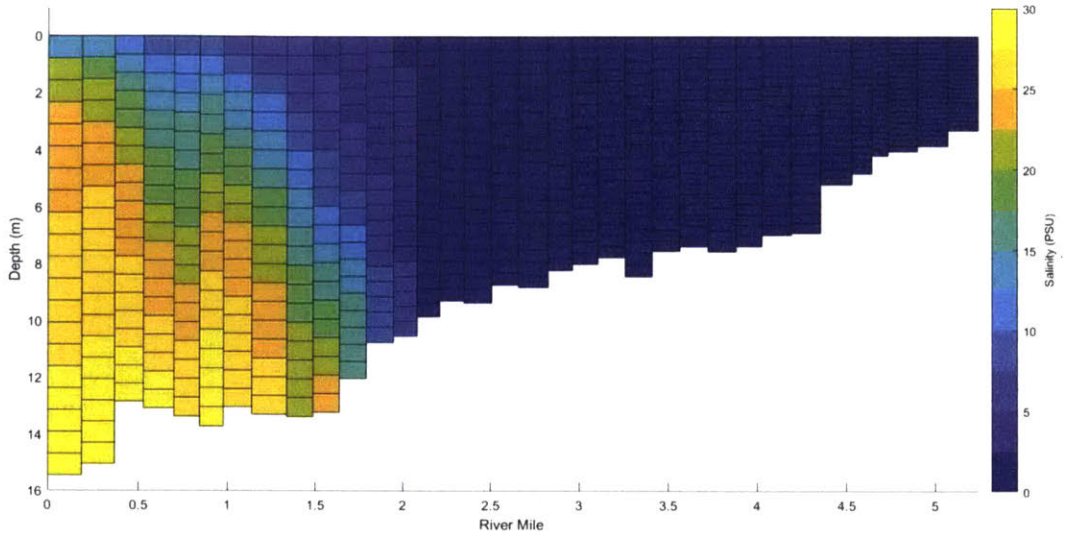

Figure 11: Longitudinal Salinity Distribution of Typical Spring Low Tide

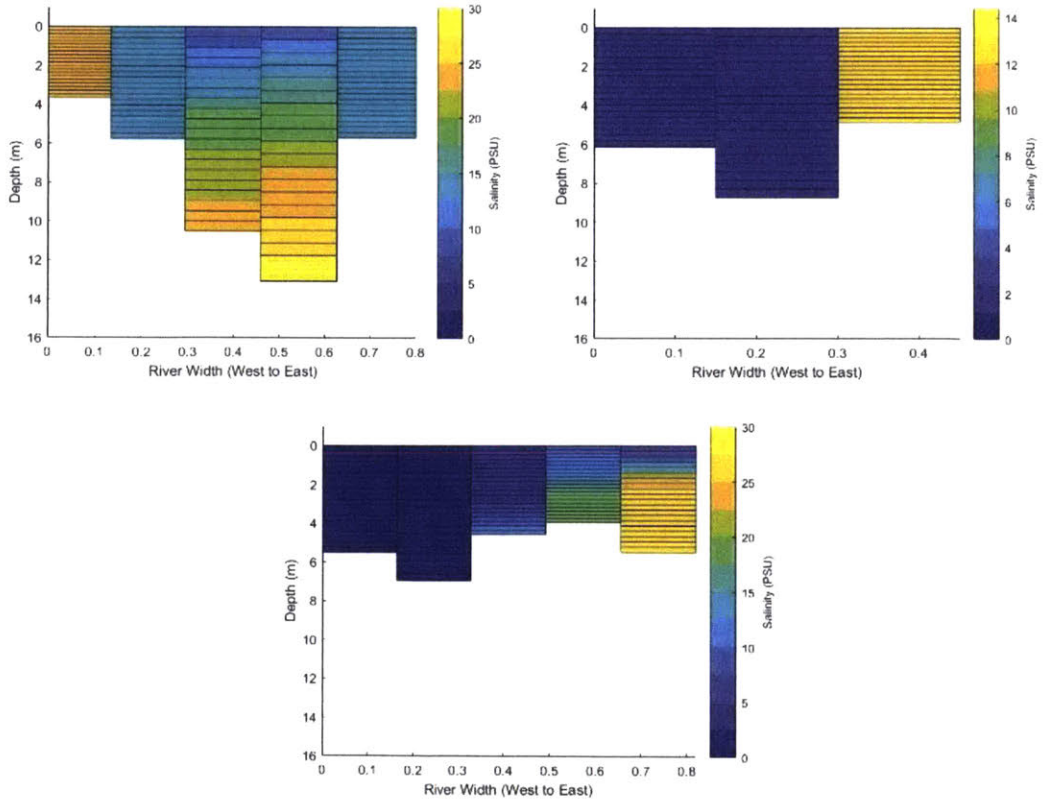

Figure 12: Selected Cross-Section Salinity Distributions of a Typical Spring Low Tide at RM 0.6 (top left), RM 2.3 (top right), and RM 4.1 (bottom center)

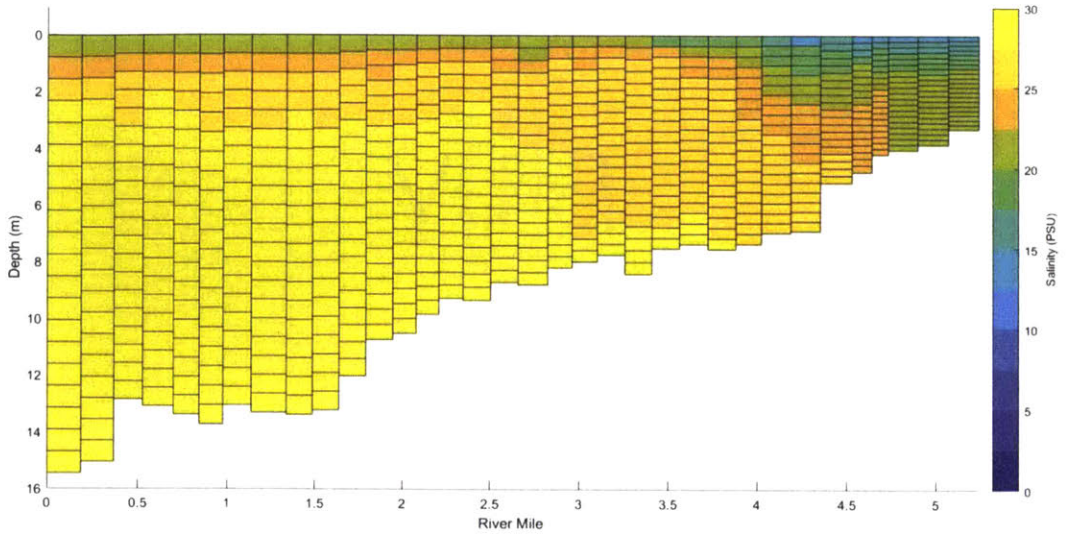

Figure 13: Longitudinal Salinity Distribution of a Typical Spring High Tide

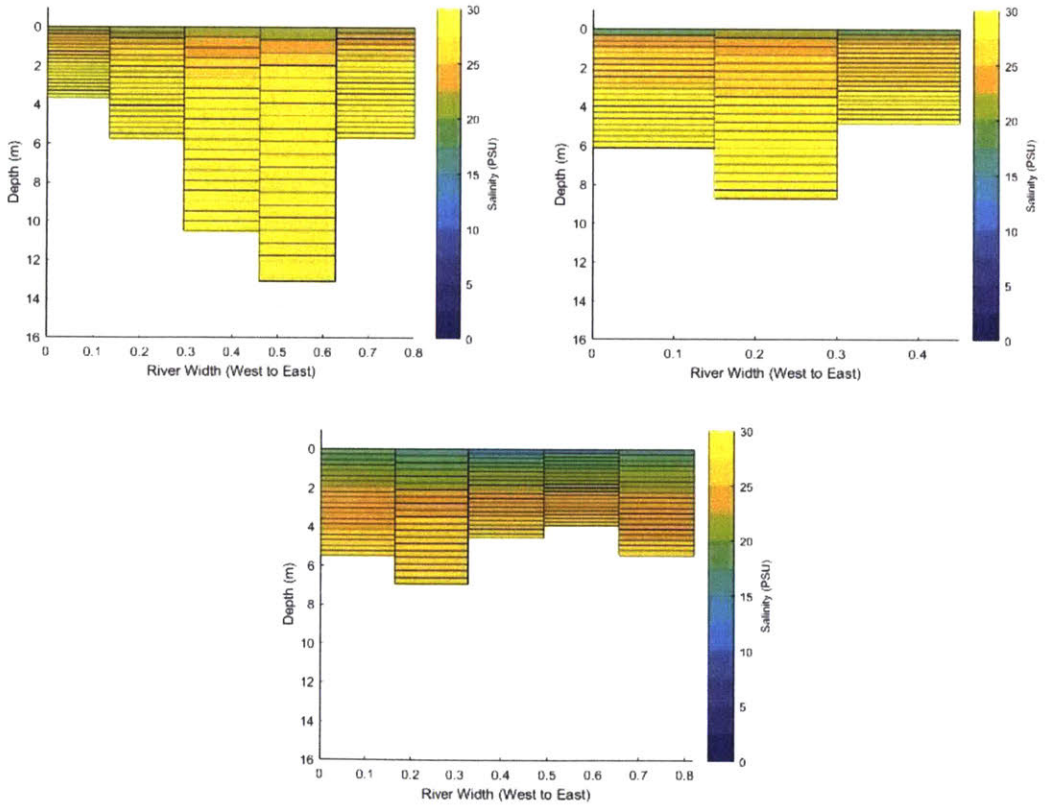

Figure 14: Selected Cross-Section Salinity Distributions of a Spring High Tide at RM 0.6 (top left), RM 2.3 (top right), and RM 4.1 (bottom center)

As seen in the above figures, the dense saltwater flows below the less-dense freshwater at any point in the tidal cycle. The extent of salinity intrusion is determined by the tidal cycle phase. More saltwater is present in the LDW during high tides, which allows for more upriver salinity intrusion, as seen in Figure 9. Conversely, less saltwater is present in the LDW during low tides, which allows for more downriver freshwater intrusion, as seen in Figure 7. Spring tides amplify this effect, causing salinity intrusion much farther upstream (Figure 11) and freshwater intrusion much farther downstream (Figure 9).

The cross-sectional distribution of salinity during neap tides tend to be laterally well mixed and vertically stratified, as shown in Figures 8 and 10. Spring high tides also exhibit mixing in the lateral, as shown in Figure 14, but tend to have less vertical stratification due to the increased salinity throughout the LDW and greater mixing energy from high tidal velocities. Spring low tides appear to be stratified in both the lateral and vertical. As expected, Figures 11 and 12 show lower salinity measurements due to low tide; however, freshwater at RM 2.3 and 4.1 dominates the western bank of the LDW. This is attributed to channel geometry creating a preferential flow path for incoming freshwater.

In both the longitudinal and cross-section distributions, isohalines are horizontal or nearly horizontal for a majority of the LDW. This is indicative of a vertically stratified estuary with a tidally-influenced salt wedge. Figures 7 through 14 reflect how the salt wedge (represented by the yellow boxes) moves upstream and downstream as influenced by the tides and river flow. To further evaluate this conclusion, the estuary Richardson number was calculated as described in Section 6.2.1 with selected values for Q (20.1 m^3/s), W (250 m), and u_t (0.1 m/s). The LDW Richardson number is approximately 20, which is much greater than the required number of 0.8 to classify an estuary as vertically stratified (Fischer et al., 1979). This confirms the LDW is a vertically stratified estuary and displays the expected characteristics, such as a tidally influenced salt wedge, inhibited vertical mixing across the density gradient, and different freshwater and saltwater flow patterns.

7.1.2 Residence Time

The mean residence time of the LDW was calculated to determine the average time a contaminant stays in the LDW, and subsequently how long it can react with the sediment and water column, before entering Elliott Bay. As described in Section 6.2.2, a residence time was calculated for each dye input location, resulting in 44 residence times for the LDW. A summary of residence times by source location is provided in Table 4 below:

Table 4 - Residence Times by Source Location

Input Source Location	Maximum Residence Time (days)	Minimum Residence Time (days)	Average Residence Time (days)
Most upstream (between RM 4.1 and RM 4.8)	2.51 (RM 4.1 bed)	1.40 (RM 4.1 surface)	1.98
Most downstream (between RM 0.1 and RM 0.8)	2.68 (RM 0.8 bed)	0.61 (RM 0.1 surface)	1.67
All surface	1.75 (RM 3.7)	0.61 (RM 0.1)	1.15
All bottom	3.00 (RM 1.7)	2.15 (RM 0.1)	2.60
All	3.00 (RM 1.7 bed)	0.61 (RM 0.1 surface)	1.91

Residence times are a function of the dye injection location and are not a property of the LDW. Contaminants that originate from the sediment bed or downstream are generally in the LDW longer than contaminants that originate at the surface or upstream. The longest residence times were observed for tracer releases at the bed on the downstream half of the LDW (between RM 1.1 and 2.6), while residence times less than a day were calculated for releases at the surface near the mouth of Elliott Bay (between RM 0.1 and 1.1).

This provides insight to flow patterns of freshwater and saltwater within the LDW. Freshwater that originates upstream flows north from the Green/Duwamish River towards Elliott Bay. The density gradient causes freshwater to flow above the intruded saltwater. Tides within Elliott Bay force downstream saltwater to initially flow south into the LDW below the freshwater. The opposite velocities of freshwater and saltwater creates shear between the freshwater layer and the saltwater layer, which causes localized mixing near the halocline and eventually dampens the flow of the saltwater. The saltwater that has mixed with freshwater is now less dense than pure saltwater and can flow with the freshwater above it. This creates a circulation within the LDW that is illustrated in Figure 15.

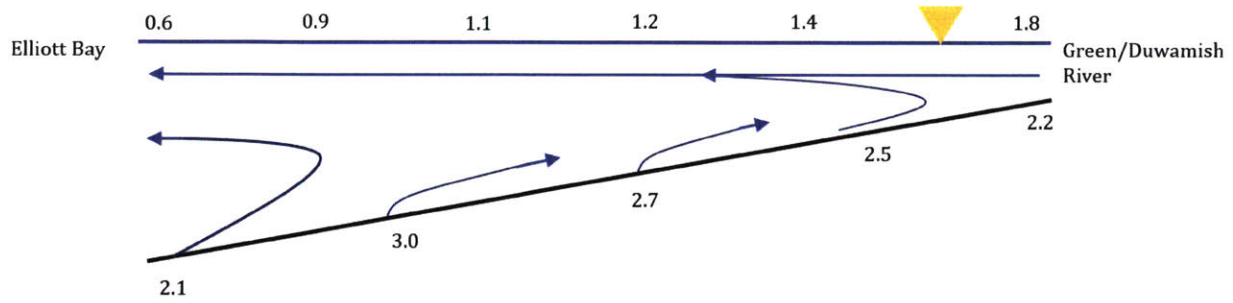

Figure 15: Density-Driven Circulation Schematic. Numbers indicate approximate residence time of input location in days.

Following this circulation pattern, referred to as the density-driven circulation, contaminants that are released downstream or at the bottom flow upstream into the LDW before being flushed out, while contaminants that are released upstream or on the surface flow downstream to Elliott Bay. Downstream sources can travel as far as RM 4.5 depending on its introduction location. In general, mid-downstream bed sources have the longest residence times, followed by upstream bed sources, downstream bed sources, upstream surface sources, and downstream surface sources.

7.2 Concentration Distribution Simulations

The LDW EFDC model simulated concentration distributions for 44 continuous, unit dye tracers over the length, width, and height of the LDW. Individual concentration distributions were time-averaged over the simulation period to reflect the concentrations that would be measured by an *in-situ* PE passive sampler. Lateral, vertical, and longitudinal concentration distributions were compared and evaluated to identify where sources in the LDW are considered distinguishable from each other.

7.2.1 East Bank Sources, West Bank Sources, and Lateral Mixing Time

Sources from the east and west banks were compared to determine a typical distance in which they were distinguishable from each other. As previously discussed, two sources were considered distinguishable if their concentration distributions were outside the PE passive sampler measurement error of approximately 20%, or ±10% (Apell & Gschwend, 2014). Once the concentration distributions fell within this range, the sources were considered indistinguishable and a PE sampler would not be able to determine the origin of the source. For this analysis, a source location always within the salt intrusion area (RM 0.5) and a source location sometimes within the salt intrusion area were selected (RM 3.7). Bank sources were introduced at each river mile at the water surface or at the sediment bed and compared at the centerline of the LDW, as shown in Figures 16 and 17.

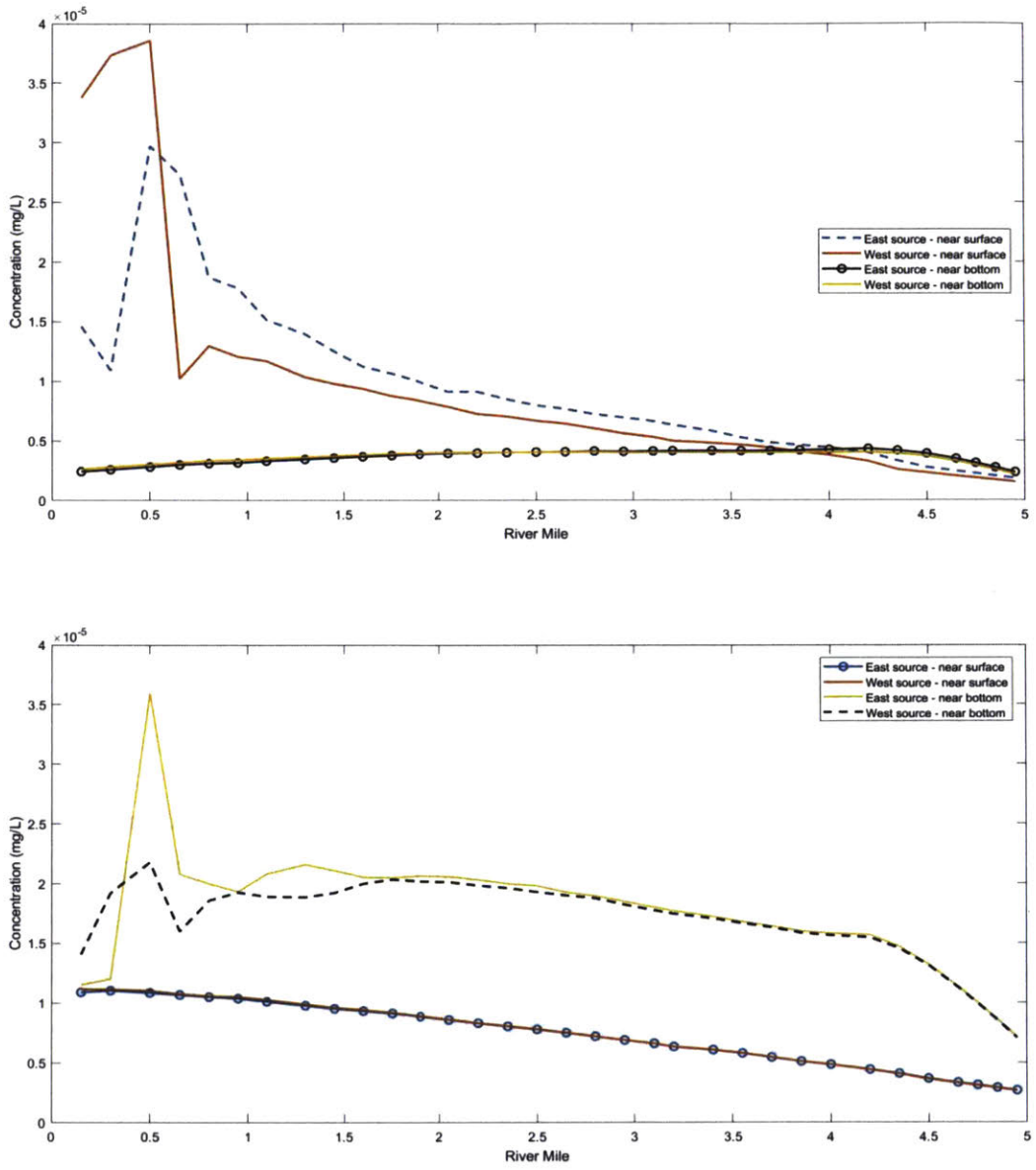

Figure 16: Longitudinal Concentration Distributions of Bank Sources Introduced at RM 0.5 near at the Water Surface (top) and Sediment Bed (bottom).

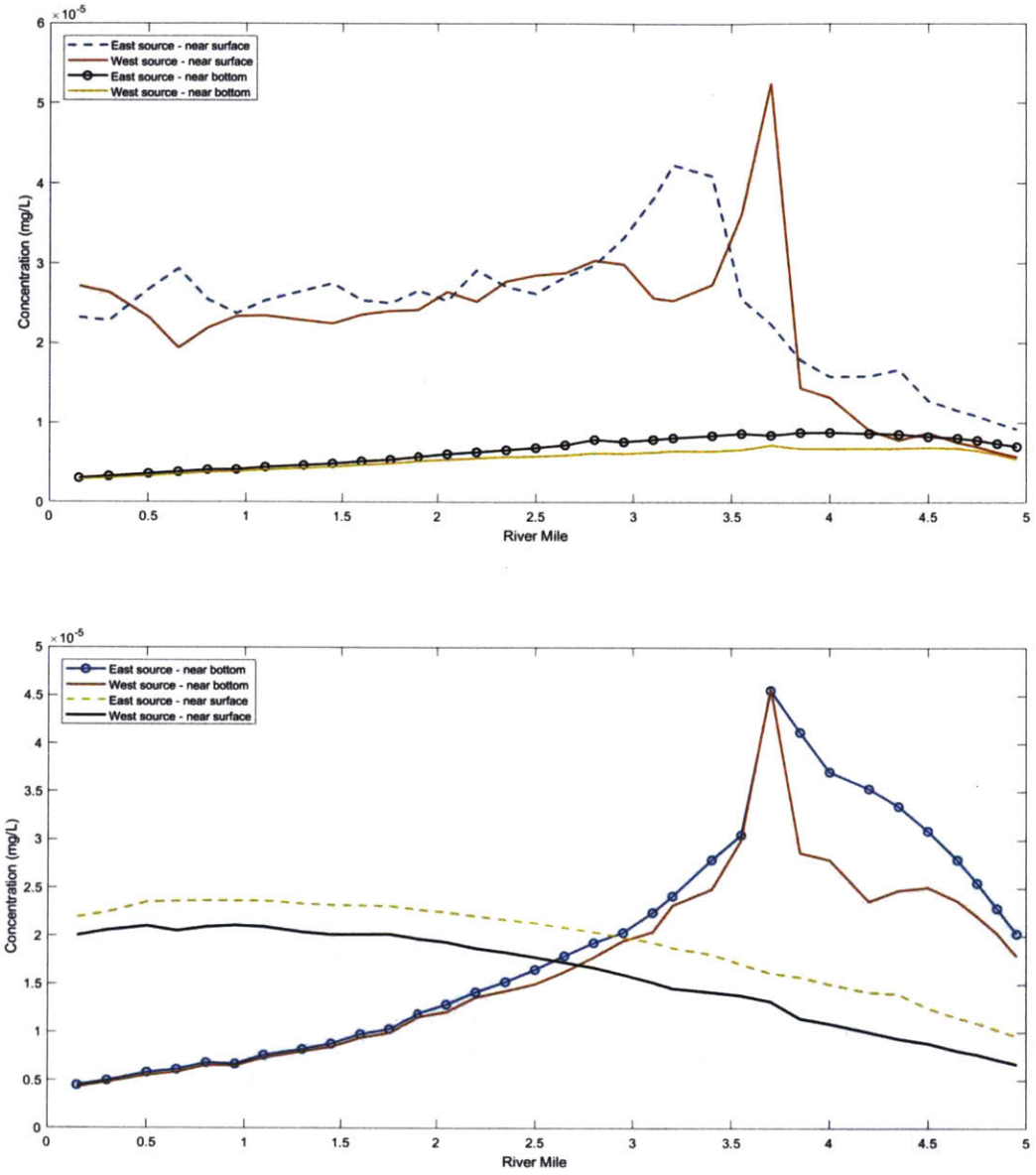

Figure 17: Longitudinal Concentration Distributions of Bank Sources Introduced at RM 3.7 at the Water Surface (top) and Sediment Bed (bottom).

The bank that the source was introduced on did not have an impact on how dye tracers mixed vertically. As shown in Figures 16 and 17, east and west bank surface sources are indistinguishable near the sediment bed; similarly, east and west bank sediment bed sources are indistinguishable near the surface. This is attributed to the hydrodynamics of the LDW that similarly affect both banks, including inhibited vertical mixing and the density-driven circulation.

Bank sources introduced at RM 0.5 are distinguishable in the centerline of the LDW at the introduction elevation for approximately 0.5 to 1.0 miles upstream from the source location. Bank sources introduced at the RM 3.7 water surface are distinguishable for approximately 0.8 miles downstream from the source location, while bank sources introduced at the sediment bed in the same location were immediately indistinguishable. However, concentration distributions downstream of downstream source locations and upstream of upstream source locations were distinguishable for approximately 0.5 to 1.3 miles. Downstream discrepancies are attributed to the short residence time of sources introduced at the water surface and the density-driven circulation at the sediment bed. Upstream discrepancies are attributed to a small tidal prism available for lateral mixing and the downstream flow direction, dominated by the freshwater flow, inhibiting the upstream transportation of contaminants.

After approximately 0.8 miles, a PE sampler would not be able to identify which bank the source is located on. This effect is due to lateral mixing of bank sources towards the center of the LDW. Cross-sectional concentration distribution maps were compared at or near the locations in which east and west bank sources were no longer distinguishable to further evaluate lateral mixing.

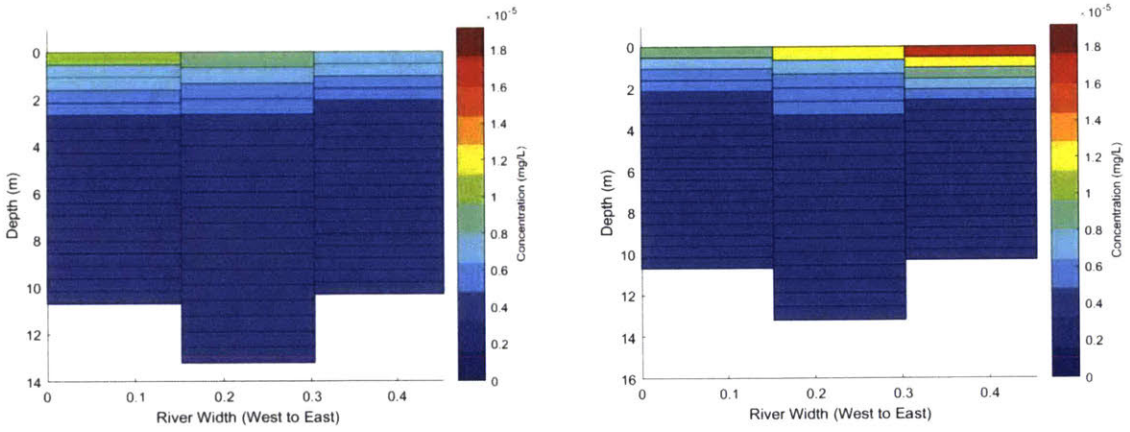

Figure 18: Cross-Section Concentration Distributions Simulated at RM 1.6 of Water Surface Sources Released at RM 0.5 West Bank (left) and East Bank (right)

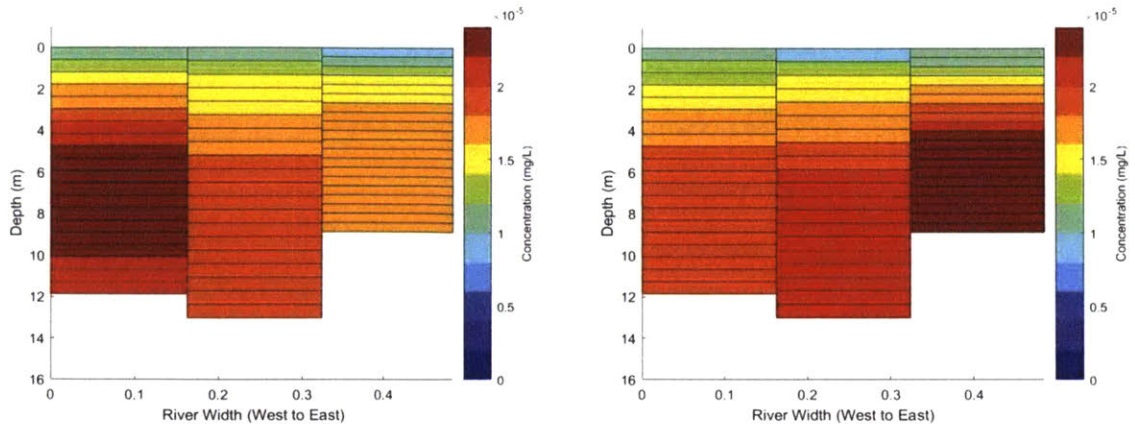

Figure 19: Cross-Section Concentration Distributions Simulated at RM 1.1 of Sediment Bed Sources Released at RM 0.5 West Bank (left) and East Bank (right)

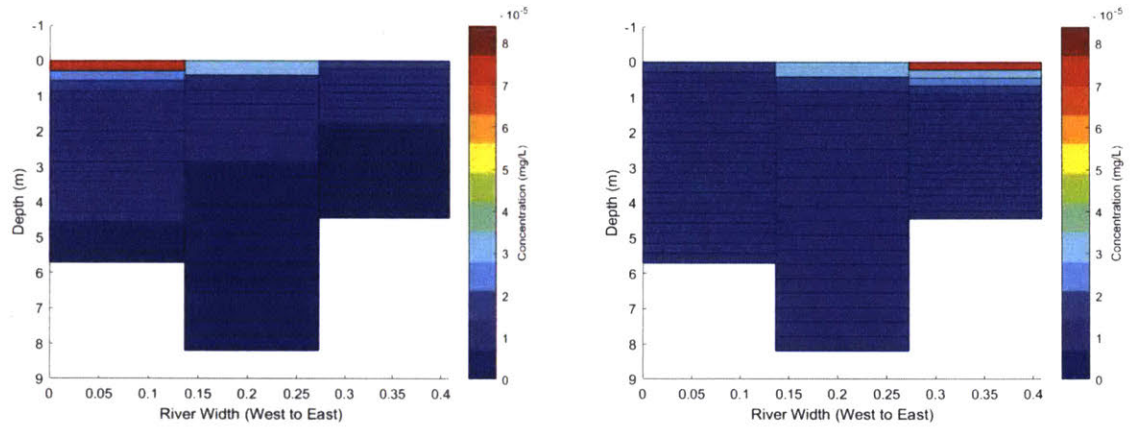

Figure 20: Cross-Section Concentration Distributions Simulated at RM 2.9 of Water Surface Sources Released at RM 3.7 West Bank (left) and East Bank (right)

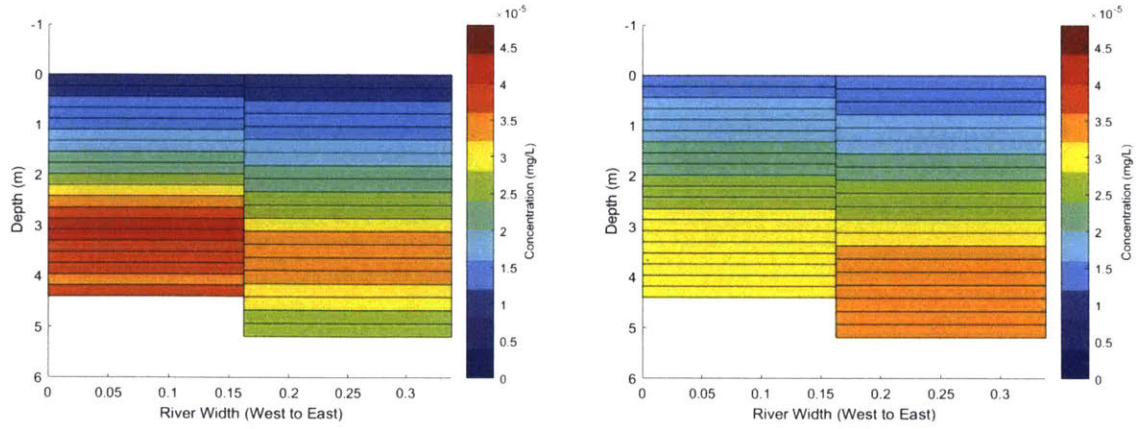

Figure 21: Cross-Section Concentration Distributions Simulated at RM 4.5 of Sediment Bed Sources Released at RM 3.7 West Bank (left) and East Bank (right). Note: the right column is considered the centerline of the channel.

Figures 18 to 21 show centerline concentration distributions are indistinguishable for east and west bank sources after approximately 0.5 to 1.0 miles. When the LDW narrows at RM 4.5, centerline concentrations are generally indistinguishable, as shown in Figure 21; however, distinguishable concentration distributions may be generated near the sediment bed. The LDW EFDC model represents the width of this portion of the LDW with two grid cells instead of three, increasing the influence of the east bank on the centerline concentrations.

As previously mentioned, lateral mixing causes bank sources to disperse towards the centerline of the channel and become indistinguishable. Following the method described in Section 6.2.3, the lateral mixing time was calculated to be approximately 1.53 days, which is less than the average residence time of 1.91 days. This confirms that, on average, there is enough time for bank sources to laterally mix to the centerline and become indistinguishable to a centerline PE passive sampler placed approximately 0.8 miles from the source location. However, as evidenced in Figures 18 through 20, if a PE passive sampler is placed near the bank of the LDW, it will be biased towards sources on that bank. It will observe higher concentrations than if that sampler was placed at the center and indicates a source is likely located within 0.8 miles on that bank

7.2.2 Surface and Bed Sources

The analysis completed for sources released on the east and west banks was continued to compare sources released at the water surface and at the sediment bed. Sources were introduced at the centerline of the LDW, within the navigation channel, at a location always within the salt intrusion area (RM 1.0), a location mostly within the salt intrusion area (RM 2.3), and a location sometimes within the salt intrusion area (RM 4.1). For each tracer release, time-averaged heat maps of longitudinal concentration distributions were compared to evaluate the vertical movement of tracer.

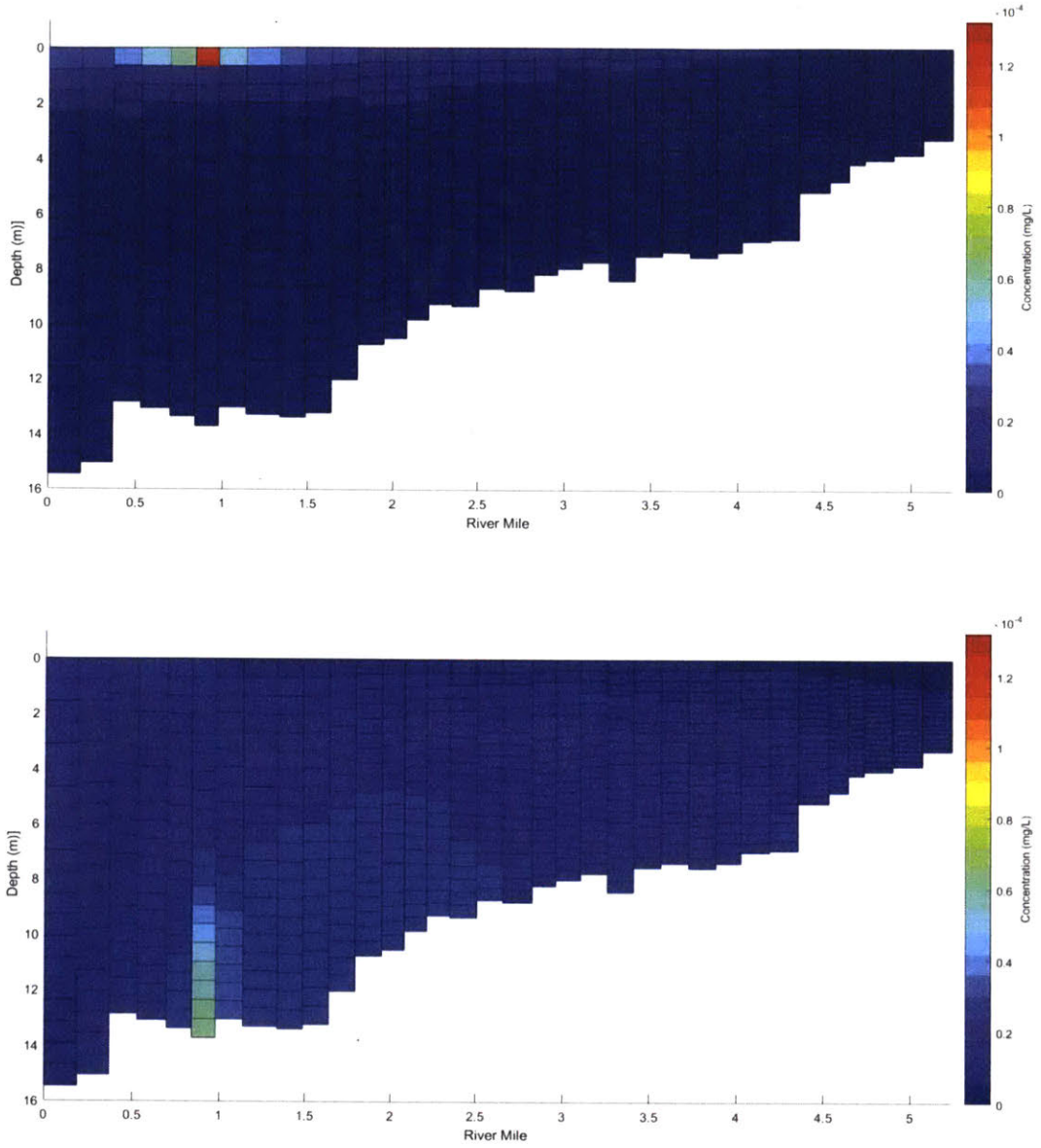

Figure 22: Longitudinal Concentration Distributions of Sources Introduced at RM 1.0 Water Surface (top) and Sediment Bed (bottom)

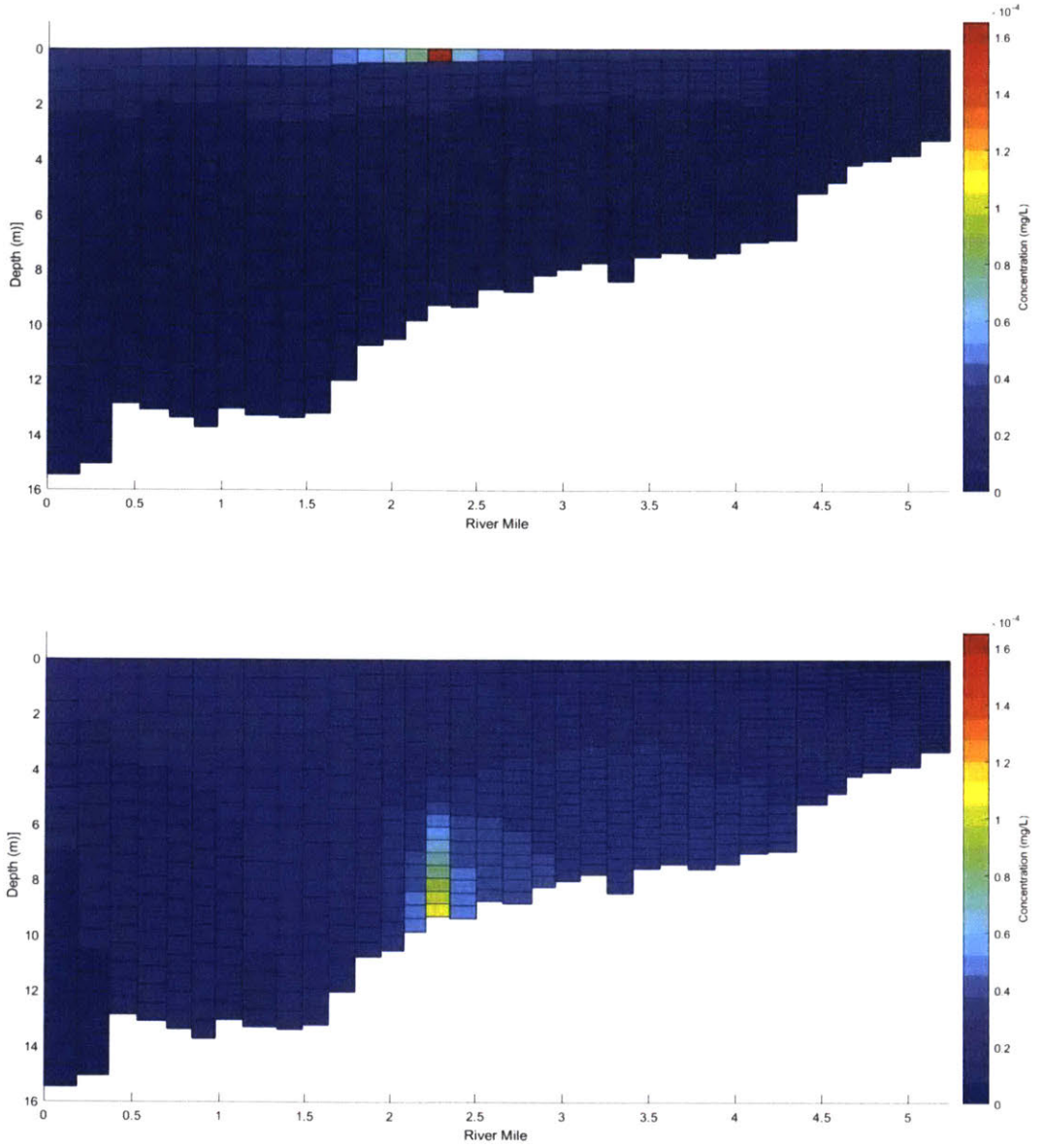

Figure 23: Longitudinal Concentration Distributions of Sources Introduced at RM 2.3 Water Surface (top) and Sediment Bed (bottom)

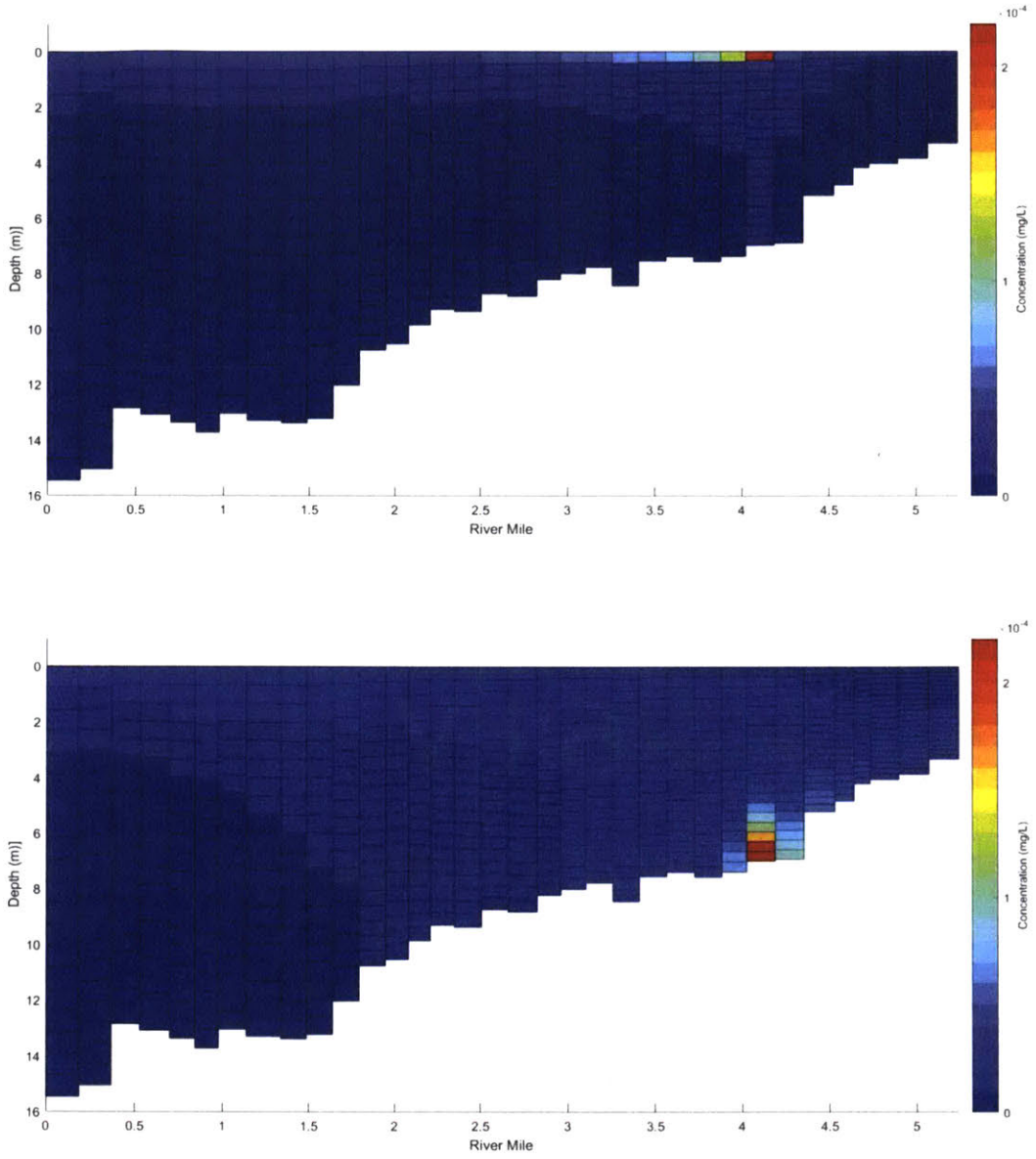

Figure 24: Longitudinal Concentration Distributions of Sources Introduced at RM 4.1 Water Surface (top) and Sediment Bed (bottom)

As shown in the Figures 22 through 24, dye tracer released at the water surface behaved similarly no matter where it was introduced in the LDW. Freshwater flow from the Green/Duwamish River dominates the flow direction at the surface of the LDW, causing downstream dispersion to dominate upstream dispersion along the water surface. The vertical density gradient inhibits vertical mixing across salt wedge, trapping surface releases at the surface of the LDW as a thin, near-surface layer.

Unlike sources introduced at the water surface, sources introduced at the sediment bed are generally introduced into saltwater because they are exposed to the density-driven circulation described in Section 7.1. Downstream sediment bed sources, represented by Figure 22, are driven upstream by tidal influence from Elliott Bay; the plume dilutes as velocity shear is introduced in the circulation. Midstream sediment bed sources initially flow upstream by tidal influence until the flow is reversed by density-driven circulation. The change from upstream flow to downstream flow is evidenced by the plume shape in Figure 23. Upstream sediment bed sources experience some mixing due to tidally-influenced density fluctuations. In all cases, the density-driven flow circulation eventually carries the diluted plume downstream and to the surface.

In general, water surface sources and sediment bed sources are distinguishable from each other in the LDW. Therefore, PE passive samplers placed at the surface will detect surface sources while samplers placed at the sediment bed will detect sediment bed sources. Inhibited vertical mixing across the salt wedge prevents the migration of water surface sources towards the sediment bed. Density-driven circulation initially causes the saltwater sediment bed sources to flow upstream. When flow is reversed, the plume concentration has diluted and low concentrations of sediment bed sources flow downstream near the water surface. When comparing sediment bed sources and water surface sources at the water surface, rising sediment bed sources result in a thicker layer of concentration than the thin layer of concentration produced by water surface sources. Therefore, a CSO or other freshwater source will likely be distinguishable from sediment bed sources in PE passive samplers due to its strong vertical concentration gradient over a short distance. Without this signature, water surface sources and sediment bed sources may not be distinguishable at the water surface near Elliott Bay. Additional upstream PE passive samplers would be necessary to determine if and where a water surface source exists in the LDW

7.2.3 Longitudinal Sources

Evaluation of longitudinal sources was completed by dividing the LDW into 16 approximately equal segments. At the approximate center of each segment, the dye tracer was introduced at the bed or

surface of the navigation channel. This generally translated to a source input for every other grid cell in the LDW EFDC model, corresponding to sources every 0.3 miles. Water surface source locations located at RM 0.5, RM 3.8, and RM 4.8 were shifted after an EFDC FORTRAN code error occurred (negative cell depths at cell center). The center sources at RM 3.8 and RM 4.8 were replaced with center sources at RM 3.7 and RM 4.7, respectively. The center source at RM 0.5 was replaced with a west bank source after it was determined to be comparable to a center source in concentration magnitude.

The longitudinal sources were compared to each other to determine the distance in which they become indistinguishable from each other. Two concentration distributions (RM 2.0 and RM 2.3) on Figures 25 and 26are bolded to visualize how adjacent sources evolve in the LDW.

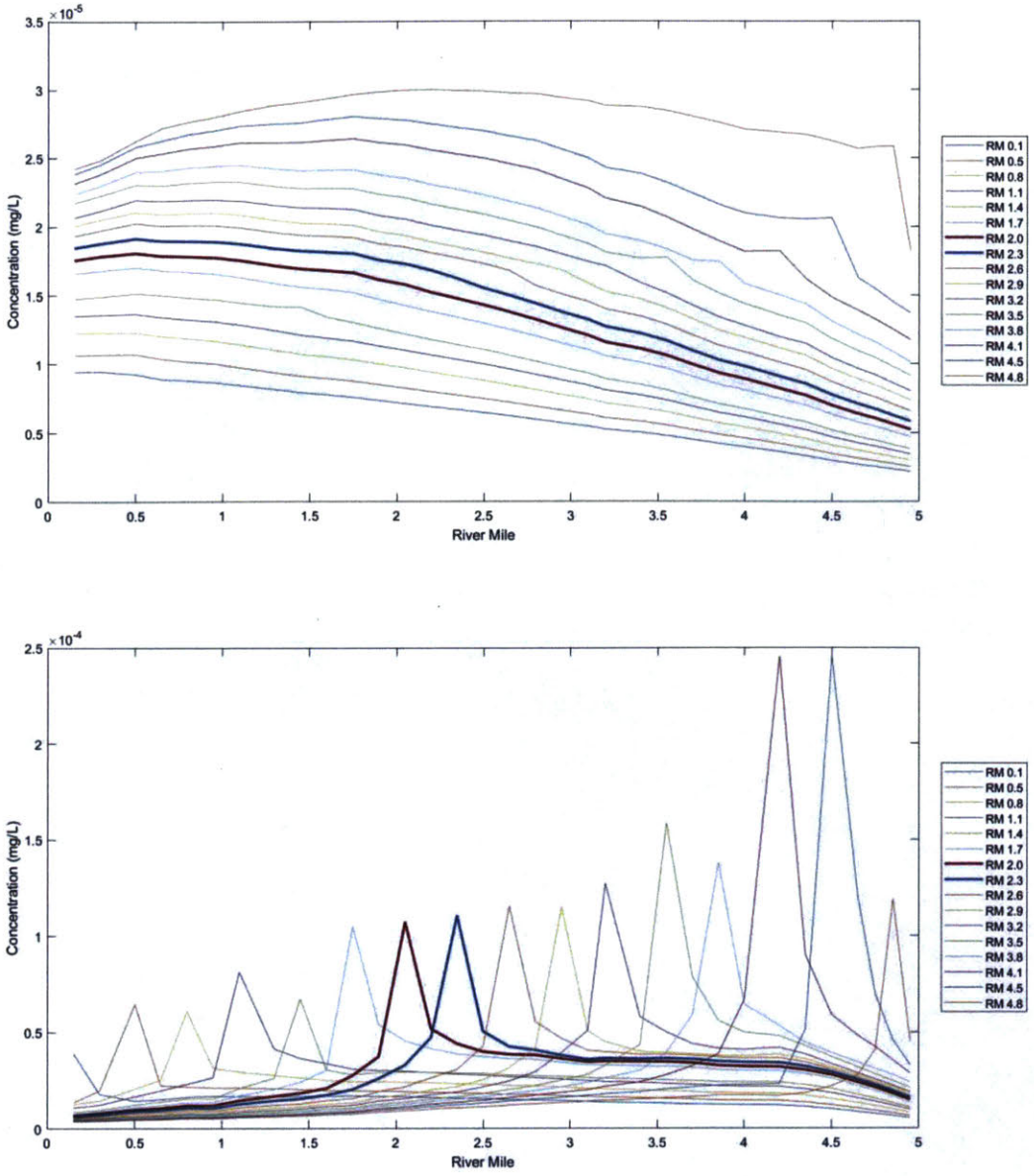

Figure 25 - Longitudinal Concentration Distributions of 16 Longitudinally Distributed Sediment Bed Sources Simulated Near the Water Surface (top) and Near the Sediment Bed (bottom).

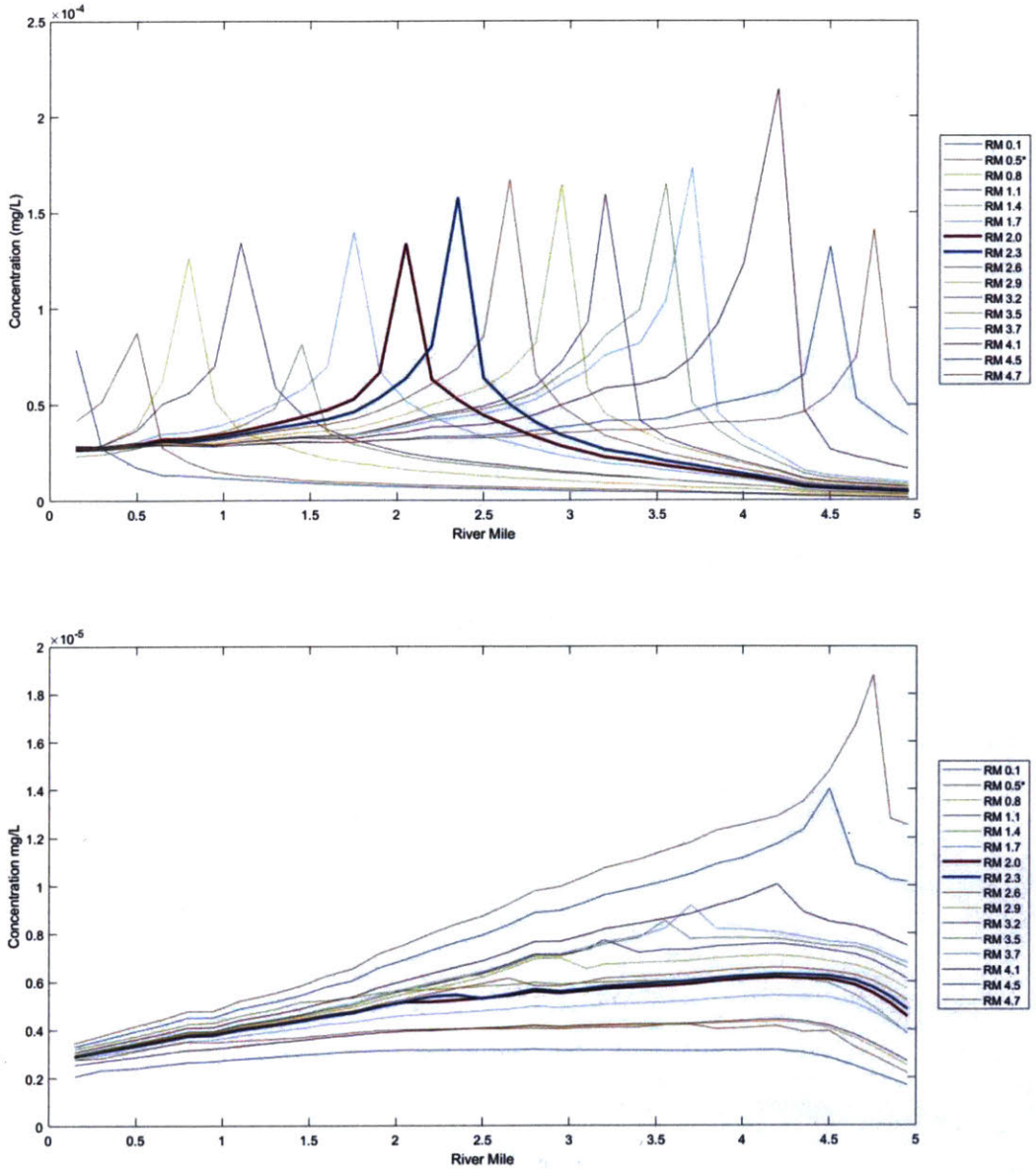

Figure 26: Longitudinal Concentration Distributions of 16 Longitudinally Distributed Water Surface Sources Simulated Near the Water Surface (top) and Near the Sediment Bed (bottom). Note: RM 0.5 is simulated as a west bank surface source.

As expected, peak concentrations are observed at the longitudinal location of the input source. Higher magnitudes of concentration distributions were observed for the upstream surface sources due to the small tidal prism available for mixing. The source elevation impacts the concentration distributions, as discussed in Section 7.2.2, so that sediment bed sources are typically not distinguishable at the surface and water surface sources are typically not distinguishable at the sediment bed. However, upstream sediment bed sources originating at RM 4.1, RM 4.5, and RM 4.8 were distinguishable at the water surface for approximately 1 mile downstream (for RM 4.5 and

4.8) and 0.3 miles upstream (for RM 4.1 and RM 4.5). Similarly, upstream water surface sources originating at RM 4.7, 4.5 and 4.1 were distinguishable at the sediment bed until the introduction of the adjacent source (i.e., source introduced at RM 4.7 was distinguishable from a source introduced at RM 4.5 until RM 4.5 and source introduced at RM 4.5 was distinguishable from a source introduced at RM 4.1 until RM 4.1). This is attributed to density-driven circulation distributing the source input within the water column and to the small tidal prism available for lateral mixing.

Adjacent sediment bed sources simulated at the sediment bed result in distinguishable concentration distributions near the source location. After the dye has traveled approximately 0.5 miles in an upstream or downstream direction, longitudinal dispersion impacts the plumes and causes adjacent sources to become indistinguishable. A summary of these distances is provided in Table 5 below.

Table 5: Summary of Distinguishable Distances of Sediment Bed Sources

Downstream Sediment Bed Source Location	Upstream Sediment Bed Source Location	Downstream distinguishable distance (miles)	Upstream distinguishable distance (miles)
RM 0.1	RM 0.5	0.2 (estimated)	0.5
RM 0.5	RM 0.8	0.5	1.0
RM 0.8	RM 1.1	0.4	0.8
RM 1.1	RM 1.4	0.7	0.2
RM 1.4	RM 1.7	0.2	1.4
RM 1.7	RM 2.0	0.4	0.2
RM 2.0	RM 2.3	0.4	0.2
RM 2.3	RM 2.6	0.5	0.4
RM 2.6	RM 2.9	0.6	0.2
RM 2.9	RM 3.2	0.4	0.3
RM 3.2	RM 3.5	0.5	0.5
RM 3.5	RM 3.8	0.3	0.3
RM 3.8	RM 4.1	0.4	0.8
RM 4.1	RM 4.5	0.7	0.4
RM 4.5	RM 4.8	1.0	0.2 (estimated)
Average (including estimations)		0.5	0.5

A similar effect is observed for adjacent water surface sources simulated at the water surface. Distinguishable concentration distributions are identified near the source location, while longitudinal dispersion causes the plumes to become indistinguishable after approximately 1.1 miles upstream and 0.4 miles downstream. A summary of these distances is provided in Table 6 below.

Table 6: Summary of Distinguishable Distances of Water Surface Sources

Downstream Water Surface Source Location	Upstream Water Surface Source Location	Downstream distinguishable distance (miles)	Upstream distinguishable distance (miles)
RM 0.1	RM 0.5*	0.5 (estimated)	0.5
RM 0.5*	RM 0.8	0.7 (estimated)	3.7
RM 0.8	RM 1.1	0.2	3.1
RM 1.1	RM 1.4	0.6	0.2
RM 1.4	RM 1.7	0.3	2.5
RM 1.7	RM 2.0	0.5	0.8
RM 2.0	RM 2.3	0.1	0.5
RM 2.3	RM 2.6	0.2	0.7
RM 2.6	RM 2.9	0.4	0.6
RM 2.9	RM 3.2	0.3	0.2
RM 3.2	RM 3.5	0.1	0.7
RM 3.5	RM 3.7	0.1	0.2
RM 3.7	RM 4.1	0.7	1.2
RM 4.1	RM 4.5	1.3	0.9 (estimated)
RM 4.5	RM 4.7	0.6	0.6 (estimated)
Average (including estimations)		0.4	1.1

In general, sediment bed sources and water surface sources had a total distinguishable distance comparable to the tidal excursion of approximately 1.2 miles, as calculated in Section 6.2.3. This translates to a longitudinal dispersion coefficient of approximately 7.5 m^2/s, calculated with an estimated distinguishable distance of 0.5 miles. The tidal excursion is greater than the source spacing of approximately 0.3 miles and effectively influences the concentration distributions within its range. A longer upstream distinguishable distance was simulated for water surface sources (approximately 1.1 miles compared to approximately 0.5). This is attributed to density-driven circulation inhibiting upstream surface water flow and dispersion, and the equivalent of two tidal excursions are required to create indistinguishable adjacent sources.

7.3 Inverse Modeling

The inverse modeling method was conducted as described in Section 6.2.4 to evaluate the importance of source location to contributing water column contamination in the LDW. The first iteration (Case A) considered an upstream sediment bed source located at RM 4.1, a downstream surface water source located at RM 1.4, and a downstream sediment bed source location at RM 0.8. The absolute calculated weight of each potential source (w) and the normalized calculated weight of each source (w_n, normalized to the sum of the weights) is provided in Table 7. The calculated water column concentration resulting from these weights (C_c), the PE passive sampler-measured water column concentrations (C_m), and the RMSE for Case A are provided in Table 8.

Table 7: Case A Potential Source Location Weights

Potential Source Location	Source weight (w)	Normalized source weight (w_n)
RM 4.1 SB	0.008	0.2
RM 1.4 WS	0	0
RM 0.8 SB	0.031	0.8
Sum	0.039	1

Table 8: Case A Measured and Calculated Total PCB Concentrations

RM	Measured Total PCB Concentration, C_m (pg/L)	Calculated Total PCB Concentration, C_c (pg/L)	RMSE (pg/L)
0.1 SB	220	419	125
0.5 SB	470	518	
2.2 SB	960	810	
4.3 SB	870	811	
4.8 SB	480	583	

The calculated absolute weights were applied to the potential source location unit concentration distributions. The modified unit concentration distributions were summed and visualized on heat maps to observe how measured data impacts the distributions. As the PE passive samplers were often not placed in the channel center, longitudinal heat maps were provided for the west bank, centerline, and east bank of the LDW in Figure 27. Locations of measured concentrations are outlined in red, while locations of potential sources are identified with an arrow.

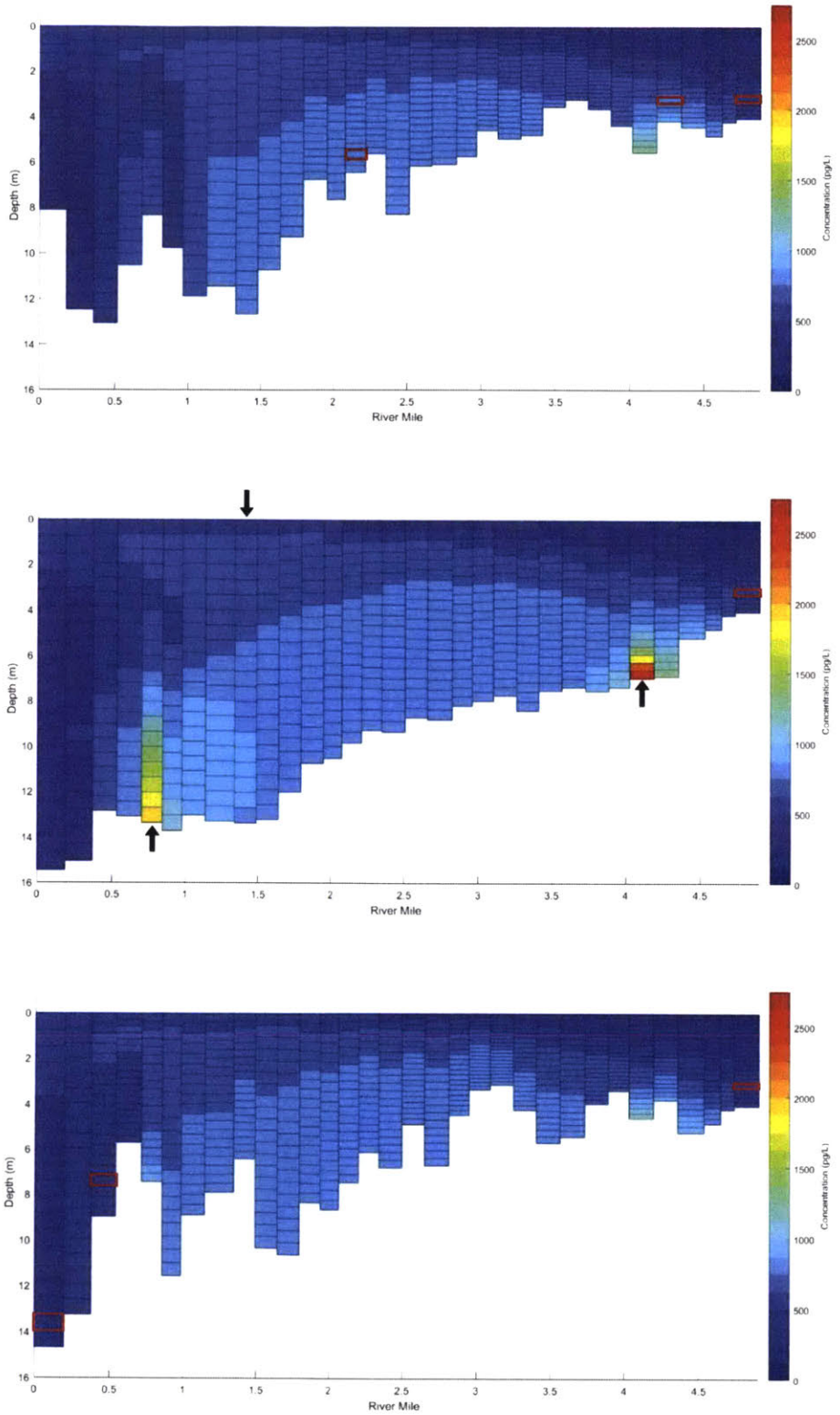

Figure 27: Case A Longitudinal Weighted Concentration Distributions at the West Bank (top), Centerline (middle), and East Bank (bottom)

The density-driven circulation drives the downstream water surface source out of the LDW before mixing upstream can occur. As such, the weight for the water surface source at RM 0.8 is zero, and the two sediment bed sources must be strong enough to generate the measured total PCB concentrations. As shown in Figure 27, the downstream sediment bed loading at RM 1.4 causes a build-up of concentration in the middle of the LDW, creating the measured concentration at RMs 0.1, 0.5, and 2.2. The upstream sediment bed loading at RM 4.1 causes a localized build-up of concentration between RM 4.0 and 4.5 before the density-driven circulation pulls it towards the water surface and downstream. This produces the measured concentrations at RM 4.3 and 4.8.

The sum of the source weight matrix (w) for Case A is 0.039; this translates to a required flux of 0.039 mg/s for these potential source locations to create the measured total PCB concentrations. Section 7.4 compares this required flux to known source information (i.e., diffusive flux and air-water exchange flux).

The procedure was repeated for each case described in Section 6.2.4. Figures, summary tables, and a brief discussion for each case are provided below.

Case B: Upstream water surface, downstream water surface, and downstream sediment bed sources compared to five sediment bed measured concentrations

Table 9: Case B Potential Source Location Weights

Potential Source Location	Source weight (w)	Normalized source weight (w_n)
RM 4.1 WS	0.050	0.7
RM 1.4 WS	0	0
RM 0.8 SB	0.022	0.3
Sum	0.072	1

Table 10: Case B Measured and Calculated Total PCB Concentrations

RM	Measured Total PCB Concentration, C_m (pg/L)	Calculated Total PCB Concentration, C_c (pg/L)	RMSE (pg/L)
0.1 SB	220	424	131
0.5 SB	470	512	
2.2 SB	960	825	
4.3 SB	870	775	
4.8 SB	480	606	

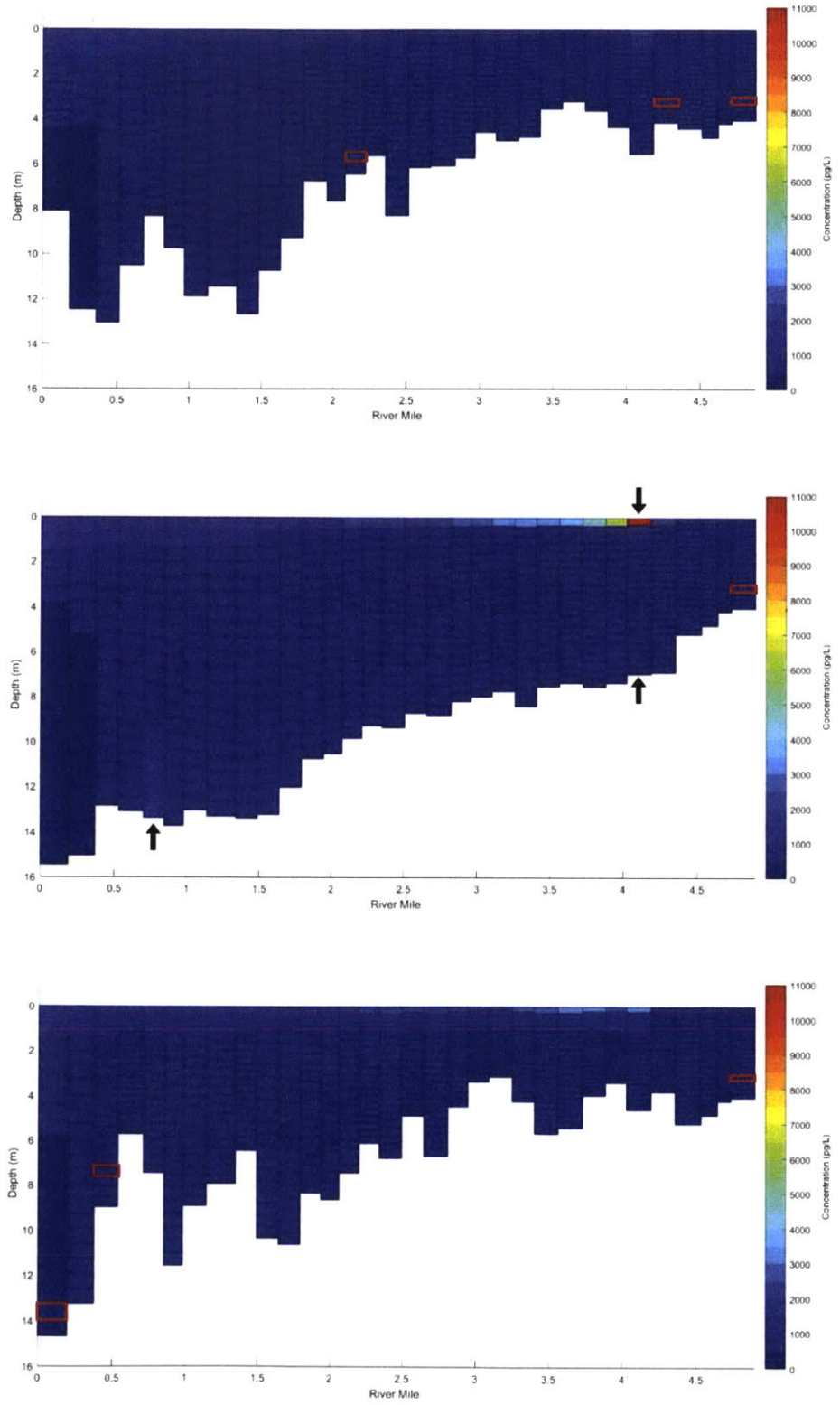

Figure 28: Case B Longitudinal Weighted Concentration Distributions at the West Bank (top), Centerline (middle), and East Bank (bottom)

When compared to Case A, a greater mass flux is required for Case B to produce the measured total PCB concentrations. The upstream water surface source at RM 4.1 has a high weight because it is the only potential source that can create the measured concentrations at the sediment bed of RM 4.3 and 4.8. The density-driven circulation does not carry the downstream sediment bed source at RM 0.8 far enough to significantly contribute to the upstream sediment bed concentrations. A significant weight is still necessary for the sediment bed source at RM 0.8 to create the measured concentrations at RM 0.1 and RM 0.5.

Excess mass is observed at the water surface downstream of the water surface source at RM 4.1, as shown in Figure 28. Freshwater flow carries this high loading downstream, generating consistently high total PCB concentrations across the LDW. As discussed in Section 7.2.2, PE samplers distributed along the water surface of the LDW would detect this relatively high concentration gradient and attribute the measured concentration to a water surface source.

Case C: Upstream, midstream, and downstream sediment bed sources compared to five sediment bed measured concentrations

Table 11: Case C Potential Source Location Weights

Potential Source Location	Source weight (w)	Normalized source weight (w_n)
RM 4.8 SB	0	0
RM 3.7 SB	0.016	0.37
RM 0.1 SB	0.027	0.63
Sum	0.042	1

Table 12: Case C Measured and Calculated Total PCB Concentrations

RM	Measured Total PCB Concentration, C_m (pg/L)	Calculated Total PCB Concentration, C_c (pg/L)	RMSE (pg/L)
0.1 SB	220	503	193
0.5 SB	470	383	
2.2 SB	960	677	
4.3 SB	870	869	
4.8 SB	480	615	

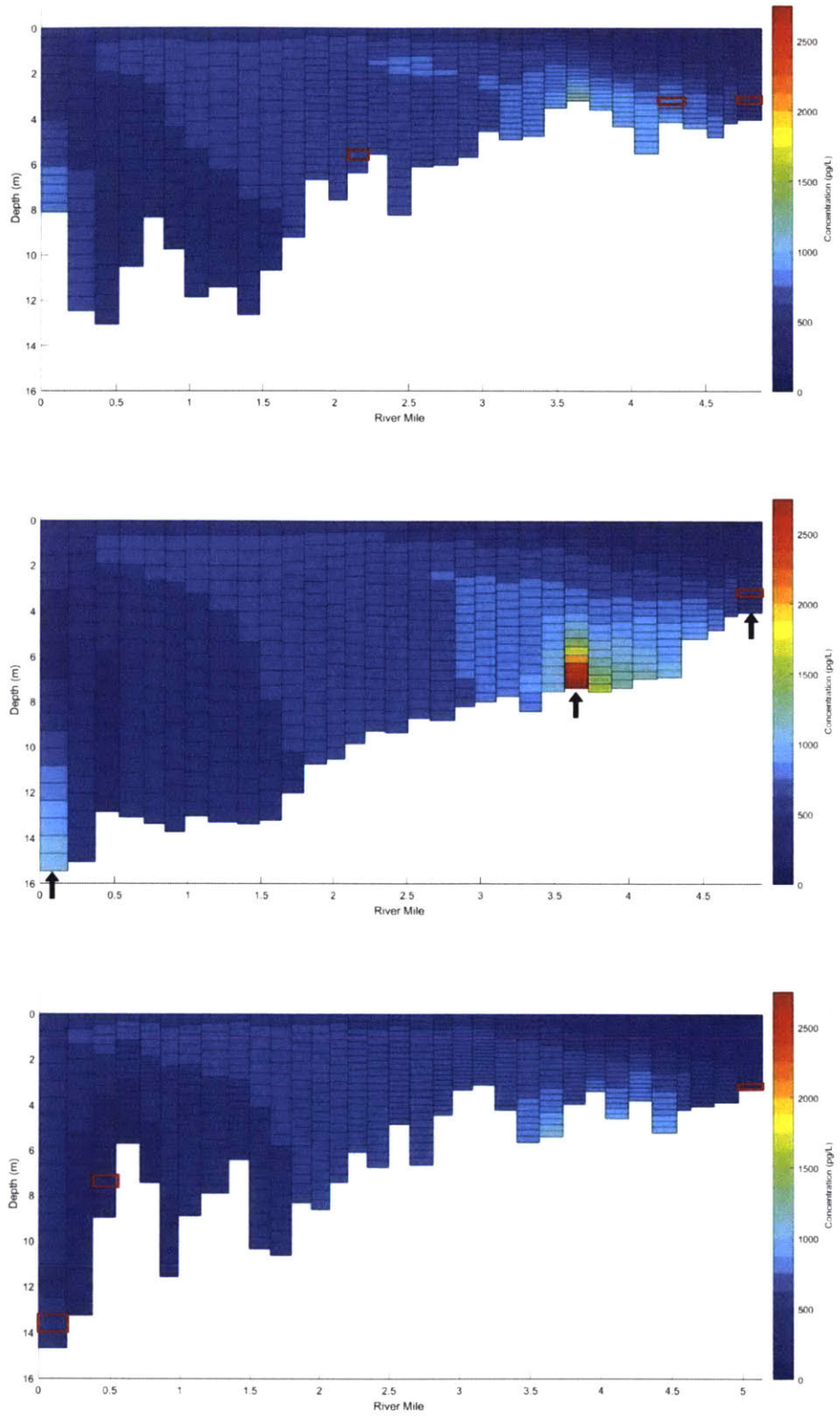

Figure 29: Case C Longitudinal Weighted Concentration Distributions at the West Bank (top), Centerline (middle), and East Bank (bottom)

The maximum concentration in Case C is approximately 3,000 pg/L, much less than the maximum concentration in Case B of approximately 11,000 pg/L. This is expected due to the smaller mass flux in Case C (mass flux of 0.042 mg/s) compared to Case B (mass flux of 0.072 mg/s). The midstream sediment bed source at RM 3.7 is strong enough to produce the measured concentrations at RMs 4.3 and 4.8 without contribution from the upstream sediment bed source at RM 4.8. Like Case A, the density-driven circulation pulls mass introduced at RM 3.7 upstream, creating a build-up of upstream concentration, before it is flushed out of the system.

The sediment bed source at RM 0.1 appears to contribute most of its mass to the measured concentrations at RM 0.1 before it is flushed out of the LDW. This is visible in Figure 29 by the band of lower concentrations between RM 0.1 and the measured concentration location at RM 0.5. The measured concentrations at RM 0.5 are likely a result of combining the potential sources from RM 0.1 and RM 3.7., as evidenced by the shape of the plume originating from RM 3.7.

Excess mass is observed midstream, approximately two meters below the water surface, as shown in Figure 29. This is attributed to the sediment bed sources at RMs 0.1 and 3.7 entering the density-driven circulation and dispersing. As discussed in Section 7.2.2, a PE sampler placed approximately two meters below the water surface would likely attribute the excess mass to a sediment bed source due to the inhibited vertical mixing between freshwater at the surface and saltwater at the sediment bed. However, PE samplers would also need to be placed at the water surface to evaluate total PCB concentrations, and resulting concentration gradients, near the surface for comparison.

Case D: Upstream and two midstream sediment bed sources compared to five sediment bed measured concentrations

Table 13: Case D Potential Source Location Weights

Potential Source Location	Source weight (w)	Normalized source weight (w_n)
RM 4.6 SB	0	0
RM 3.7 SB	0	0
RM 2.6 SB	0.034	1
Sum	0.034	1

Table 14: Case D Measured and Calculated Total PCB Concentrations

RM	Measured Total PCB Concentration, C_m (pg/L)	Calculated Total PCB Concentration, C_c (pg/L)	RMSE (pg/L)
0.1 SB	220	194	166
0.5 SB	470	268	
2.2 SB	960	743	
4.3 SB	870	952	
4.8 SB	480	687	

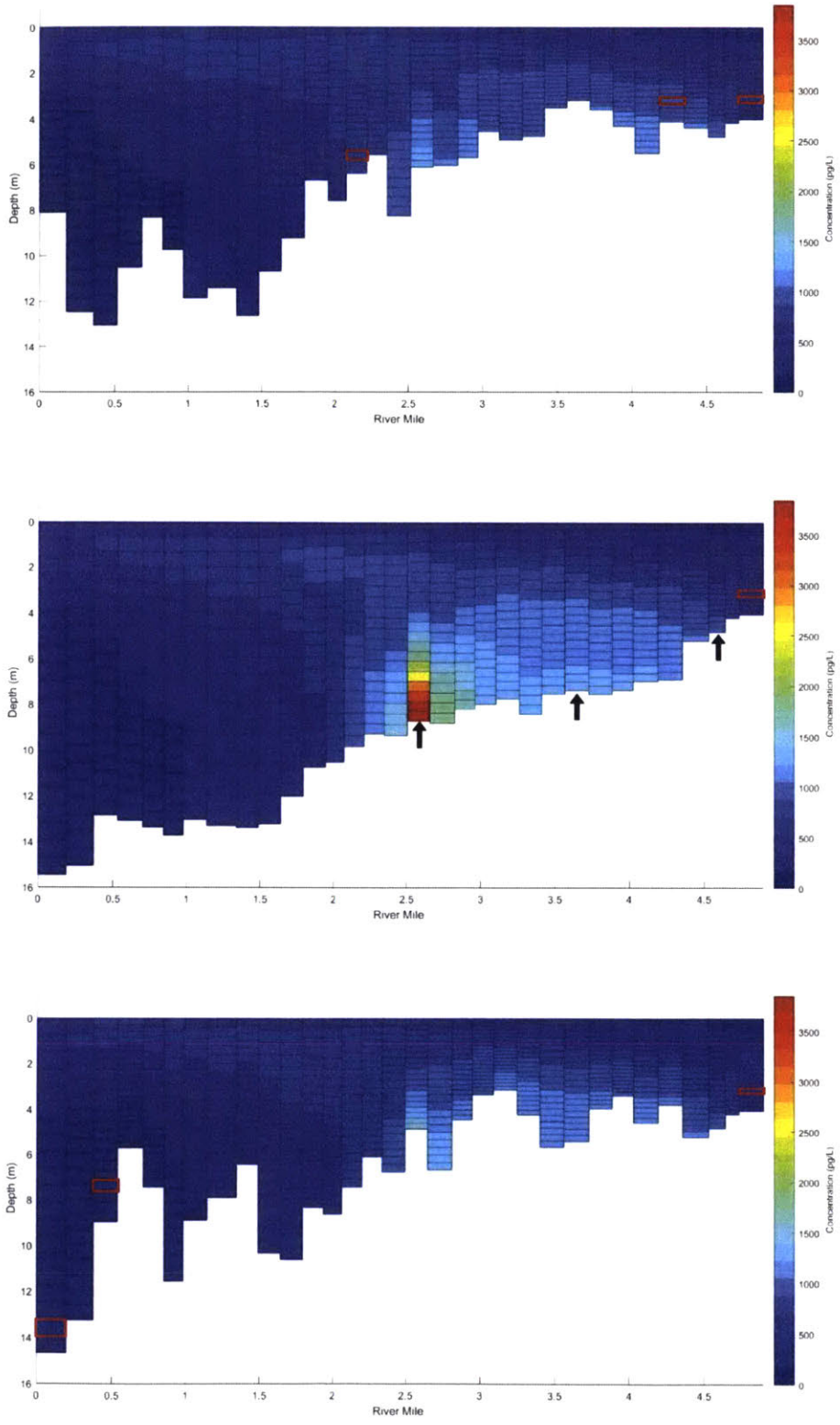

Figure 30: Case D Longitudinal Weighted Concentration Distributions at the West Bank (top), Centerline (middle), and East Bank (bottom)

Like Case C, the most upstream sources in Case D, located at RMs 4.6 and 3.7, do not contribute to the measured concentrations. The sediment bed source at RM 2.6 can produced all measured total PCB concentrations due to its calculated mass flux and dispersion by the density-driven circulation. While the calculated mass flux for Case D (0.034 mg/s) is slightly less than Case C (0.042 mg/s), higher maximum concentrations were observed in Case D (4,000 pg/L) than Case C (3,000 pg/L). This is due to the different number of potential sources in each case; the sole source in Case D provides all the mass in the system, creating concentration build-up at its location. The two sources in Case C have individual weights less than the source in Case D, so that the concentration build-up near the source locations in Case C is less than Case D.

As shown in Figure 30, excess mass is observed downstream of RM 2.6 near the water surface and upstream of RM 2.6 near the middle and near the sediment bed of the channel. As discussed with Case C, PE passive samplers placed two meters below the water surface would identify the source as a sediment bed source due to inhibited vertical mixing. However, PE passive samplers placed only at the water surface may attribute this concentration to a water surface source. Both are necessary to correctly determine the concentration gradient near the water surface and subsequently attribute the sources as sediment bed sources.

Case E-1: One upstream water surface, one upstream sediment bed, one downstream water surface, and one downstream sediment bed sources compared to five sediment bed measured concentrations

Table 15: Case E-1 Potential Source Location Weights

Potential Source Location	Source weight (w)	Normalized source weight (w_n)
RM 4.7 WS	0.027	0.51
RM 4.5 SB	0	0
RM 0.8 WS	0	0
RM 0.8 SB	0.026	0.49
Sum	0.053	1

Table 16: Case E-1 Measured and Calculated Total PCB Concentrations

RM	Measured Total PCB Concentration, C_m (pg/L)	Calculated Total PCB Concentration, C_c (pg/L)	RMSE (pg/L)
0.1 SB	220	419	130
0.5 SB	470	515	
2.2 SB	960	823	
4.3 SB	870	780	
4.8 SB	480	606	

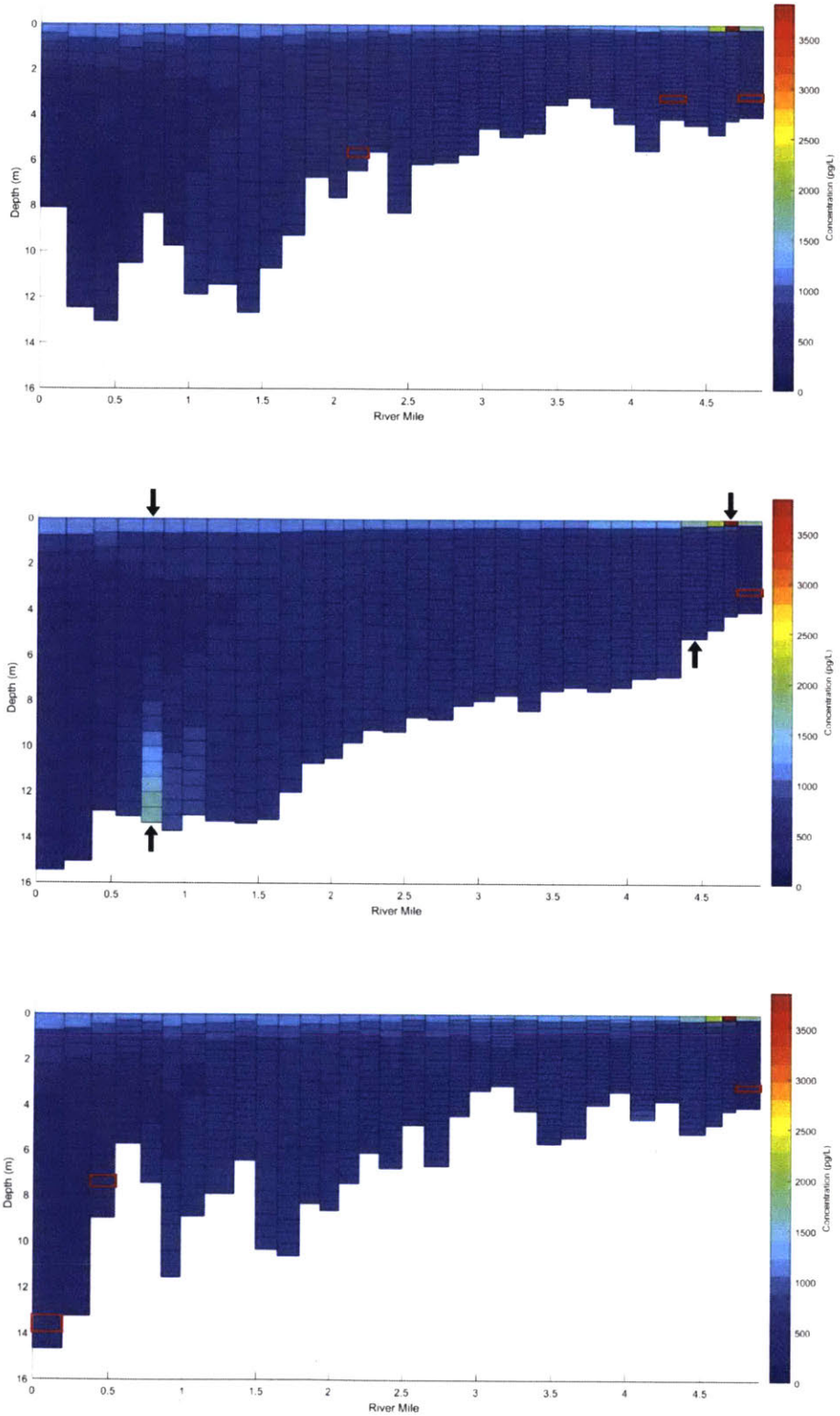

Figure 31: Case E-1 Longitudinal Weighted Concentration Distributions at the West Bank (top), Centerline (middle), and East Bank (bottom)

The Inverse Model selected the upstream water surface source at RM 4.7 to be the best fit for the upstream sediment bed measured concentrations at RM 4.3 and 4.8. The potential sediment bed source at RM 4.5 may not be carried far enough by the density-driven circulation to build concentration at the measured locations before it is flushed out of the LDW. To generate the sediment bed concentrations measured at RM 4.3 and 4.8, the water surface source at RM 4.7 must have a high mass flux, which is reflected as a high buildup of concentration near the source location. The sediment bed source located at RM 0.8 is the main contributor to the measured concentrations at RMs 0.1, 0.5, and 2.2. The density-driven circulation pulls the mass loading upstream before it leaves the system, resulting in concentration building up between RMs 0.8 and 3. The water surface source at RM 4.7 contributes to the measured concentration at RM 2.2 due to the high loading introduced to the system at the source location.

Like Case B, excess mass is observed in Figure 31 at the water surface downstream of the water surface source at RM 4.7 due to freshwater flow carrying the loading downstream. A PE sampler placed at the water surface would detect this high concentration, and resulting concentration gradient, down the length of the LDW and attribute it to a water surface source.

Case E-2: One upstream water surface, one upstream sediment bed, one downstream water surface, and one downstream sediment bed sources compared to five sediment bed measured concentrations

Table 17: Case E-2 Potential Source Location Weights

Potential Source Location	Source weight (w)	Normalized source weight (w_n)
RM 4.6 WS	0	0
RM 4.1 SB	0.0028	0.07
RM 1.4 WS	0	0
RM 1.4 SB	0.036	0.93
Sum	0.039	1

Table 18: Case E-2 Measured and Calculated Total PCB Concentrations

RM	Measured Total PCB Concentration, C_m (pg/L)	Calculated Total PCB Concentration, C_c (pg/L)	RMSE (pg/L)
0.1 SB	220	327	72.5
0.5 SB	470	413	
2.2 SB	960	953	
4.3 SB	870	804	
4.8 SB	480	564	

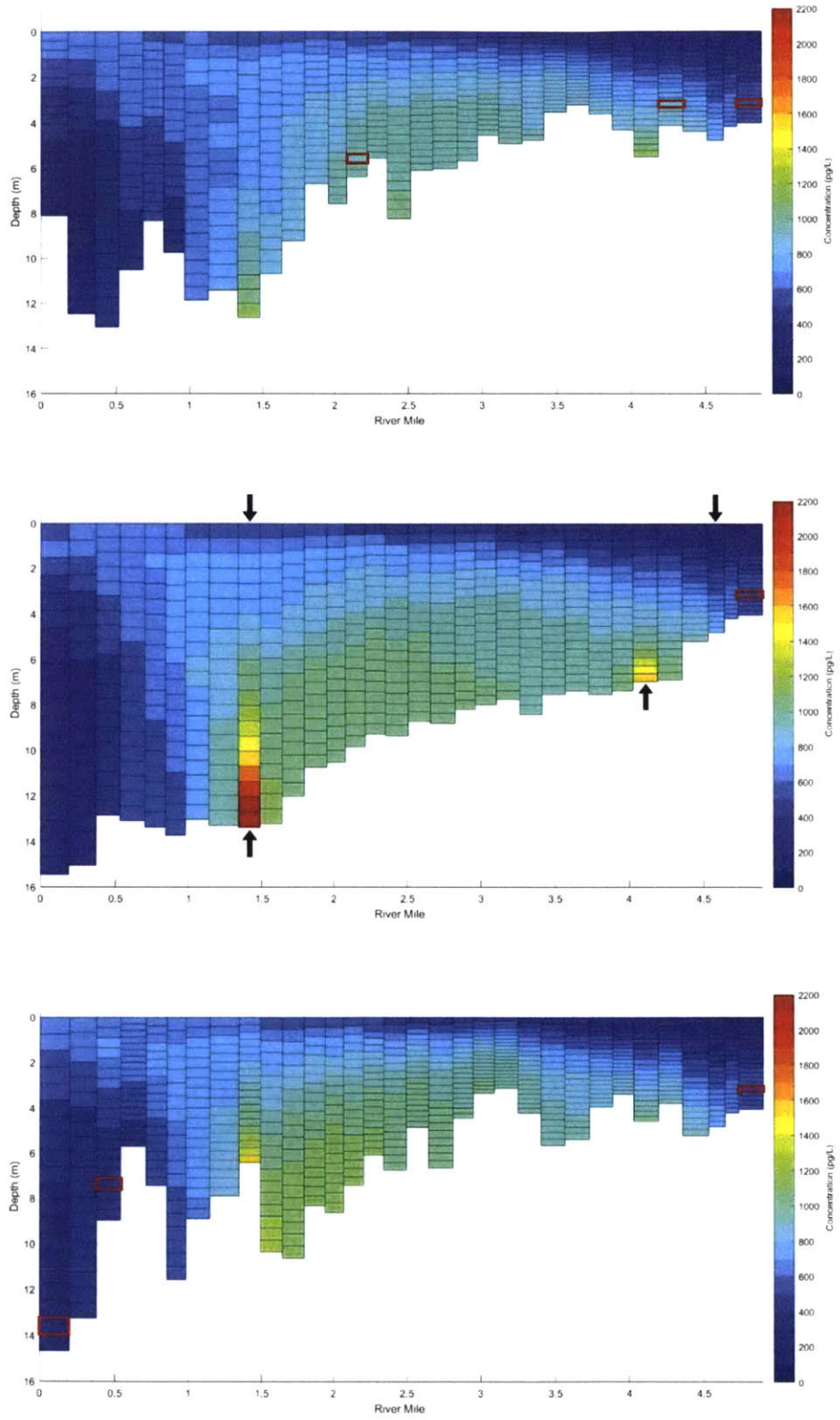

Figure 32: Case E-2 Longitudinal Weighted Concentration Distributions at the West Bank (top), Centerline (middle), and East bank (bottom)

Case E-2 simulates different potential source locations in the same vicinity as the potential source locations in Case E-1. This results in mass loadings from the two selected sediment bed source locations (RM 4.1 and RM 1.4) and no mass loading from the two selected water surface source locations (RM 4.6 and RM 1.4). As evidenced by the RMSE, the Inverse Model achieved a better fit for the measured concentrations with Case E-2 than Case E-1 (72.5 versus 130). While this doesn't indicate Case E-2 is more likely to occur in the LDW than Case E-1, it does show that sediment bed sources are a better fit for sediment bed measured concentrations than water surface sources.

The sediment bed source at RM 1.4 generates most of the concentration distribution observed in Figure 32. The midstream unit concentration distribution originating from RM 1.4 is higher than that originating from RM 4.1, as seen in Figure 23. As such, the higher weight of the RM 1.4 source provides most of the mass for the measured concentrations in this case. The source located at RM 4.1 supplements the signature from RM 1.4 for the measured concentrations at RM 4.3 and 4.8, and it does not significantly contribute to the measured concentrations at RM 2.2, 0.5, and 0.1.

Case E-2 exhibits a similar pattern of excess mass as Case A; mass builds up midstream near the sediment bed and the mid-depth before the density-driven current removes it from the LDW. PE samplers placed at the midstream sediment bed or at the downstream surface water would detect these areas of excess mass. Additional PE samplers would be required in the midstream water column and upstream surface water to appropriately measure the vertical concentration gradient and assign the excess mass to sediment bed sources, not additional upstream water surface sources.

Case F-1: One upstream water surface, one upstream sediment bed, one downstream water surface, and one downstream sediment bed sources compared to three sediment bed and two surface water measured concentrations

Table 19: Case F-1 Potential Source Location Weights

Potential Source Location	Source weight (w)	Normalized source weight (w_n)
RM 4.5 SB	0.007	0.18
RM 4.5 WS	0.001	0.04
RM 0.8 SB	0.031	0.78
RM 0.8 WS	0	0
Sum	0.040	1

Table 20: Case F-1 Measured and Calculated Total PCB Concentrations

RM	Measured Total PCB Concentration, C_m (pg/L)	Calculated Total PCB Concentration, C_c (pg/L)	RMSE (pg/L)
0.1 SB	220	423	204
0.9 WS	280	597	
2.2 SB	960	812	
4.3 SB	870	705	
4.7 WS	420	287	

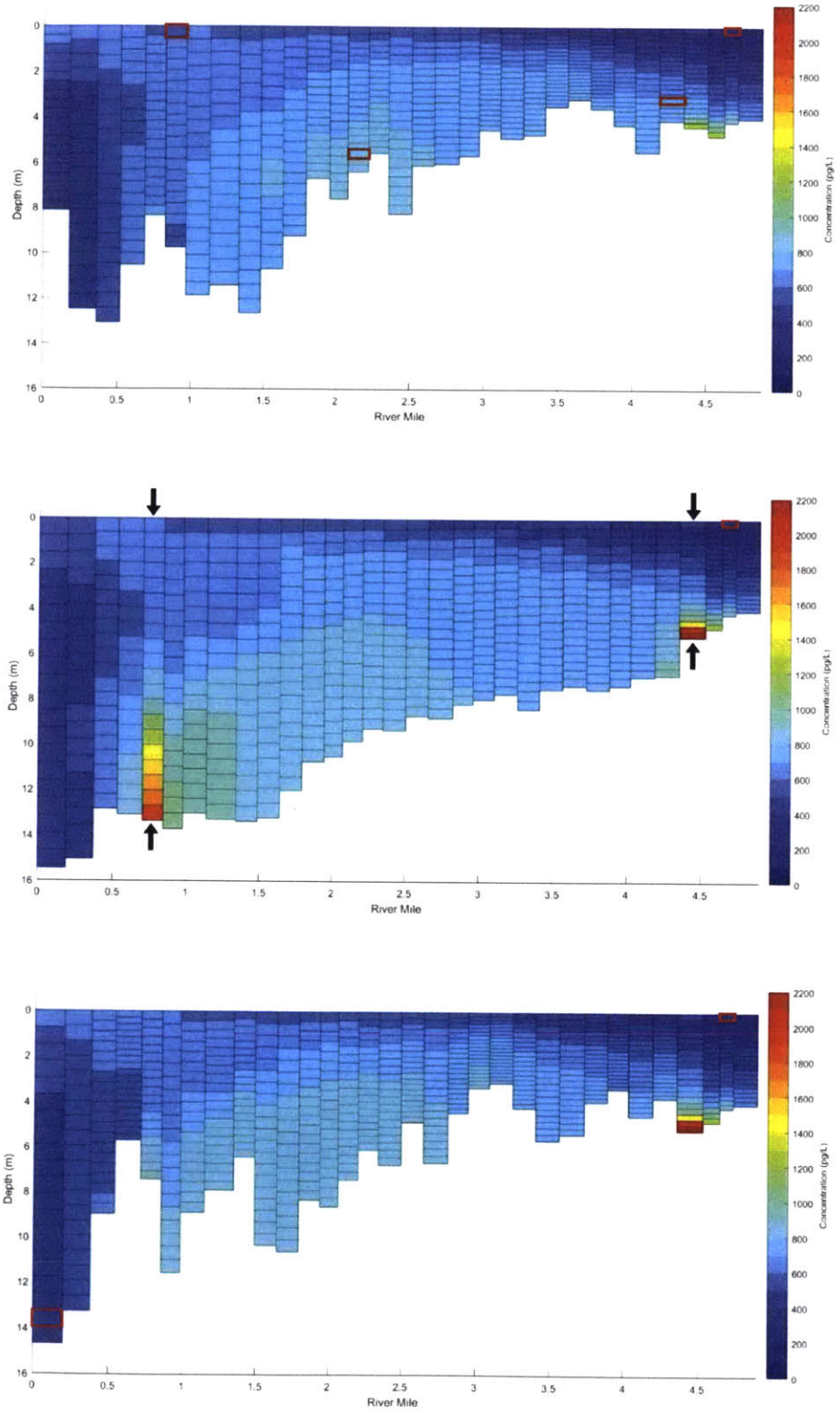

Figure 33: Case F-1 Longitudinal Weighted Concentration Distributions at the West Bank (top), Centerline (middle), and East Bank (bottom)

Case F-1 expands Case E by substituting two measured sediment bed concentrations (RM 0.5 and 4.8) for two measured water surface concentrations (RM 0.9 and 4.7). While the measured surface water concentrations and the measured sediment bed concentrations were collected one year apart, this analysis assumed conditions do not significantly change in one year.

The addition of measured water surface sources slightly altered the distribution of the weighted unit concentrations from Case E-2; a small weight was assigned to the upstream water surface source at RM 4.5, while most of the mass flux still originates from the downstream sediment bed source at RM 0.8. As such, the downstream sediment bed source still generates most of the mass observed in Figure 31. The upstream sediment bed source contributes to the concentrations measured at the sediment bed of RM 4.3 and the water surface of RM 0.9; however, the density driven circulation pulls this source downstream, preventing significant contribution to the water surface source at RM 4.7. Therefore, a mass flux from the potential water surface source at RM 4.5 is necessary. Tidal influence at RM 4.5 disperses the mass flux upstream towards RM 4.7, which supplements the mass originating from the sediment bed of RM 0.8.

The water surface source at RM 4.5 is carried downstream with freshwater flow, increasing water surface concentrations downstream of its location, as observed on Figure 33. This slightly increases the measured concentrations along the water surface and is subsequently captured by the measured water surface concentration at RM 0.9. However, a majority of the mass flux originates from sediment bed samples, particularly from RM 0.8. Higher concentrations of total PCBs at the water surface than at the sediment bed, in addition to vertical concentration gradient measurements, would be necessary to differentiate a potential water surface source location from a potential sediment bed source location.

Case F-2: One upstream water surface, one upstream sediment bed, one downstream water surface, and one downstream sediment bed sources compared to three sediment bed and two surface water measured concentrations

Table 21: Case F-2 Potential Source Location Weights

Potential Source Location	Source weight (w)	Normalized source weight (w_n)
RM 4.1 SB	0.003	0.07
RM 4.6 WS	0.002	0.06
RM 1.4 SB	0.032	0.87
RM 1.4 WS	0	0
Sum	0.037	1

Table 22: Case F-2 Measured and Calculated Total PCB Concentrations

RM	Measured Total PCB Concentration, C_m (pg/L)	Calculated Total PCB Concentration, C_c (pg/L)	RMSE (pg/L)
0.1 SB	220	299	167
0.9 WS	280	591	
2.2 SB	960	867	
4.3 SB	870	747	
4.7 WS	420	310	

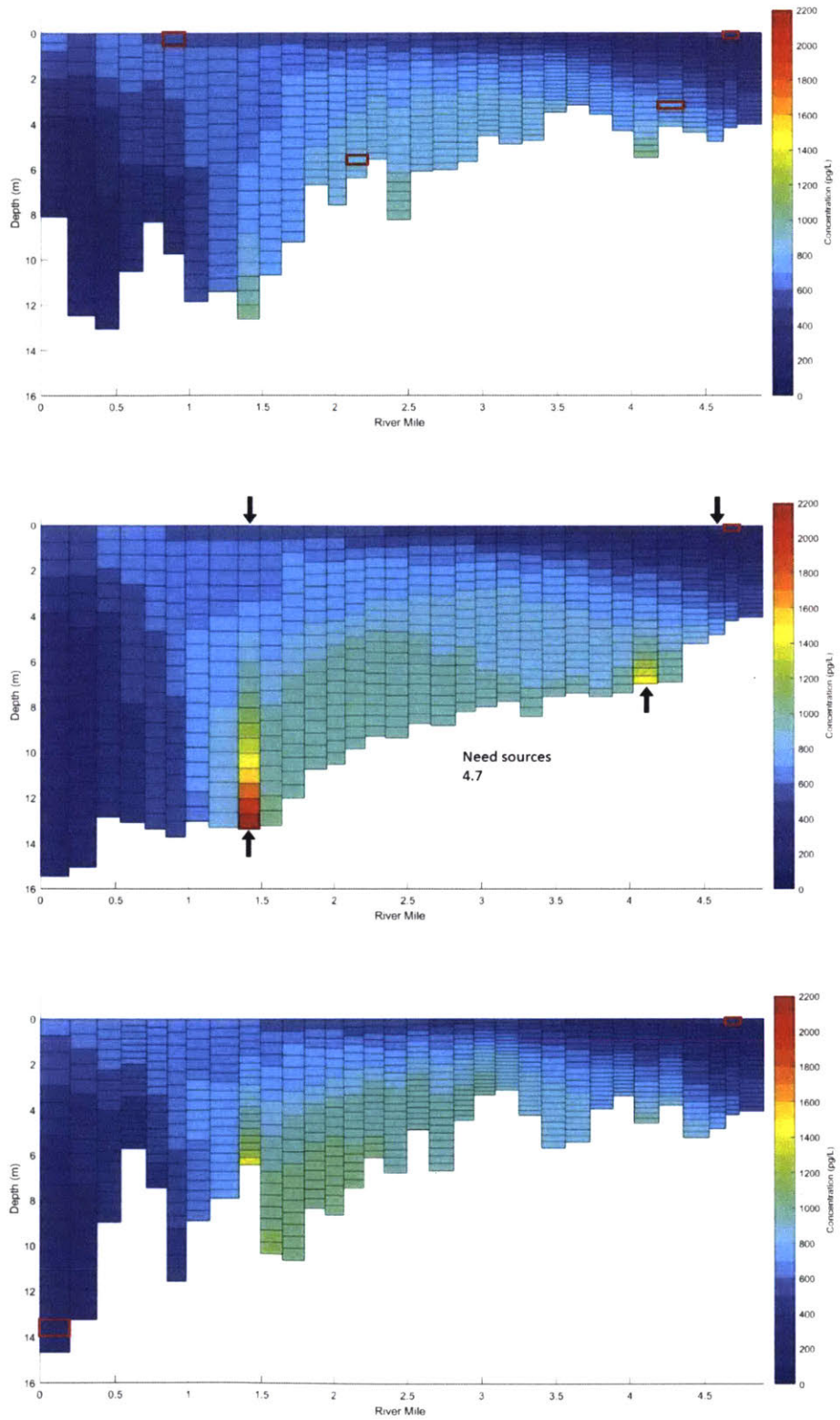

Figure 34: Case F-2 Longitudinal Weighted Concentration Distribution at the West Bank (top), Centerline (middle), and East Bank (bottom)

Case F-2 simulates different potential source locations in the same vicinity as the potential source locations in Case F-1. Unlike the difference between Case E-1 and E-2, which resulted in a potential water surface source location shifting to a potential sediment bed source location, the difference between Case F-1 and F-2 is a redistribution of mass flux among the same potential source vicinities. The upstream sediment bed source decreased its mass flux, the upstream water surface source increased its mass flux, and the downstream sediment bed source increased its mass flux. Based on the RMSE, Case F-2 (RSME of 167) is a better fit for the measured data than Case F-1 (RSME of 204). While this doesn't indicate Case F-2 is more likely to occur in the LDW than Case F-1, it does show that the distribution of the Case F-2 sources is a better fit for the measured concentrations than Case F-1.

While the plume shapes are generally the same in both Case F simulations, the sediment bed source locations in Case F-2 (RM 1.4 and 4.1) are closer together than in Case F-1 (RM 0.8 and 4.5). This causes a build-up of mass that results in higher midstream concentrations near the sediment bed, as shown in Figure 34. A PE sampler placed in this area can detect this concentration; with other PE sampler data, it may indicate the presence of two sediment bed sources instead of a new midstream sediment bed source.

Case G-1: One upstream water surface, one upstream sediment bed, one downstream water surface, and one downstream sediment bed sources compared to five sediment bed and three surface water measured concentrations

Table 23: Case G-1 Potential Source Location Weights

Potential Source Location	Source weight (w)	Normalized source weight (w_n)
RM 4.5 SB	0.004	0.12
RM 4.5 WS	0.001	0.02
RM 0.8 SB	0.032	0.86
RM 0.8 WS	0	0
Sum	0.037	1

Table 24: Case G-1 Measured and Calculated Total PCB Concentrations

RM	Measured Total PCB Concentration, C_m (pg/L)	Calculated Total PCB Concentration, C_c (pg/L)	RMSE (pg/L)
0.1 SB	220	421	233
0.5 SB	470	517	
0.9 WS	280	516	
2.0 WS	280	484	
2.2 SB	960	790	
4.3 SB	870	619	
4.7 WS	420	221	
4.8 SB	480	488	

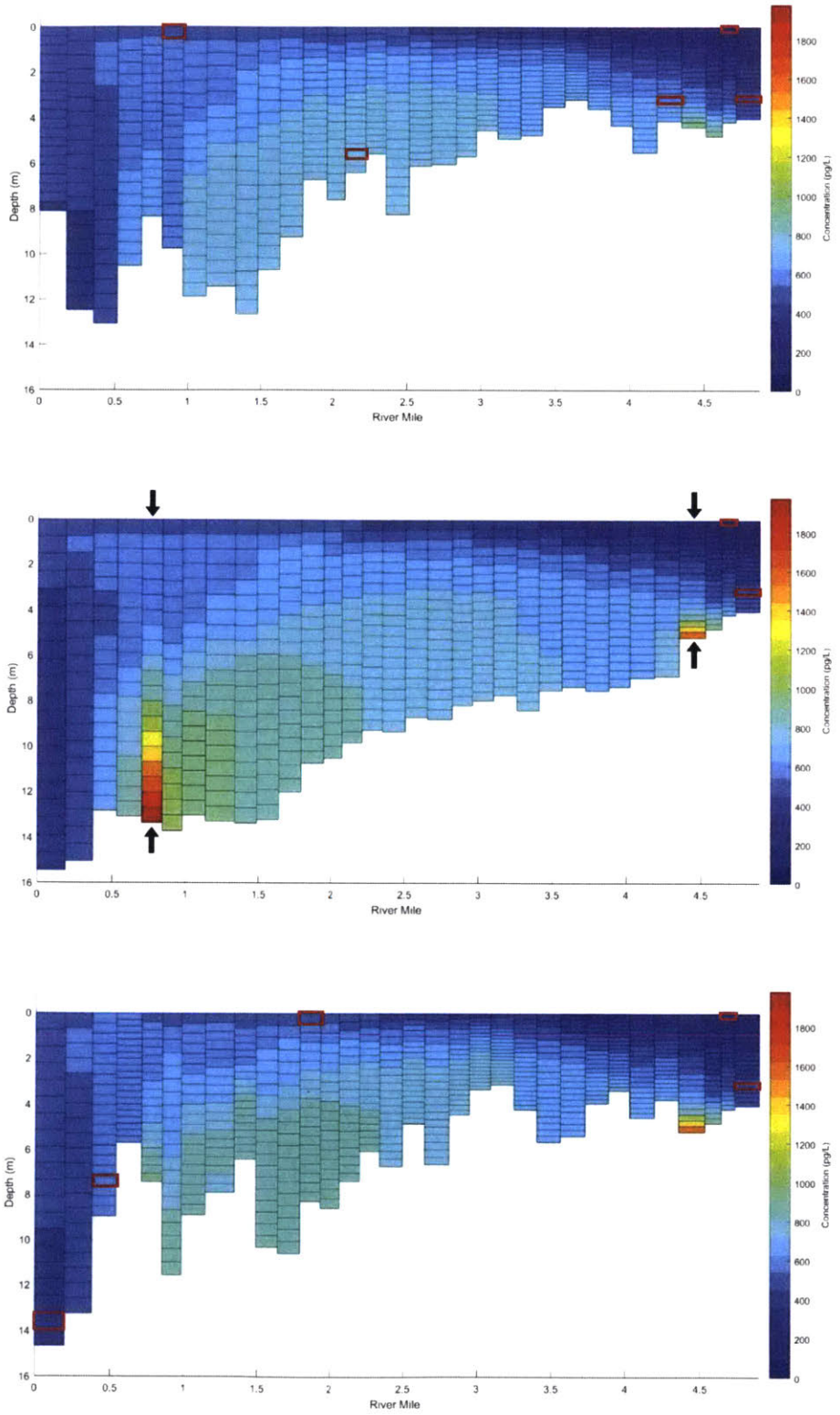

Figure 35: Case G-1 Longitudinal Weighted Concentration Distributions at the West bank (top), Centerline (middle), and East Bank (bottom)

Case G-1 mirrors Case F-1; the downstream sediment bed source at RM 0.8 contributes the most mass to the system and is the main source for all measured concentrations. The upstream sediment bed source at RM 4.5 contributes to the concentrations measured at the sediment bed of RM 4.3, the water surface of RM 2.0, and the water surface of RM 0.9; however, the density driven circulation pulls this source downstream, preventing significant contribution to the water surface source at RM 4.7. Therefore, a mass flux from the potential water surface source at RM 4.5 is necessary. Tidal influence at RM 4.5 disperses the mass flux upstream towards RM 4.7, which supplements the mass originating from the sediment bed of RM 0.8.

Compared to Case F-1, slightly increased concentrations are observed downstream near the sediment bed due to the reintroduction of the measured concentration at RM 0.5, as shown in Figure 35. In addition, the total mass flux required and the RMSE differs for both cases (Case G-1 mass flux is 0.037 mg/s with RSME 233, while Case F-1 mass flux is 0.039 mg/s with RSME 2014). Otherwise, the plume evolution, general concentration distribution, and general conclusions are similar for Case G-1 and Case F-1.

Case G-2: One upstream water surface, one upstream sediment bed, one downstream water surface, and one downstream sediment bed sources compared to five sediment bed and three surface water measured concentrations

Table 25: Case G-2 Potential Source Location Weights

Potential Source Location	Source weight (w)	Normalized source weight (w_n)
RM 4.1 SB	0.0003	0.01
RM 4.6 WS	0.001	0.04
RM 1.4 SB	0.034	0.95
RM 1.4 WS	0	0
Sum	0.036	1

Table 26: Case G-2 Measured and Calculated Total PCB Concentrations

RM	Measured Total PCB Concentration, C_m (pg/L)	Calculated Total PCB Concentration, C_c (pg/L)	RSME (pg/L)
0.1 SB	220	305	203
0.5 SB	470	384	
0.9 WS	280	543	
2.0 WS	280	502	
2.2 SB	960	883	
4.3 SB	870	675	
4.7 WS	420	249	
4.8 SB	480	469	

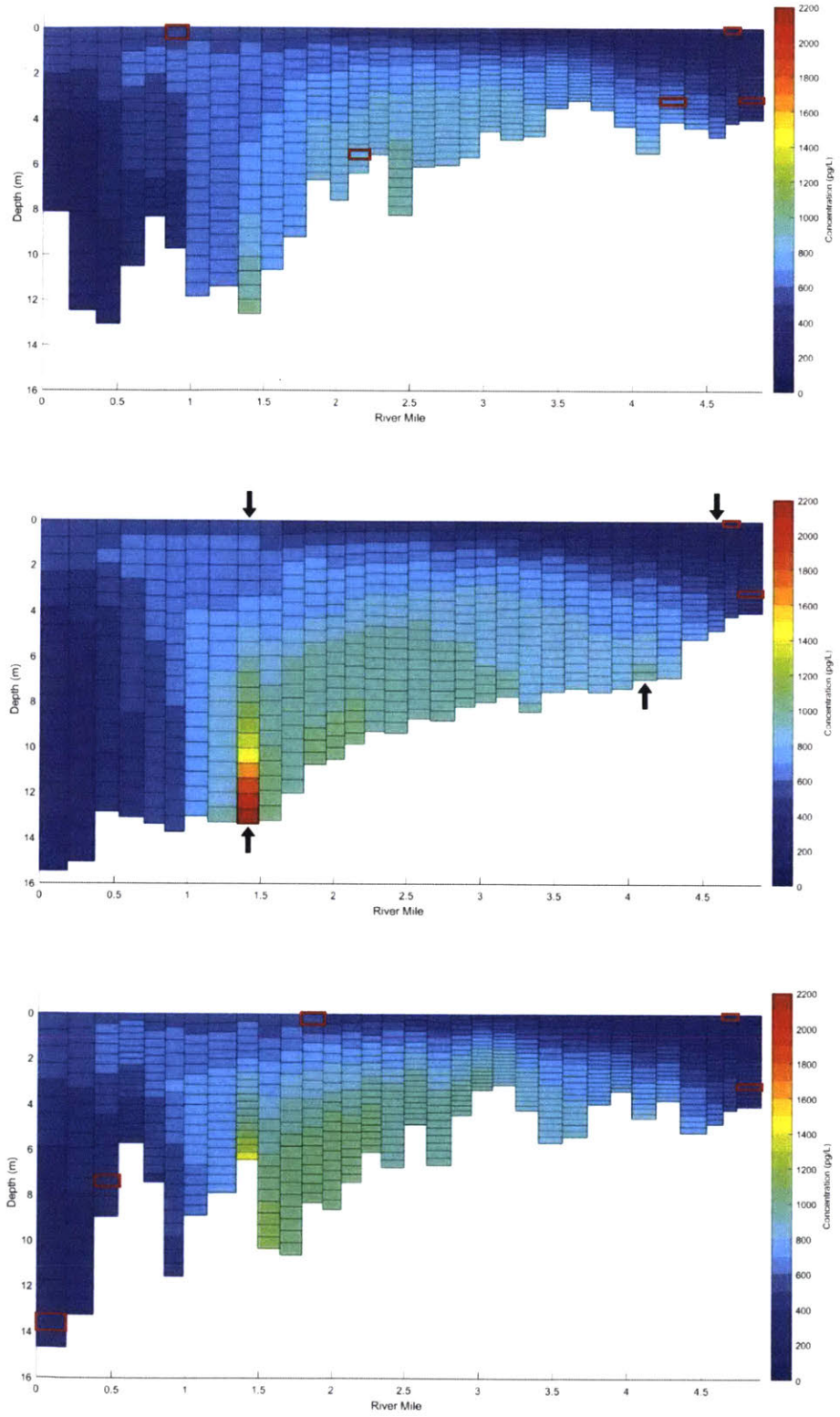

Figure 36: Case G-2 Longitudinal Weighted Concentration Distributions at the West Bank (top), Centerline (middle), and East Bank (bottom)

Case G-2 mirrors Case F-2; the downstream sediment bed source at RM 1.4 contributes the most mass to the system and is the main source for all measured concentrations observed in Figure 36. The upstream surface water source at RM 4.1 contributed to the measured concentrations at the water surface of RMs 0.9, 2.2, and 4.7 and at the sediment bed of RM 4.3. The upstream sediment bed source at RM 4.1 had the smallest mass flux, but it supplemented the source at RM 1.4 for the water surface measured concentrations and the upstream sediment bed measured concentration at RM 4.3.

Compared to Case G-1, the mass flux for the downstream sediment bed source and the upstream water surface source in Case G-2 were comparable. However, the mass flux for the upstream sediment bed source decreased by an order of magnitude between the cases (Case G-1 had a mass flux for RM 4.5 of 0.004, while Case G-2 had a mass flux for RM 4.1 of 0.0003). This indicates the distance between the upstream potential sources and downstream potential sources is important to mass flux. A greater distance between upstream and downstream sediment bed sources requires a higher mass input from upstream sediment bed sources because the downstream source is not carried far enough to generate the measured concentrations as the plume concentration decreases. Alternatively, it indicates that potential downstream sediment bed sources placed further upstream into the salt wedge experience more transport due to the density-driven circulation and do not need significant contribution for upstream sediment bed sources to generate the measured concentrations.

7.4 Comparison to Known Source Information

The Inverse Model produced estimated mass fluxes (the sum of the weights) that would be required from potential source locations to produce the measured total PCB concentrations in the water column of the LDW. A summary of these fluxes, and the associated RMSE, by case is provided in Table 27.

Table 27: Summary of Mass Fluxes Predicted by the Inverse Model

Case	RSME (pg/L)	Calculated Flux (mg/s)
A	125	0.039
B	131	0.072
C	193	0.042
D	166	0.034
E-1	130	0.053
E-2	72.5	0.039
F-1	204	0.040
F-2	267	0.037
G-1	233	0.037
G-2	203	0.036
Mean	163	0.043

MIT previously studied two potential source fluxes, as described in Section 4.0: diffusive sediment-water flux from the sediment bed and air-water exchange flux from the water surface. The resulting fluxes from these analyses were approximately 130 ng/m^2/day (Prendergast et al., 2018) and 63 ng/m^2/day (Apell & Gschwend, 2017), respectively. Over the entire surface area of the LDW (1,800,000 m^2), these fluxes sum to approximately 0.004 mg/s, an order of magnitude lower than the Inverse Model requires.

Known source fluxes are not large enough to create the measured water column concentrations. Therefore, one or more "missing sources" are present and contribute to the measured concentrations observed in the LDW. Potential missing sources include resuspension of the sediment bed by propwash, additional sorbed or dissolved PCBs introduced from CSOs or upstream sources, desorption of PCBs from the sediment bed and banks, bioirrigation of porewater by benthic organisms, and groundwater seeps meeting the banks of the LDW. Additional PE passive sampler measurements (for dissolved phase) and traditional sediment sampling would be required in suspected areas of PCB contamination to further evaluate potential source locations and fluxes.

Except for Case B, the maximum concentration for the Inverse Model Cases was an order of magnitude higher than the measured water column concentrations (Case B was two orders of magnitude higher). This indicates the source location has likely not been directly measured by PE passive samplers, but it is located near the higher measured concentrations. Considering the general trends observed in the Inverse Model Cases, the water column and surface water data indicate a missing source may be on the sediment bed, generating concentration near RMs 2.2 and 4.3, and may be at the water surface, contributing to the measured concentrations near RM 4.7. Additional measured water column concentrations are necessary, particularly at the water surface and mid-depth, to more fully evaluate vertical, horizontal, and longitudinal concentration gradients, plot a potential plume shape, and hypothesize where sources are most likely located.

8.0 Conclusion

The LDW EFDC model appropriately characterized the LDW as a vertically stratified, salt wedge estuary. The extent of salinity intrusion from Elliott Bay depends on the spring-neap tidal cycle and the strength of freshwater flow from the Green/Duwamish River. This results in a density-driven circulation that initially carries dense saltwater upstream within the salt wedge before flow is reversed by freshwater flowing downstream. Due to this flow pattern, mean residence times are longer for sources that originate at the mid-downstream sediment bed, followed by upstream bed sources, downstream bed sources, upstream surface sources, and downstream surface sources.

Potential source locations in the LDW were evaluated by spatially comparing unit strength concentration distributions of lateral, vertical, and longitudinally distributed sources. The calculated lateral mixing time (1.5 days) was less than the average residence time of the LDW (1.9 days); as such, sources that originate on opposite banks were generally indistinguishable by a PE passive sampler placed at the center of the LDW within a mixing distance of approximately 0.8 miles. However, PE passive samplers placed near the bank of the LDW will be biased towards sources on that bank, indicating a potential source is likely located on that bank within 0.8 miles. Concentration distributions from vertical separated sources were generally distinguishable from each other midstream and upstream due to inhibited vertical mixing across the salt wedge. While both sediment bed sources and surface water sources result in measurable concentrations at the downstream water surface, the vertical concentration gradient was much higher for water surface sources than for sediment bed sources. As such, water surface sources are distinguishable from sediment bed sources due to their thin layer of high concentration trapped at the water surface. Longitudinally distributed sources were generally distinguishable for approximately 0.5 miles; longer distances were simulated for water surface sources because the density-driven circulation inhibits upstream surface water flow and dispersion. The tidal excursion (1.2 miles) was greater than the source spacing (approximately 0.3 miles) and comparable to the distinguishable distance (approximately 1 to 1.4 miles), indicating the tidal excursion effectively creates indistinguishable unit strength concentration distributions.

The importance of source location to contributing water column contamination was evaluated with an Inverse Model. Ten cases were conducted to determine the mass flux required to generate a set of PE passive sampler measured concentrations. Different combinations of measured water column samples collected near the sediment bed and at the surface water were input to the model for comparison to a variety of modeled unit strength concentration distributions. The Inverse Model

weighted the unit concentration distributions with non-negative least squares techniques (to prevent a negative mass flux). The fluxes were applied to the unit concentration distributions to calculate a weighted water column concentration, which was compared to the measured water column concentrations using RSME. For the 10 cases, the average RSME was approximately 163 pg/L (compared to an average concentration of approximately 560 pg/L) and the average mass flux was approximately 0.043 mg/s.

Compared to known source fluxes, the calculated mass flux is an order of magnitude higher, indicating one or more missing sources continue to impact the LDW. However, general trends observed during Inverse Modeling provided insight to potential source locations. The maximum concentration observed at modeled potential source locations was typically an order of magnitude higher than the measured water column and surface water concentrations considered. Therefore, the source location(s) has likely not been directly measured by PE passive samplers; but, the source(s) may have been indirectly measured at the locations of highest measured concentrations. The water column and surface water data considered for this study indicate a missing source may be near the midstream sediment bed, the upstream sediment, and the upstream water surface.

As previously discussed, additional measured water column concentrations are necessary, particularly at the water surface and mid-depth, to more fully evaluate vertical, horizontal, and longitudinal concentration gradients, plot a potential plume shape, and hypothesize where sources are most likely located. PE passive sampling data collected in 2016 will provide a better understanding of freely dissolved water column PCB concentrations, and this combined method of modeling and PE passive sampling can be used to better understand contamination source locations with new data.

References

AECOM. (2012). *Executive Summary: Final Feasibility Study, Lower Duwamish Waterway, Seattle, Washington.* Seattle.

AECOM. (2016). *Removal Action Construction Report: Phase 1: Sediment and Upland Cleanup.* Seattle.

Anchor Environmental, LLC. (2007). *Duwamish/Diagonal Sediment Remediation Project 4-Acre Residuals Interim Action Closure Report.*

Apell, J., & Gschwend, P. (2014). Validating the Use of Performance Reference Compounds in Passive Samplers to Assess Porewater Concentrations in Sediment Beds. *Environmental Science & Technology, 48*, 10301-10307.

Apell, J., & Gschwend, P. (2016). In situ passive sampling of sediments in the Lower Duwamish Waterway Superfund site: Replicability, comparison with ex situ measurements, and use of data. *Environmental Pollution, 218*, 95-101.

Apell, J., & Gschwend, P. (2017). The atmosphere as a source/sink of polychlorinated biphenyls to/from the Lower Duwamish Waterway Superfund site. *Environmental Pollution, 227*, 263-270.

Apell, J., & Prendergast, D. (2015, May). Dissolved PCB Measurements Using Polyethylene Passive Sampler: Unpublished Raw Data. Seattle, Washington.

Boeing. (n.d.). *Cleaning an Urban Waterway*. Retrieved April 4, 2018, from Boeing: http://www.boeing.com/principles/environment/duwamish/cleanup.page

Boeing. (n.d.). *Duwamish Waterway*. Retrieved April 4, 2018, from Boeing: http://www.boeing.com/principles/environment/duwamish/index.page

Dynamic Solutions International, LLC, EFDC Explorer. (2016). *Overview of the EFDC EPA Model.* Retrieved from www.eemodelingsystem.com/efdc-epa/2016_03_EFDC_EPA_Description.pdf

EcoChem, Inc., Anchor Environmental, LLC. (2005). *Duwamish/Diagonal CSO/SD Sediment Remediation Project Closure Report.* Seattle.

Fischer, H., List, E., Koh, R., Imberger, J., & Brooks, N. (1979). *Mixing in Inland and Coastal Waters.* San Diego: Academic Press.

Hilton, A., McGillivary, D., & Adams, E. (1998). Residence time of freshwater in Boston's Inner Harbor. *J. Waterway, Port, Coastal and Ocean Engineering, 124(2)*, 82-89.

Integral Consulting, Inc. (2015). *Lower Duwamish Waterway Slip 4 Early Action Area: Long-Term Monitoring Data Report Year 3 (2015).* Seattle.

Integral Consulting, LLC. (2013). *Removal Action Completion Report Residential Yards Cleanup.* Seattle.

Integral Consulting, LLC. (2017). *Removal Action Construction and Completion Report: Phase 2: Adjacent Streets and Residential Yards Study Area, Phase 2: Adjacent Streets and Stormwater.* Seattle.

Ketchum, H. (1951). The exchanges of fresh and salt waters in tidal estuaries. *J. Marine Res., 10*, 18-38.

King County. (1999). *King County Combined Sewer Overflow Water Quality Assessment for the Duwamish River and Elliott Bay. Appendix B1: Hydrodynamic Fate and Transport Numerical Model for the Duwamish River and Elliott Bay.* Seattle.

King County. (2016, December 28). *Norfolk CSO sediment remediation project.* Retrieved April 3, 2018, from King County: https://www.kingcounty.gov/services/environment/wastewater/sediment-management/projects/Norfolk.aspx

King County Department of Natural Resources. (2005). *Norfolk CSO Sediment Remediation Project Five-Year Monitoring Program: Final Monitoring Report - Year Five, April 2004.*

King County Water and Land Resources Division. (2016). *Duwamish Diagonal Sediment Remediation Project: 2011 and 2012 Monitoring Report.* Seattle.

Lower Duwamish Waterway Group. (n.d.). *A rich history, a cleaner future.* Retrieved April 5, 2018, from Discover the Duwamish: http://www.ldwg.org/discover.html

Polytechnic Institute of New York University. (2013, March 7). *Least Squares with Examples in Signal Processing.* Retrieved April 24, 2018, from Polytechnic Institute of New York University Electrical and Computer Engineering: http://eeweb.poly.edu/iselesni/lecture_notes/least_squares/least_squares_SP.pdf

Prendergast, D. (2017, December 8). Inverse Model EFDC. Cambridge, Massachusetts.

Prendergast, D., Apell, J., Adams, E., & Gschwend, P. (2018). Characterizing the Diffusive Sediment-Water Fluxes of Polychlorinated Biphenyls Using Passive Sampling, and Estimating Their Contributions to Estuarine Mass Balances: Manuscript in Progress. Cambridge, Massachusetts. Retrieved November 10, 2017

United States Geological Survey. (2018, April 25). *USGS 12113390 Duwamish RIver at Golf Course at Tukwila, WA.* Retrieved April 25, 2018, from National Water Information System: https://waterdata.usgs.gov/wa/nwis/uv/?site_no=12113390&PARAmeter_cd=00060,00065

US EPA. (2010, September 30). Action Memorandum for a Non-Time-Critical Removal Action at the Terminal 117 Early Action Area of Lower Duwamish Waterway Superfund Site, Seattle, Washington. Seattle, Washington.

US EPA. (2014). *Record of Decision: Lower Duwamish Waterway Superfund Site.* US EPA Region 10.

US EPA. (2017, August). *Next Steps: Jorgenson Forge Sediment Cleanup.* Retrieved from US EPA: https://semspub.epa.gov/work/10/100059613.pdf

US EPA. (2018, January 23). *Hazardous Waste Cleanup: Boeing Plant 2, Tukwila, Washington.* Retrieved April 5, 2018, from US EPA: https://www.epa.gov/hwcorrectiveactionsites/hazardous-waste-cleanup-boeing-plant-2-tukwila-washington

US EPA. (2018). *Lower Duwamish Waterway, Seattle, WA.* Retrieved April 1, 2018, from US EPA: https://cumulis.epa.gov/supercpad/SiteProfiles/index.cfm?fuseaction=second.Cleanup&id=1002020#bkground

Washington State Department of Ecology. (2004). *Lower Duwamish Waterway Source Control Action Plan for the Duwamish/Diagonal Way Early Action Cleanup.* Bellevue: Washington State Department of Ecology.

Washington State Department of Ecology and Leidos. (2016). *Lower Duwamish Waterway Source Control Stategy.* Bellevue.

Washington State Department of Ecology. (n.d.). *Jorgenson Forge Corp.* Retrieved March 30, 2018, from Washington State Department of Ecology: https://fortress.wa.gov/ecy/gsp/Sitepage.aspx?csid=3689

Washington State Department of Ecology. (n.d.). *North Boeing Field Georgetown Steam Plant.* Retrieved April 3, 2018, from Toxic Cleanups - Sites: https://fortress.wa.gov/ecy/gsp/Sitepage.aspx?csid=4765

Washington State Department of Ecology. (n.d.). *Source Control.* Retrieved March 30, 2018, from Washington State Department of Ecology: https://ecology.wa.gov/Spills-Cleanup/Contamination-cleanup/Cleanup-sites/Toxic-cleanup-sites/Lower-Duwamish-Waterway/Source-control

Windward Environmental, LLC. (2010). *Remedial Investigation Report Final.* Seattle.

Windward Environmental, LLC. (2017). *Lower Duwamish Waterway Slip 4 Early Action Area Long-Term Monitoring Data Report: Year 4 (2016).* Seattle.